# Permafrost patch size near the margins of discontinuous permafrost, southern Yukon and northern B.C.

Olivier Bellehumeur-Génier

Thesis submitted to the

Faculty of Graduate and Postdoctoral Studies

in partial fulfillment of the requirements

for the degree of Master of Science in Geography

uOttawa

Department of Geography, Environment and Geomatics

University of Ottawa

# Acknowledgment

I would like to express my most sincere acknowledgments to my supervisor Dr. Antoni Lewkowicz, for his professional mentoring throughout this thesis research. Without his help and time, I wouldn't have been able to make this project. I would like to acknowledge my two examiners, Dr. Sharon Smith and Dr. Denis Lacelle, who gave their time and ideas to ensure that this thesis would work and that to improve quality of the thesis. Special thanks to Philip Bonnaventure and Robert Way for the numerous discussions on the results. Without those exchanges the final conclusions could not have been reached. This project would not have been possible without the help of Benoit Faucher, who probed the active layer thousands of times, helped carry the heavy ERT equipment, and gave countless hours for this project.

I would like to thank my family who has always been there for me. Their support helped me bring this project to completion. Thank you to Diane Génier, my godmother who always loved the adventurous spirit and the wild landscape of the North and encouraged me to pursue of this degree.

Finally, this project wouldn't have been possible without financial support from the Natural Science and Engineering Research Council of Canada, the Northern Scientific Training Program, the University of Ottawa and Yukon College.

# Abstract

This research focused on measuring permafrost patch size and related variables between Fort St. John, BC and Whitehorse, YT. Methods used included electrical resistivity tomography, climate monitoring, active layer measurement, analysis of historical aerial photos, and on-site near-vertical aerial imaging. Where permafrost is present along the transect, mean annual air temperature (2010-2014) varied from -3.3 ºC to -0.9 ºC, mean annual ground surface temperature from 0.7 ºC to 2.4 ºC and mean annual ground temperature from -0.3 ºC to 0.2 ºC (at TTOP). Permafrost patches are in the order of 10 – 50 000 $m^2$ in area and there is a strong positive log-log relationship between patch area and maximum permafrost thickness. A conceptual model of permafrost patch size evolution under a warming climate is proposed. It is concluded that permafrost patch size depends on site-specific characteristics, the time since permafrost began to degrade and the local climate conditions.

# Table of Contents

# List of Figures

# List of Tables

# CHAPTER 1: INTRODUCTION AND BACKGROUND

## 1.1 Background

### 1.1.1 Introduction

Permafrost was initially introduced as a term for "*permanently frozen ground*" (Muller, 1943), but this definition was revised to "*ground that remains at or below 0°C for at least 2 consecutive years*" (French, 2007). Even though this definition is widely used, it is common to refer to permafrost as perennially frozen soil, referring in this instance to the state of the water and not strictly the temperature of the ground (French, 2007). Permafrost is also known as perennially cryotic soil which means that the ground remains below 0ºC, a definition that addresses the fact that moisture in permafrost could be unfrozen, partially unfrozen, frozen or even absent (French, 2007). It is estimated that more than 20% of the world's land area falls into permafrost zones and that this is the case for about 50% of Canada's land area (Brown et al., 2001; French, 2007).

Permafrost presence is controlled regionally by climate, but locally it is highly dependent on the ecosystem in which it develops, this being especially true near the southern margin of its distribution (Shur and Jorgenson, 2007; Smith and Riseborough, 1996). With predicted global surface temperature increases ranging from 1.1°C to 6.4°C to the end of the 21$^{st}$ Century and an accentuated warming in lands north of 60° latitude, permafrost degradation in northern Canada could become a serious problem for infrastructure and communities (AMAP, 2012; Bindoff et al., 2013). Future development of northern Canada in the light of global climate change creates the need for better knowledge of permafrost distribution and its

possible evolution. Models, such as the thickness and continuity conceptual model proposed by Roger Brown (1970) (Figure 1.1) are central to our collective understanding of permafrost distribution. Such concepts (Figure 1.1) need to be proven and validated, but new technology such as spaceborne remote sensing has not yet been able to produce information on permafrost body dimensions in the ground (Kaab, 2008). Airborne remote sensing has proven to be successful in acquiring information on permafrost ground characteristics, but this technology is expensive and not readily available (Kaab, 2008; Minsley et al., 2012; Pastick et al., 2013).

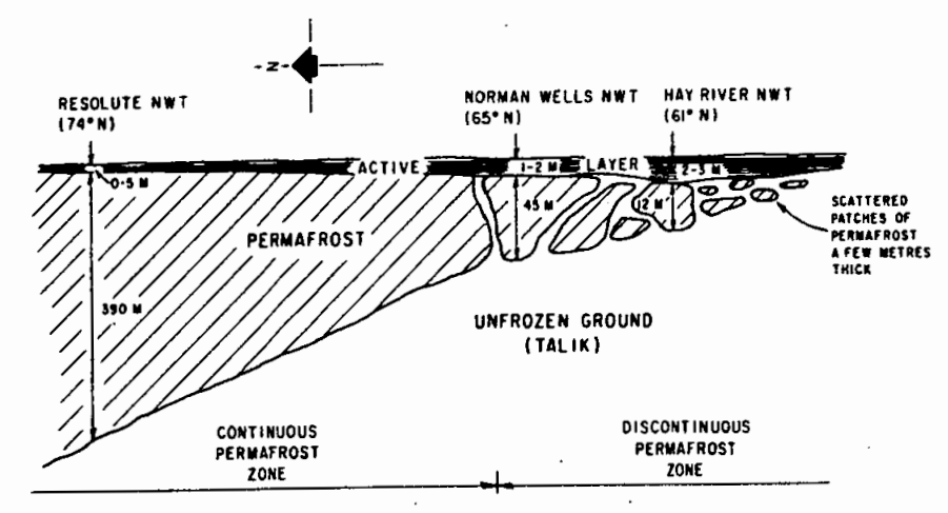


Figure 1.1: Conceptualization of permafrost thickness and continuity in Canada (Brown, 1970)

Consequently, *in situ* measurements such as active layer probing, climate and ground data analysis, on site near-vertical imaging and electrical resistivity tomography (ERT) are needed to better understand local permafrost conditions. ERT creates a 2-D profile of the ground based on the soil's resistance to an input of electric current and this allows the limits of a permafrost body to be defined by the gradient between frozen and un frozen soil (Loke, 1999). This technique has been

widely used in Europe for the study of permafrost (Hilbich et al. 2009; Kneisel et al., 2000) and has also proven effective in Western Canada (James et al., 2013; Lewkowicz et al., 2011; Miceli, 2012).

### 1.1.2 Research Objectives

This research focused on field determination of permafrost patch size and measurement of related variables from the southern limit of the isolated permafrost patches zone to near the boundary between sporadic discontinuous and extensive discontinuous permafrost, on a southeast to northwest transect in western Canada. It aimed to fill the knowledge gap concerning permafrost patchwork dimensions and dynamics at the southern margin of permafrost. A better understanding of permafrost patch size should help in upscaling point measurements of ground temperature and active layer depth to larger scale permafrost models and to the validation of regional or global models. To undertake this investigation, climate data from the last four years were collated, air photos from the present and the past were examined, thaw depths were measured, and extensive ERT surveys were made at each site. The results expected from this research were:

- Patch size is influenced by local controls near the southern margin of permafrost.
- Correlations are present between mean annual air temperature and permafrost patch size and thickness along the transect.
- Permafrost spatial breakdown follows Brown's (1970) conceptual model (Figure 1.1).

### 1.1.3 Permafrost Classification

Permafrost is a perennially frozen ground, defined as earth materials that remain at or below 0°C for at least two consecutive years (Brown and Péwé, 1973; French, 2007). The active layer is the near-surface ground layer underlain by permafrost that undergoes seasonal thaw (French, 2007). The active layer thickness varies greatly between regions, with a thin active layer in the High Arctic and a thicker active layer in the sub-Arctic (French, 2007). The presence of salts or clay minerals at the top of permafrost can result in seasonal thaw even if the soil remains in a cryotic (below 0°C) state, affecting the apparent active layer thickness (French, 2007). The transient layer is an ice-rich ground layer found in the near-surface between the active layer and the top of permafrost that thaws on a decadal or centennial time scale (Shur et al., 2005).

Permafrost varies greatly in thickness, from more than 600 m thick in the far north of Canada, to only a few meters thick at its southern limit (French, 2007). Permafrost is linked to climate and can be found in regions of high latitude (sub-Arctic, Arctic) and high elevation (mountain regions and high plateaus) (French, 2007). These two factors are independent, as exemplified by the Tibetan plateau where the latitudinal position is not favourable for the permafrost formation, but its elevation permits the presence of permafrost (French, 2007).

The relative percentage of permafrost presence across a region is the main characteristic used to classify the distribution of permafrost. The continuous permafrost zone is an area where more than 90% of the land is underlain by

permafrost, with the exception of deep rivers, large lakes and water bodies (French, 2007). The extensive discontinuous zone has between 90% and 50% of the land underlain by permafrost and it presents heterogeneous patterns with perennially unfrozen ground interfingering with permafrost patches (French, 2007). The sporadic discontinuous permafrost zone has between 50% and 10% of the area underlain by permafrost and represents separate patches of permafrost surrounded by unfrozen ground. The isolated patches zone has less than 10 % of its area underlain by permafrost (Heginbottom et al., 1995). There is more than one classification internationally, but in this thesis the Canadian permafrost definitions (Heginbottom et al., 1995) and those of the International Permafrost Association (IPA) Permafrost and Ground Ice Map (Brown et al., 2001) are used.

The climate in a specific location can either be favourable, neutral or unfavourable for permafrost (Shur and Jorgenson, 2007). Since the climate may change through time, areas where the climate was favourable in the past may be neutral or even unfavourable for permafrost in the present or future. Under a warming climate, permafrost may disappear completely or may persist due to the specific attributes of a location in the landscape (Shur and Jorgenson, 2007). This variability is due to the complex interactions between permafrost, vegetation succession and soil properties in evolving environments (Shur and Jorgenson, 2007). Feedbacks among these variables influence the thermal properties of the ground, potentially creating a thermal offset that can preserve permafrost even though the mean ground surface temperature exceeds 0°C (Lewkowicz et al., 2011)

Shur and Jorgenson (2007) described five categories of permafrost to explain the interaction between the climate, ecosystem and permafrost: (1) Climate-driven; (2) Climate-driven ecosystem-modified; (3) Climate-driven ecosystem-protected; (4) Ecosystem-driven; and (5) Ecosystem-protected. Climate-driven permafrost is found in cold regions where the climate is responsible for the formation of permafrost independent of the vegetation cover. Climate-driven ecosystem-modified permafrost was formed during a period of colder climate, but vegetation succession and the ecosystem evolution have caused a modification of the permafrost. The permafrost's resistance to degradation is altered positively or negatively by the ecological succession. Climate-driven ecosystem-protected permafrost was formed in a colder climate but is sustained in warmer conditions by a protective ecosystem component. Ecosystem-driven permafrost is dependent on ground cover (such as peat) and environmental settings that influence thermal conductivity. This permafrost type is characterized by downward freezing under a low thermal gradient. Because of this dependence on the ecosystem, it is more vulnerable to natural or anthropogenic disturbance that may result in the degradation of the permafrost with little possibility of recovery (Shur and Jorgenson, 2007). Ecosystem-protected permafrost remains protected by the ecosystem in areas of mean annual air temperature (MAAT) between -2 and 2°C and possesses the same characteristics as ecosystem-driven permafrost. If the permafrost is in disequilibrium with the environment due to warming or disturbance, degradation will begin and the permafrost will not redevelop after degradation (Shur and Jorgenson, 2007).

### 1.1.4 Thermal Dynamics of Permafrost

At a macro-scale, climate represents the most important control over permafrost, but there are many local controls (Smith and Riseborough, 2002; Throop et al., 2012). The link between permafrost and climate can be examined through the relative values of the MAAT (Mean Annual Air Temperature), MAGST (Mean Annual Ground Surface Temperature), MAGT (Mean Annual Ground Temperature) and TTOP (Temperature at Top of Permafrost), which summarize the thermal regime of permafrost (Smith and Riseborough, 1996, 2002) (Figure 1.2). The MAAT represents the regional climatic conditions at a specific location. The MAGT, MAGST and TTOP, on the other hand, represent the interaction between the regional setting and the local site conditions, such as lithology, vegetation and snow cover (Smith and Riseborough, 1996, 2002).

### 1.1.5 Surface and Thermal Offsets

Permafrost presence and thickness under equilibrium conditions depend on the relationships between air and ground temperatures, known as offsets (Figure 1.2) (Smith and Riseborough, 1996, 2002) and the geothermal gradient. The latter relates to the geothermal heat flux which flows from the Earth's centre towards the surface (French, 2007). The surface offset (MAGST - MAAT) is affected by surface variability in snow cover (nival offset) and/or vegetation (vegetation offset), which act as insulators, intercept solar radiation and influence the ground thermal regime by modifying the water balance (Smith and Riseborough, 1996, 2002). The thermal offset (TTOP - MAGST) assuming equilibrium is caused by changes in the thermal conductivity of the ground when thawed or frozen. This variability in thermal

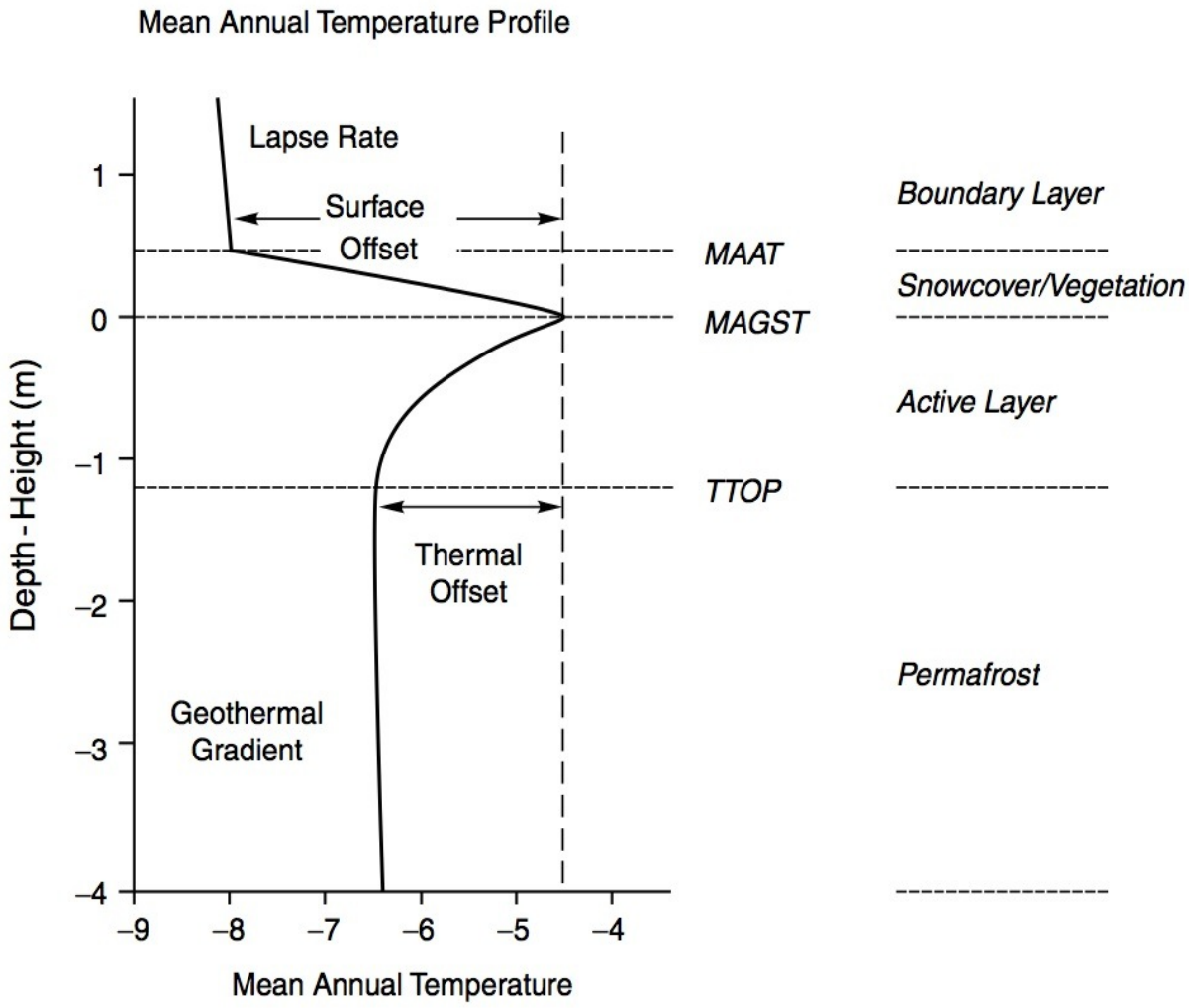


Figure 1.2: Thermal profile of the ground according to the TTOP model (from Smith and Riseborough, 2002)

conductivity is linked to the water content, its physical phase and the thermal properties of the soil particles (French, 2007; Smith and Riseborough, 1996, 2002). In areas of discontinuous permafrost, the presence of perennially frozen ground is linked to the relationship between MAAT and TTOP (TTOP = MAAT + Surface offset + Thermal offset) (Smith and Riseborough, 2002). The southernmost limit of discontinuous permafrost under the TTOP model is controlled by the influence of the thermal conductivity ratio on the thermal offset, while the northernmost limit of discontinuous permafrost is related to snow cover and the nival offset (Smith and Riseborough, 2002).

### 1.1.6 Permafrost Local Controls

Permafrost distribution is climatically controlled at a larger scale, but its small-scale distribution is governed by local controls such as relief, rock type, surficial geology, drainage, vegetation, forest fire and snow cover (Brown 1970; French, 2007; Smith and Riseborough, 1996). In the discontinuous permafrost zone, the relationship between permafrost and terrain is generally more complex than in the continuous zone (French, 2007). The occurrence of permafrost, the boundaries of permafrost patches, the permafrost thickness, and depth of the frost table are mainly influenced by the local setting (Brown, 1970; Cheng, 2004).

Relief's main influence on permafrost resides in the amount of solar radiation received by the ground and the amount of snow that can accumulate on the slope (Brown, 1970). For example, in mountainous part of northern British Columbia and southern Yukon, permafrost may occur beneath a north-facing slope but not beneath an adjacent south-facing slope due to insolation variations (French, 2007).

Rock type mainly affects the continuous permafrost zone where the climate is sufficiently cold to produce permafrost in any location (Brown, 1970; French, 2007). Rock type influences the ground albedo and thermal conductivity (French, 2007). Albedo values can vary from 10 to 40% between rock-covered ground and bare ground (French, 2007). Different rock types and ground cover will greatly influence conductivity, evaporation rate and diffusion properties of the ground, thereby influencing permafrost characteristics (Brown, 1970; French, 2007).

Drainage impacts permafrost local conditions through modification of the ground thermal regime. The quantity of moisture in the ground just before the start of winter and the quantity of moisture that remains after the spring thaw influence the heat transfer between the ground and the atmosphere (Brown, 1970). At the southern margin of the discontinuous permafrost zone, permafrost and drainage are closely related (French, 2007). In the isolated patches zone, permafrost is often found in poorly drained peaty sites, which insulate the ground from solar radiation in the summer and have higher thermal conductivities in winter when the ice content of the peat increases, thus creating a large thermal offset (Brown, 1967; Brown, 1970; French, 2007). Poor drainage can also create stagnant water bodies of different sizes. Taliks, which are layers of ground that remain unfrozen year-round in permafrost areas, are commonly found beneath a body of water that do not freeze to the bottom, due to the high volumetric heat capacity of unfrozen water and its capacity to transfer atmospheric heat by convection in summer (French, 2007).

Vegetation has one of the most complex relationships with the ground thermal regime. The most fundamental effect of vegetation is its ability to intercept solar

radiation and snow before it reaches the ground. The type of vegetation found will greatly influence snow distribution at a location. Vegetation and drainage are also closely related: poorly drained peat cover is common over permafrost bodies in the discontinuous zones (Brown, 1970; French, 2007). The peat and organic cover are essential to the preservation of permafrost at the southern margin (Brown, 1970). In North America, permafrost is often present in boreal forest dominated by spruce, which has a dense canopy that reduces the solar radiation reaching the ground and intercepts snowfall, allowing deeper penetration of cold in winter (French, 2007).

Forest fires are common in the boreal forest of North America and their influence on permafrost varies depending on the rate of burning and the nature of the pre-existing and recovering vegetation at the site, although permafrost is not directly affected by the fires heat, but rather by the loss of ground cover (French, 2007). In the event of a forest fire over peat terrain, if the peat cover is still intact the permafrost will persist. A forest fire in 1958 in the northern Yukon resulted in a 2.4 m degradation of permafrost and a ground temperature rise to ≥ -0.2°C (Burn, 1998). Over the following 41 years the active layer also thickened compared to an undisturbed neighbouring forest site, but it was calculated that more than 1000 years would be needed to completely eliminate the permafrost (Burn, 1998).

The capacity of snow to influence permafrost at a small scale is linked to its insulating properties and its high albedo (French, 2007). The latter can reach 90% for a fresh snow cover and therefore reduces solar energy absorption (Zhang, 2005). Snow insulation capacity is remarkable: its thermal diffusivity is approximately 10 times lower than that of frozen ground depending on his density (Williams and Smith,

1989). Snow depths at a site vary as a function of the micro-topography, vegetation and dominant winds (Brown, 1970; French, 2007). The duration of the snow cover can influence permafrost significantly. If the snowpack develops early in autumn, it can reduce heat flow out of the ground. In spring, a late-lying snow cover can shield the surface from solar radiation and prevent heat entering the ground (French, 2007; Goodrich, 1982; Williams and Smith, 1989).

### 1.1.7 Permafrost and Climate Change

Current model projections of Global Mean Surface Temperature Change from the IPCC (2013) range from increases of 0.3°C to 1.7°C from 1986-2005 to 2081-2100 in scenario RCP2.6 to increases of 2.6°C to 4.8°C from 1986-2005 to 2081-2100 in scenario RCP8.5 (Figure 1.3). Global warming will be amplified in the Arctic by as much as two times the global rate of warming (Bindoff et al., 2013; IPCC, 2013). Given that permafrost is primarily a product of climate, rising atmospheric temperatures and changes in global precipitation distribution will result in overall warming of permafrost (Smith and Riseborough, 2002; Throop et al., 2012 Vaughan et al., 2013). Permafrost has the potential to release large quantities of greenhouse gases such as methane, carbon dioxide and nitrous oxide into the atmosphere, thus increasing global warming rates (Hartmann et al., 2013; Schaefer et al., 2011; Schuur et al., 2009; Schuur et al., 2015; Zimov et al., 2006). Permafrost degradation also has the potential to seriously affect northern communities due to potential change in soil strength and ground stability that could damage infrastructure and by alter the landscape and vegetation (AMAP, 2012; IPCC, 2013).

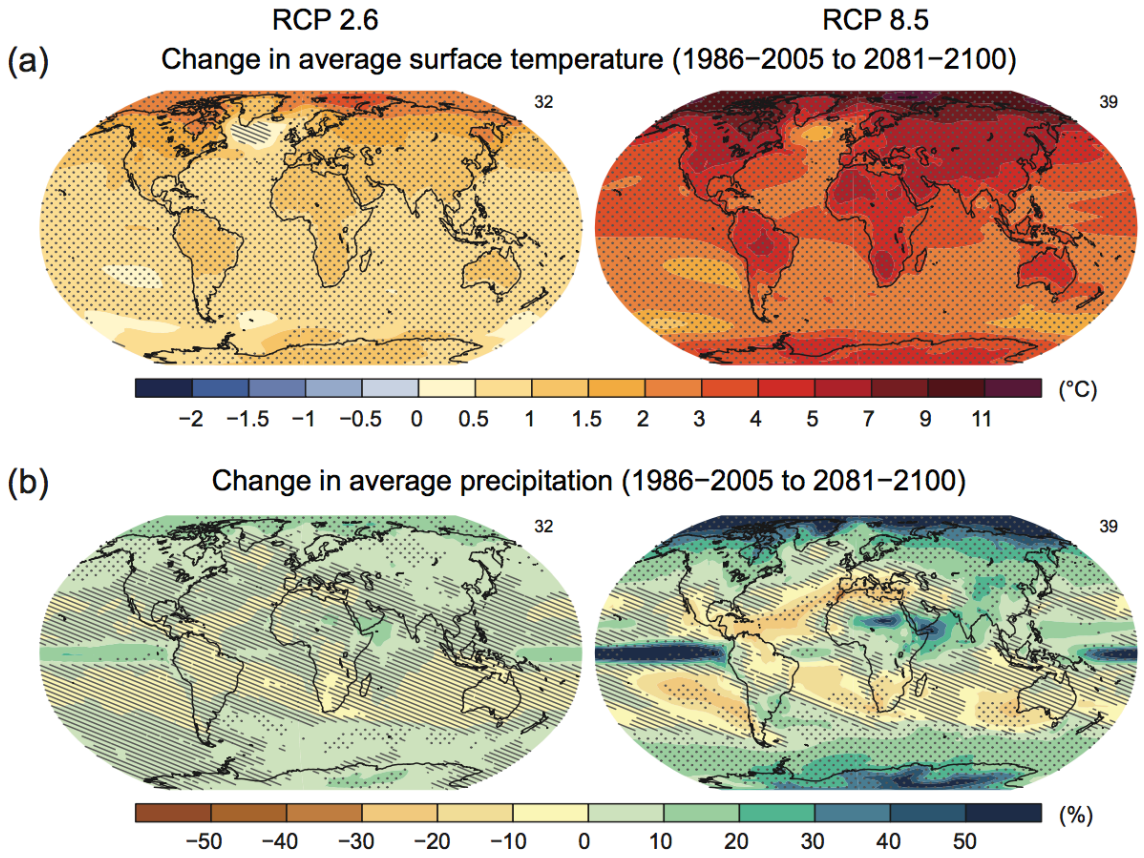


Figure 1.3: Predicted change in average surface temperature and average precipitation from 1986-2005 to 2081-2100 for scenarios RCP 2.6 and RCP 8.5 (from IPCC, 2013).

Smith et al. (2015) observed changes in discontinuous permafrost temperatures ranging from 0.1 to 0.15°C per decade from 1984 to 2015 for Wrigley and Norman Wells boreholes in the southern Mackenzie Valley. Changes in temperatures at Alert boreholes in the Canadian high Arctic from 1978 to 2015 range from 0.32 to 0.50°C per decade (Smith et al., 2015). Permafrost warming in Canada is greater at high latitudes in the continuous zone with higher rates of change than in the discontinuous zone (Smith et al., 2015, Smith et al., 2010). Permafrost warming near the southern margin of permafrost, such as in the southern Mackenzie valley or Yukon, and in mountainous regions is slower and indicates that thaw is occurring

internally, with ground temperatures remaining very close to 0°C for long periods (Lewkowicz et al., 2011; Smith et al., 2015; Smith et al., 2010). This is due to the absorbed heat being converted into latent heat associated with partial melting of the interstitial ice in the ground, which results in a diminished rate of ground warming (Romanovsky et al., 2010).

### 1.1.8 Electrical Resistivity Tomography

#### *1.1.8.1 ERT Basics*

Electrical resistivity tomography (ERT) or Direct Current Resistivity (DC resistivity) is a geophysical technique that measures subsurface resistance to an electrical current. This method is one of the most commonly used and most efficient geophysical methods to detect, differentiate and characterize structures within frozen material or permafrost (Hauck and Kneisel, 2008). ERT is performed by passing electrical current into the ground using two current electrodes. Two potential electrodes then receive the output signal that is sent to the recorder (Hauck and Kneisel, 2008; Hilbich et al., 2008; Loke, 1999).

$$\rho_a = K\frac{\Delta V}{I}, \quad \text{Eq. [1]}$$

Resistivity ($\rho_a$) (Eq. 1) is calculated by dividing the voltage difference ($\Delta V$) by the current (I) and then multiplying this by a geometric factor (K) that depends on the configuration of the four electrodes (Hauck and Kneisel, 2008; Loke, 1999). The result is termed an apparent resistivity of subsurface material, representing a value

for homogeneous ground. An inversion conversion is then needed to convert the apparent resistivities into “true” resistivities.

ERT uses a multi-electrode system and two-dimensional data inversion to represent ground conditions (Hauck and Kneisel, 2008). As the distance between the electrodes increases, the electrical signal penetrates deeper and gathers more information about the subsurface (Hauck and Kneisel, 2008; Loke, 1999). A linear array of electrodes can be used to create a 2-D subsurface profile which shows both vertical and horizontal changes in conditions (Hilbich et al., 2008; Loke, 2011). Three-dimensional ERT surveys can also be produced if information on the resistivity perpendicular to the initial transect is collected, creating a detailed representation of a ground body (Loke, 2011).

#### *1.1.8.2 The Wenner array*

The Wenner array is one of the most commonly used electrode arrays in permafrost studies (Hauck and Kneisel, 2008; Lewkowicz et al., 2011). This array achieves the strongest electrical signal and can penetrate to moderate depth due to its small geometric factor (Loke, 1999). The strength of the Wenner array resides in its capacity to resolve vertical changes because of its high resolution at the centre of the profile (Loke, 1999). The technique is more limited at resolving horizontal differences, especially near its edges where there is low depth of penetration of the signal (Loke, 1999).

#### *1.1.8.3 ERT Post-Processing*

In order to analyze the resistivity data collected in the field, the resistivity values need to be converted from “apparent” resistivity to “true” resistivity. To do so, inversion computer software such as RES2DINV is used to invert the data and convert it into a two-dimensional profile of the transect. The relationship between apparent and true resistivity is complex and programs such as RES2DINV simplify the process and demand minimal user input, thus making the technique more accessible (Loke, 1999).

The post-processing starts with the visualization of a pseudo-section, a preliminary display of the resistivity values. Before running the inversion, it is necessary to inspect the resistivity values for bad data points in the profile and add the surface topography if applicable (Loke, 2011). A single apparent resistivity profile could have multiple inversion results based on the type of inversion model selected (Loke, 1999). Each inversion model has different parameters affecting the inversion process. A “Robust Model Inversion” is normally used when examining permafrost as this best represents the sharp boundaries and homogeneous body (Loke, 2011) associated with permafrost profiles, making it the optimal inversion method to define permafrost patch boundaries at a location.

#### *1.1.8.4 ERT Limitations*

ERT is one of the most effective geophysical techniques to investigate permafrost in the field, but it does have some limitations that should be taken into

consideration (Hauck and Kneisel, 2008; Kneisel et al. 2008; Vonder Muhll et al., 2002).

First, knowledge of the resistivity signature of the earth materials is needed to fully interpret the ERT survey results. However, materials have overlapping resistivities (Table 1.1), necessitating careful interpretation of the field data (Hauck and Kneisel, 2008). Resistivity values in a survey may vary due to lithological differences, moisture state, moisture content and the chemical properties of pore water (Hauck and Kneisel, 2008). The moisture effects on electrical resistivity are particularly important in the analysis of permafrost as frozen water in the ground produces a high electrical resistivity in comparison to unfrozen water (Hauck, 2002; Hauck et al., 2003; Hauck and Kneisel, 2008).

Second, electrode spacing impacts the spatial resolution of the ERT survey. Larger spacings create a coarser spatial resolution in the profile (Loke, 1999) making small subsurface features, such as a thin active layer, hard to characterize or identify. Greater electrode spacings, however, facilitate the surveying of larger portions of terrain. Smaller electrode spacings offer greater resolution but are labour intensive and also have lower penetration depth.

Third, good coupling between the electrodes and the subsurface material is essential in order to obtain reliable results (Hauck et al., 2003). This can be challenging in dry, coarse and rocky terrain (Vonder Muhll et al., 2002).

Finally, the interpretation of the ERT inversion profile in the post-processing stage can be challenging. The inversion process can create areas of low accuracy

Table 1.1: Material threshold to electrical resistivity (adapted from Hauck and Kneisel, 2008)

| **Material** | **Range of resistivity (Ω m)** |
|---|---|
| Clay | 1-100 |
| Sand | 100-5 x $10^3$ |
| Gravel | 100-4 x $10^2$ |
| Granite | 5 x$10^3$-$10^6$ |
| Gneiss | 100-$10^3$ |
| Schist | 100-$10^4$ |
| Groundwater | 10-300 |
| Frozen Sediments<br>ground ice<br>mountain permafrost | 1 x $10^3$-$10^6$ |
| Glacier ice (temperate) | $10^6$-$10^8$ |
| Air | infinity |

(i.e. artefacts), within the profile and this could lead to misinterpretation of results (Hilbich et al., 2009).

These weaknesses explain the necessity of combining ERT with traditional field methods to examine permafrost. Climate data, borehole temperatures and frost probing greatly help in the analysis of the ERT profiles and all the methods complement each other (Kneisel et al. 2008; Miceli, 2012).

## 1.2. Study Area

### 1.2.1 Physical Location

The study area extends between Fort St John, BC and Whitehorse, YT along 1200 km of the Alaska Highway corridor (Figure 1.4). This transect is located in the isolated patches and sporadic discontinuous permafrost zones (Heginbottom et al., 1995).

### 1.2.2 Previous Research

In 1964, Roger Brown performed a survey along this route to identify permafrost bodies and he found permafrost at about 55% of the sites that he examined (Brown, 1967). These sites were generally north-facing, poorly drained, had a thick organic mat and exhibited scattered black spruce or tamarack.

James (2010) repeated Roger Brown's survey in 2007 and 2008 in order to investigate changes in permafrost along this transect. James (2010) revisited 55 of the original 86 sites examined by Brown and 81% of the sites that no longer had

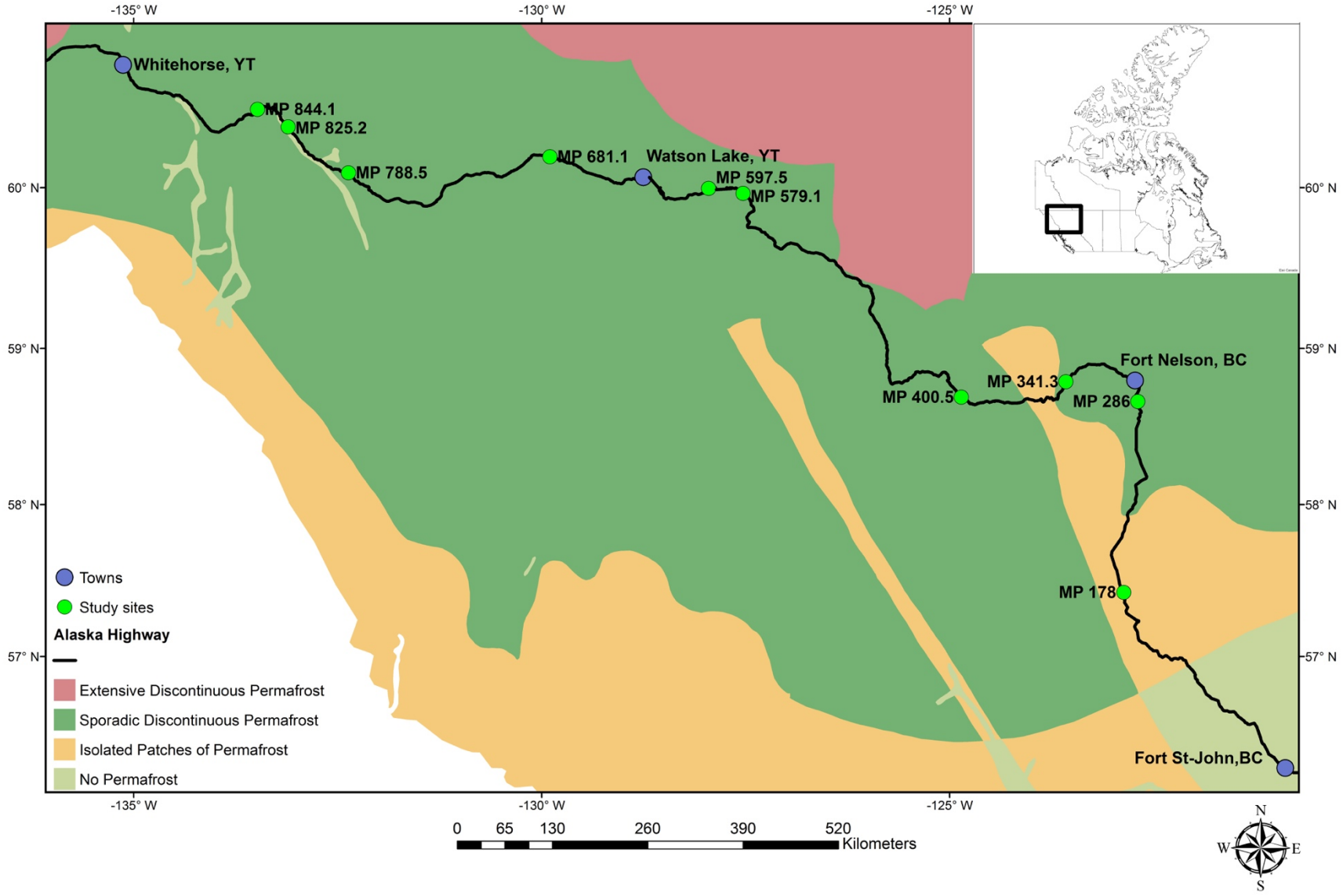


Figure 1.4: Study area map. Permafrost zones based on Heginbottom and al. (1995). Shapefile downloaded via ArcGIS online database.

permafrost were concentrated in the southern section of the transect, between Fort Nelson, BC and Fort St-John, BC. James et al. (2013) found that the MAAT had increased by 1.5°C to 2.0°C since the mid-1970s, the active layer appeared to be thicker than in 1964 and that permafrost degradation had occurred at almost half of the permafrost sites examined by Brown. An organic mat was usually present where the permafrost had persisted (James et al., 2013). James (2010) equipped five of

field sites examined in this thesis (MP 286, MP 400, MP 597, MP 681, MP 844) with air and ground surface temperature monitoring equipment in August 2007.

Miceli (2012) installed fixed electrode arrays at the five sites mentioned above plus MP 178, MP 341, MP 579, MP 788 and MP 825 (all of which were examined by Brown (1967)), in order to examine seasonal variations in resistivity. These are also the ten field sites studied in this thesis. Miceli (2012) added ground temperature and snow depth monitoring equipment at two additional locations on each of the pre-existing sites and matched the entire installation at the other five in August 2010. She found that permafrost thickness in this area rarely exceeded 25 m with most permafrost being less than 15 m thick (James et al., 2013; Miceli, 2012). Miceli (2012) observed that the majority of the permafrost along the transect only occupied a part of the landscape and that the permafrost was vulnerable to thaw, especially in zones of hydrological disturbance (Miceli, 2012). Measured TTOP temperatures were close to 0°C and if temperatures continued to rise, permafrost would be expected to actively degrade (Lewkowicz et al., 2011). It was also suggested that the

presence of permafrost might be responsible for the large thermal offsets observed at the sites (James, 2010; Lewkowicz et al., 2011).

### 1.2.3 Climate

The study region is located in the Boreal Cordillera, Taiga Plains, Montane Cordillera and Boreal Plains ecozones of Canada (Environment Canada, 2016a; Rowe, 1972). The climatic zones identified as being traversed by the transect vary among sources. Taylor et al. (1997) divided the region into two major units: the Northwest Forest and the Yukon/North BC Mountains. The Northwest Forest area includes the northeast portion of British Columbia (MP 47 to MP 342), with elevations ranging from 900 to 1200 m asl. This zone is characterized by temperature differences that can reach 40°C between winter and summer months (Taylor et al., 1997). The summers are normally short, there are extended cold winters and annual precipitation is >500 mm. The Yukon/North BC Mountains region represents the Yukon portions of the transect (MP 350 to MP 620 and MP 750 to MP 790) with topography varies between mountains and lowlands and an average annual precipitation >500 mm (Taylor et al., 1997).

Wahl et al. (1987) offered a more detailed perspective on the climate of the Yukon portion of the transect and identified three different regions: the Liard Basin, the Pelly-Cassiar Mountains and the Upper Yukon-Stikine Basin. The Liard Basin climatic region is traversed by the northeast section of the transect (MP 620 to MP 690). Its precipitation ranges between 400 and 600 mm per year and the topography is lower with a milder climate (Wahl et al., 1987). The Pelly-Cassiar Mountains region

(MP 690 to 750 and MP 790 to MP 870) has some of the highest elevations in the study area and is located in the southern Yukon (Wahl et al., 1987). Annual precipitation ranges from 500 to 700 mm and the climate is temperate in the winter and cool in the summer (Wahl et al., 1987). The Upper Yukon-Stikine Basin (MP 870 to MP 1500) is characterized by relatively low annual precipitation (300 mm/year) and high wind velocity due to the orographic effect of the St-Elias Coast Mountains (Wahl et al., 1987). The western end of the study transect is in this region which exhibits a continental climate with elevations ranging from 600 to 2000 m asl. The three climatic regions mentioned have MAATs ranging between 0°C and -4°C, with the western portion of the transect displaying warmer temperatures than the eastern portion at the same latitude (Wahl et al., 1987).

The annual mean temperatures of the four climate stations with the longest records along the transect are shown in Figure 1.5. The coldest part of the transect is located in the northeast section near Watson Lake, YT, while the warmest part is in the south, near Fort St. John, BC. From the 1940s until about 1973, all four stations were subject to a cooling trend. From 1973 to 1978, there was a rapid warming, followed by a slow warming through to the present day. Table 1.2 also shows that there was an increase in MAAT, but only slight changes in rainfall, snowfall and total precipitation at the four stations between the 1961-1990 and 1981-2010 climatic normals. In detail, snowfall decreased at the stations from the 1950s to the 1970s and then increased from the 1970s through to present, except at Whitehorse where no trends were apparent (Figure 1.6).

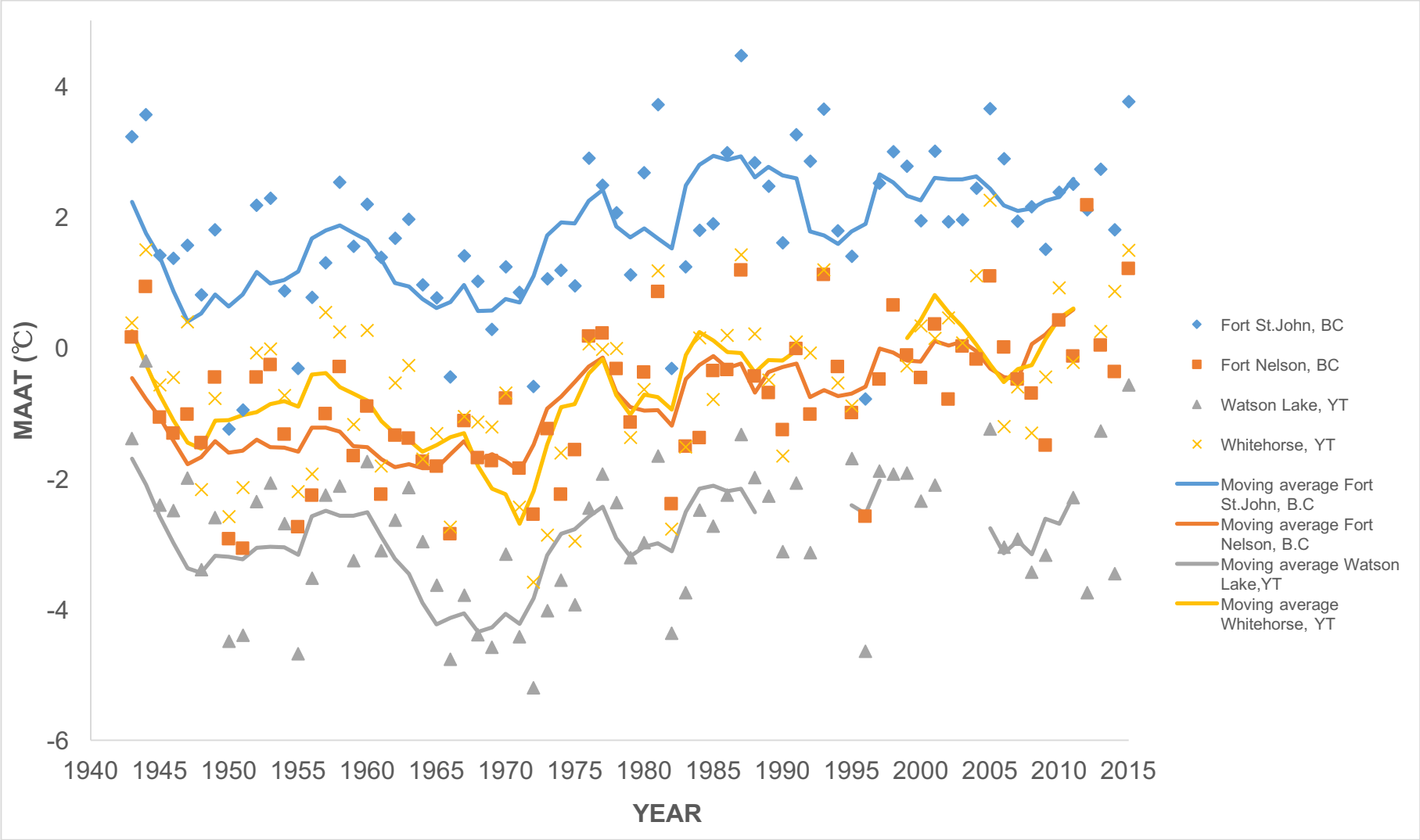


Figure 1.5: Time series (1943-2015) of annual mean temperature for four climate stations in northern British Columbia and Yukon (Source: Environment Canada, 2016b). Lines are 5-year running means. Missing years due to poor data quality: Watson Lake 1993,1994, 2002-2004, 2010 and Whitehorse 1996-1998, 2012.

Table 1.2: Climate normals (1961-1990; 1971-2000; 1981-2010) for the four main climate stations on the transect in northern British Columbia and Yukon. (Source: Environment Canada, 2016b).

| Station | Latitude | Longitude | Elevation | 1961-1990 | | | | 1971-2000 | | | | 1981-2010 | | | |
|---|---|---|---|---|---|---|---|---|---|---|---|---|---|---|---|
| | | | | MAAT (ºC) | Rainfall (mm) | Snowfall (cm) | Precipitation (mm) | MAAT (ºC) | Rainfall (mm) | Snowfall (cm) | Precipitation (mm) | MAAT (ºC) | Rainfall (mm) | Snowfall (cm) | Precipitation (mm) |
| Fort St.John | 56°14'N | 120°44'W | 694.9 m | 1.6 | 296 | 198 | 468 | 2.0 | 313 | 186 | 467 | 2.3 | 292 | 190 | 445 |
| Fort Nelson | 58°50' N | 122°35' W | 381.9 m | -1.1 | 306 | 191 | 449 | -0.7 | 320 | 178 | 452 | -0.4 | 313 | 191 | 452 |
| Watson Lake | 60°06' N | 128°49'W | 687.4 m | -3.1 | 257 | 219 | 414 | -2.9 | 255 | 197 | 404 | -2.4 | 262 | 196 | 416 |
| Whitehorse | 60°42'N | 135°04'W | 706.2 m | -1.0 | 160 | 145 | 269 | -0.7 | 163 | 145 | 267 | -0.1 | 161 | 142 | 263 |

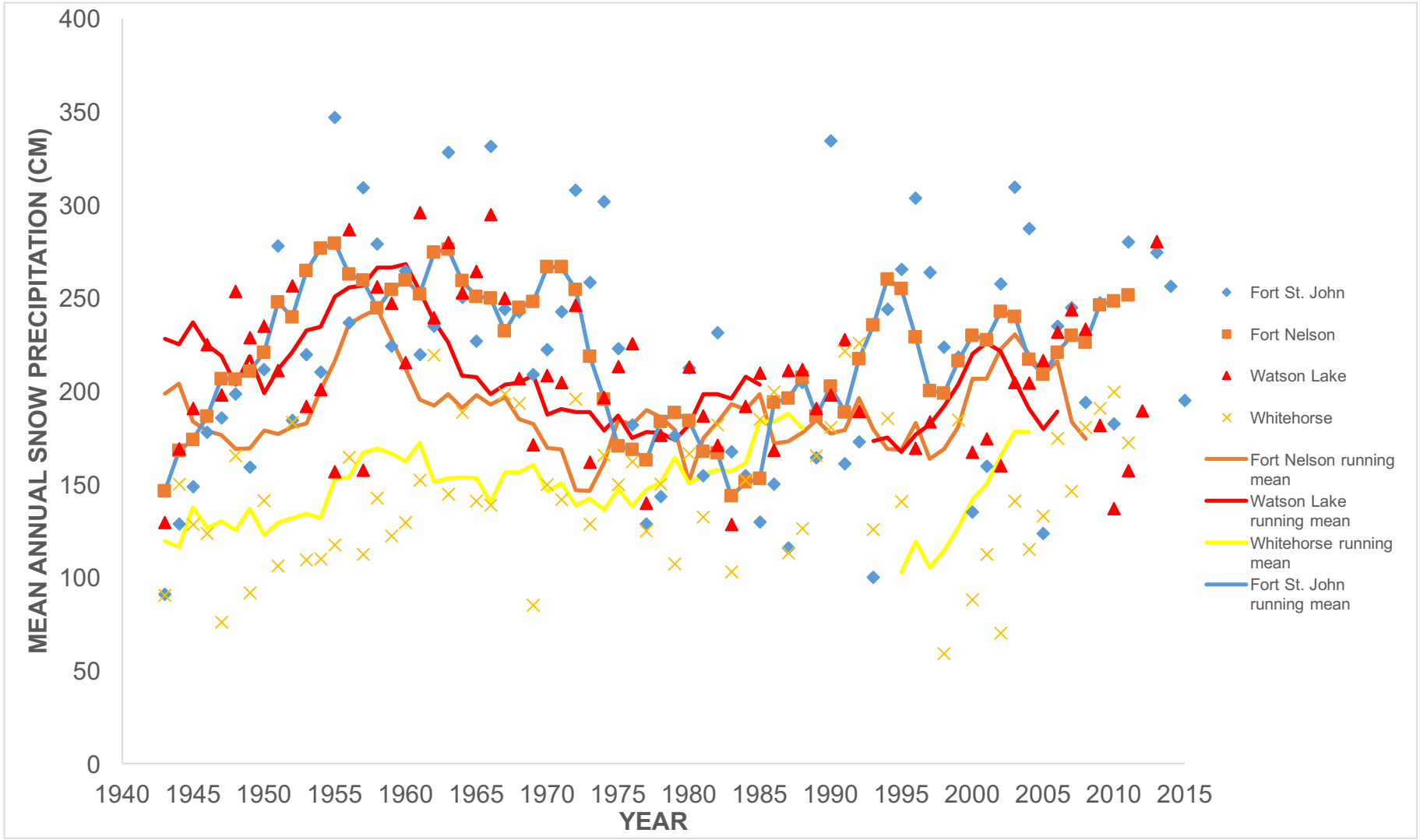


Figure 1.6: Time series (1943-2015) of mean annual snowfall for four climate stations in northern British Columbia and Yukon (Source: Environment Canada, 2016b). Lines are 5-year running means. Missing years due to poor data quality: Watson Lake 1979, 1993-1995, 1998, 1999, 2014, 2015 and Whitehorse 1996, 1997, 2012-2015.

### 1.2.4 Vegetation

The entire study route is forested with the exception of poorly drained sites, active alluvial fans and sites altered by humans (James et al., 2013). Most of the study sites have black spruce trees (*Picea mariana*), which are stunted in poorly drained ground (Brown, 1967; James et al., 2013). Other species found in the study area are white spruce (*Picea glauca*), tamarack (*Larix laricina*), subalpine fir (*Abies lasiocarpa*), lodgepole pine (*Pinus contorta*), aspen (*Populus tremuloides*), balsam poplar (*Populus balsamifera*), paper birch (*Betula papyrifera*), dwarf birch (*Betula nana*), willow. Mosses, lichens, sedges and labrador tea form ground covers (James et al., 2013; Miceli, 2012, Rowe, 1972).

### 1.2.5 Topography

The topography along the transect is highly variable with numerous mountain ranges, intermontane valleys and plateaux (Brown, 1967). The Alaska Highway itself generally follows the lower-lying parts of the landscape with elevations varying from 300 m asl to 1200 m asl (Brown, 1967). The highest point on the transect is Summit Lake, BC within Stone Mountain Provincial Park, which is at approximately 1280 m asl (Brown,1967; Miceli, 2012).

### 1.2.6 Glaciation and Holocene Climate Change

The glacial history of Yukon and British Columbia is complex, with multiple glaciations and the influence of two major ice sheets over the region (Church and Ryder, 2010; Duk-Rodkin, 2004). In the Yukon, lobes of the Cordilleran ice sheet

advanced northeastward and westward and the Laurentide ice sheet advanced westward in the northern portion of the territory (Duk-Rodkin, 2004). In British Columbia, the central and eastern portion of the province was mainly influenced by the Cordilleran Ice sheet and the northeastern portion was influenced by the Laurentide ice sheet (Church and Ryder, 2010). The glaciations in Yukon have been named as the Pre-Reid glaciations (2.9 Ma to 400.5 ka BP), the Reid glaciation (300 to 230 ka BP) and the McConnell glaciation (23.9 to 10.7 ka BP) (Duk-Rodkin 2004). It is believed that Pre-Reid glaciations were the most extensive in the region and that the McConnell glaciation was the least extensive (Duk-Rokin, 2004). In British Columbia, the last Pleistocene glacial episode is known as the Fraser glaciation. It started in the mountain ranges around 30 ka BP, but the ice only emerged from them around 20 ka BP and the glacial maximum was reached at approximately 15 ka BP (Church and Ryder, 2010). Except in the northwest Yukon which was never glaciated, numerous earlier glacial events may have occurred in the study region over the last several million years, but proof of such events is rare because succeeding glacial advances destroyed or altered the evidence (Church and Ryder, 2010; Duk-Rodkin, 2004).

Given the glacial history, the surficial geology is dominated by till and veneers of glacial deposits, with limited areas of glaciolacustrine and colluvial deposits, especially in northern British Columbia. Brunisols are the dominant soil type in Yukon with a small proportion of luvisols and cryosols (Smith, 2004). In British Columbia, soils are predominantly luvisolic, but brunisol and organic soils are common in northern B.C (Church and Ryder, 2010).

The start of the Holocene in southern Yukon was marked by a rapid warming that began around 12 ka BP (Gajewski et al., 2014). The climate during the Holocene was highly variable with warm and dry conditions in the first half of the period, followed by cold events at 8000, 5500 and 3000 BP (Church and Ryder, 2010). The last cold event was the Little Ice Age in the 18$^{th}$ century and it was the most severe of the Holocene (Church and Ryder, 2010). The Mount Logan Ice core analyzed by Fisher et al., (2008) and the paleoclimate reconstruction performed by Viau et al., 2008 (illustrated in Figure 1.7 by Gajewski et al., (2014)) demonstrate the high variability of the climate during the Holocene. At least some of the permafrost found along the transect most likely formed during the Little Ice Age, when temperatures were colder than at present and permafrost may have been more extensive (Vitt et al., 1994, Zhang et al., 2006).

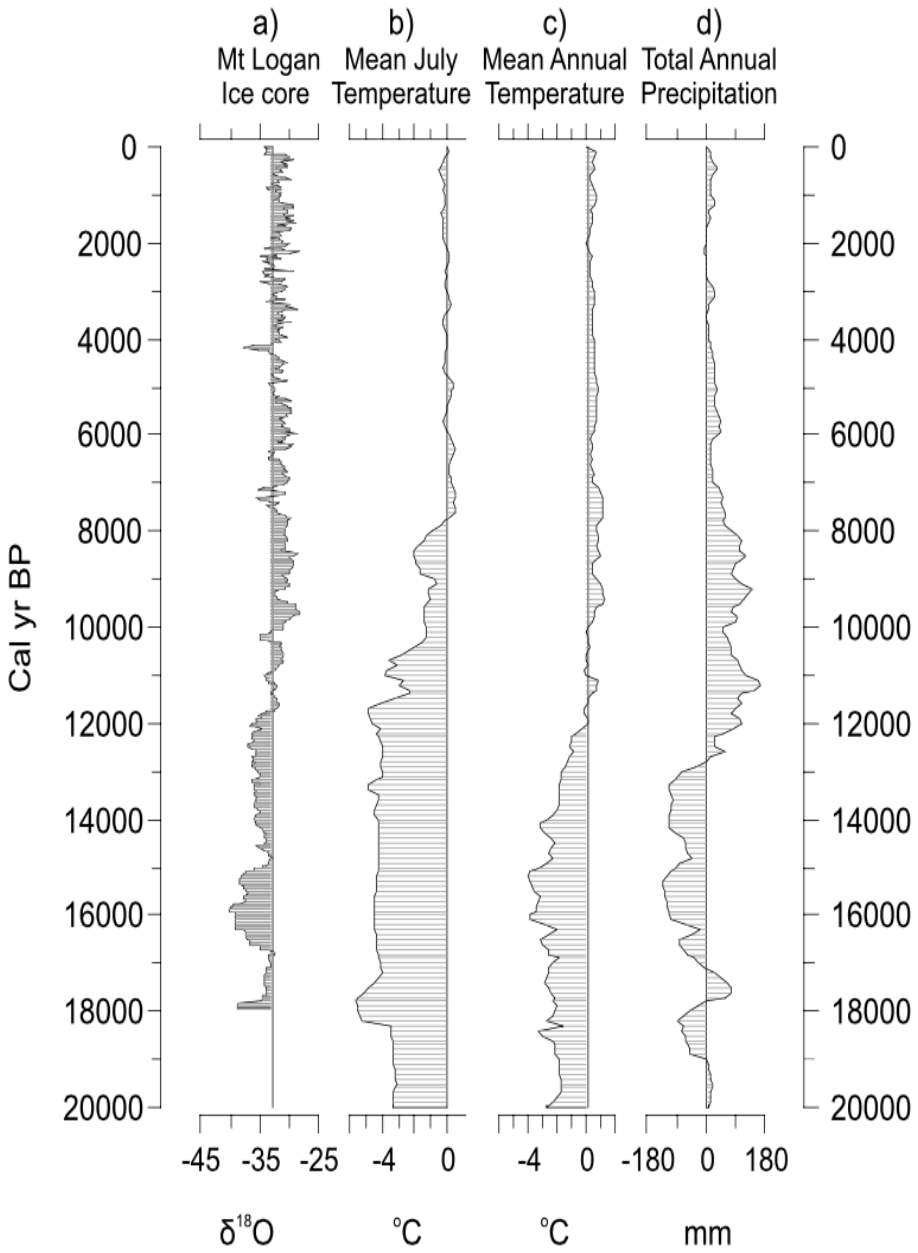


Figure 1.7: Climate of southwestern Yukon from the full glacial to the present (from Gajewski et al., 2014). A) Oxygen Isotope ratios from Mt. Logan ice core from Fisher et al., (2008), b) pollen-based mean July air temperature anomalies (from present) for southwestern Beringia (60°-65° N; 125°-150° W), c) eastern Beringia (Alaska and Yukon) mean annual air temperature anomalies and d) eastern Beringia total annual precipitation anomalies (Viau et al., 2008).

# CHAPTER 2: ARTICLE

I here thereby confirm my participation in the creation of this article with my co-author and thesis supervisor Dr. Antoni G. Lewkowicz. The fieldwork was undertaken by me with training and supervision offered at the first field sites by Dr. Lewkowicz. The data processing and analysis were performed by me and revised and edited by my co-author Dr. Lewkowicz. The ideas and concepts presented in this paper are my original contribution, but they include elements that developed or evolved through discussions with my thesis supervisor. The article was written by me, and revised and edited by Dr. Lewkowicz.

# Permafrost patch size near the margins of discontinuous permafrost, northern British Columbia and southern Yukon, Canada

Olivier Bellehumeur-Génier & Antoni G. Lewkowicz
*Department of Geography, Environment and Geomatics*
*University of Ottawa, Ottawa, Ontario, Canada*

## ABSTRACT

Permafrost patch area, permafrost thickness and related variables were determined at ten sites along a 1200 km transect in the isolated patches and sporadic discontinuous permafrost zones, between Fort St. John, BC and Whitehorse, YT. Methods used included electrical resistivity tomography, borehole temperature monitoring, climate data collection, active layer measurement, analysis of historical aerial photos, and on-site near-vertical aerial imaging. The observations revealed discrete permafrost patches ranging from 10 to 50 000 $m^2$ in area and from a few meters to 50 m in thickness. There was a strong positive log-log relationship between permafrost patch area and maximum thickness even though permafrost boundaries at a given site were mainly influenced by local controls such the thickness of the organic mat, changes in surficial deposits and the presence of standing or running water to promote or eliminate permafrost. Evidence along the transect, such as tilted trees, taliks, progressively decreasing average apparent resistivity of the ground over time, a paucity of significant correlations among functional variables and the small range of mean annual ground temperatures (-0.3°C to 0.2°C), suggest that the permafrost is degrading. A conceptual model was developed that illustrates the evolution under climate warming of a unitary permafrost body which warms and then breaks down into smaller patches as

degradation progresses. We conclude that the permafrost patch size depends on the local site settings, the current site climate, and if the latter represents conditions that exceed the ability of the ecosystem to protect the permafrost, the time since it became climatically unsustainable. The importance of time underlines the need for detailed transient modelling to predict the evolution of permafrost near the margins of its distribution.

## 2.1 Introduction

Permafrost patch size and spacing in the discontinuous permafrost zones are significant for upscaling from point measurements of ground temperatures and active layer thickness, such as those in the Global Terrestrial Network for Permafrost, and hence for the validation of regional or global climate models. Little is known, however, about fine-scale permafrost characteristics from the southern margin of the isolated patches zone through to the boundary between extensive discontinuous and continuous permafrost. This research focused on initiating such measurements along a southeast to northwest oriented transect along the Alaska Highway between Fort St. John, BC and Whitehorse, YT.

Roger Brown's survey along the Alaska Highway in 1964 found permafrost at about 55% of the sites he examined (Brown, 1967). These sites were generally north-facing, poorly drained, and had a thick organic mat. The survey was repeated in 2007 and 2008 in order to investigate the changes in permafrost along the transect (James et al., 2013). MAAT had increased by 1.5°C to 2.0°C since the mid-1970s, the active layer appeared to be thicker than in 1964, and permafrost degradation had occurred at almost half of the permafrost sites examined by Brown

(James et al., 2013). Lewkowicz et al. (2011) measured TTOP temperatures at some of the sites and observed that they were generally very close to 0°C. They concluded that if temperatures continued to rise, permafrost would actively degrade. It was also suggested that the presence of permafrost might be responsible for the large thermal offsets observed at some sites (Lewkowicz et al., 2011). Miceli (2012) used fixed electrode arrays at ten of Brown's survey sites to examine seasonal variations in electrical resistivity. She found that permafrost thickness was generally less than 15 m thick and rarely exceeded 25 m. The present study builds on this earlier work but focuses on assessing the dimensions of permafrost bodies along the transect.

### 2.2 Study Area

The study area extends along 1200 km of the Alaska Highway corridor (Figure 2.1), traversing the entire isolated patches zone and much of the sporadic discontinuous permafrost zone (Heginbottom et al., 1995). Mean annual air temperature (MAAT) varies between 2°C and -3°C (Environment Canada, 2016b) and the entire study route is forested with the exception of poorly drained sites, active alluvial fans and sites altered by human activity. Ten field sites were established along the transect (Figure 2.1; Appendix M) most of which have a cover of black spruce (*Picea mariana*), often stunted (Brown, 1967; James et al., 2013). Other species found in the study area are white spruce (*Picea glauca*), tamarack (*Larix laricina*), subalpine fir (*Abies lasiocarpa*), lodgepole pine (*Pinus contorta*), aspen (*Populus tremuloides*), balsam poplar (*Populus balsamifera*), paper birch (*Betula papyrifera*), dwarf birch (*Betula nana*) and willow. Mosses, lichens, sedges and labrador tea form ground covers (James et al., 2013; Miceli, 2012). Permafrost

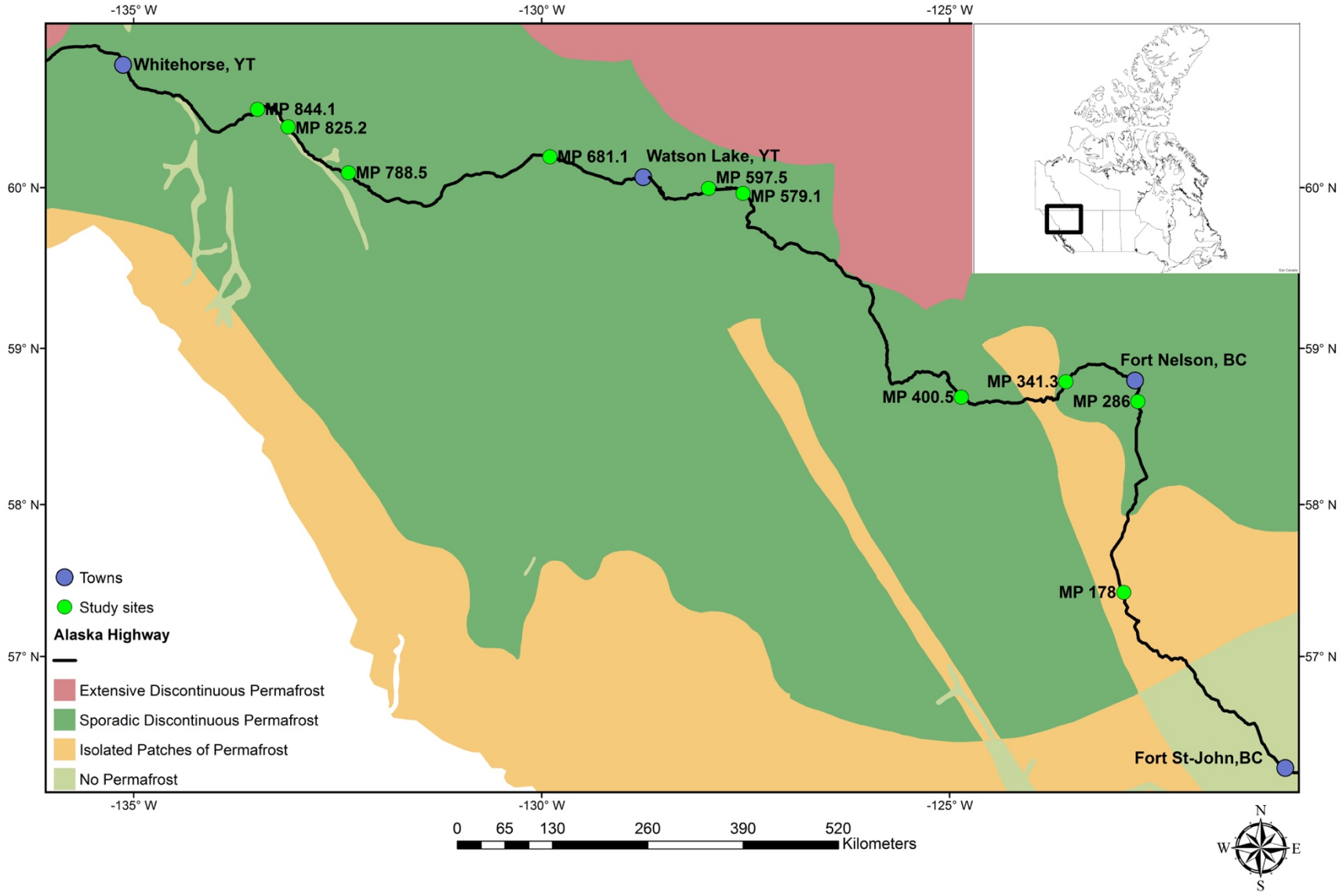


Figure 2.1: Study area map. The study sites are identified by the milepost (MP) number originally used by Brown (1967). Permafrost zones based on Heginbottom and al., (1995). Shapefile downloaded via ArcGIS online database.

was present at all ten sites in 1964 (Brown, 1967) and has persisted through to the present (James, 2010).

### 2.3 Methods

Each study site has with three monitoring stations located 20-40 m apart, equipped with Onset Hobo Pro data loggers (accuracy ± 0.2°C) recording surface temperatures and ground temperatures within the active layer and at the top of permafrost at two-hour intervals. The main station is also equipped with the same type of logger to measure shielded air temperature, and all three stations have stakes with stacked Thermochron iButtons (accuracy ± 1°C) with located 5, 10, 20, 30, 40 ,60, 80, 100 cm above the surface to infer snow depth (Lewkowicz, 2008). Four sites also have a shallow borehole (up to 5 m deep) equipped with an RBR logger (resolution better than ± 0.1°C) or Onset Hobo Pro loggers with external thermistors that record ground temperatures at intervals of 2-8 hours. The climate and ground temperature records acquired cover three years from October 1, 2010, to September 30, 2013, but logger malfunction, surface inundation or damage by animals resulted in loss of data at some sites. In these cases, correlations for daily air temperature were undertaken between site data and nearby sites or Environment Canada climate stations. In all cases, $r^2$ values for the correlations equalled or exceeded 0.97. When appropriate, a blended version of the air temperature record was created by merging the simulated values with the original data. At sites where logger malfunction was chronic, a blended year average was created to obtain the MAAT. Snow cover records include a fourth year of data and run from 2010-2011 to 2013-2014

A 120 cm long frost probe was used to measure the depth to the frost table in August 2014 to confirm the presence of permafrost. Frost probing surveys were undertaken during initial examination of the sites and were used to roughly delimit the permafrost bodies. The surveys started from a known permafrost location on the permanent electrode array (see below) and expanded over an area of approximately 500 x 500 m. More intensive probing was conducted where the environmental settings were judged most likely to produce permafrost, but the probing was also done randomly. By the end of this first survey, rough limits of permafrost bodies were established and flagged, and the spatial variation in environmental setting was also noted. During the second phase of fieldwork, extensive probing was done along the ERT transect at 1 m intervals, to verify the geophysical interpretations and environmental conditions were also noted at 1 m intervals.

An Unmanned Aerial Vehicle (UAV) was used to obtain aerial images of the sites. The UAV was the DJI Phantom 2 Vision+ quadracopter, which is equipped with a 14 megapixel camera, with a resolution of 4384 x 3288 (DJI, 2014). Each image was obtained at an altitude of approximately 90 m above the ground and at a gimbal angle of 90°. The UAV field pictures were compared visually to historical air photos in the National Air Photo Library in Ottawa and to satellite imagery from Google Earth Pro to determine any changes that may have occurred over time at the site. Attempts to georeference the images in order to create 3D models of the sites were unsuccessful due to equipment limitations and the high density of trees. A differential GPS would have proven helpful to mark locations used in the post-processing of the images.

The main technique used to define permafrost patch boundaries was electrical resistivity tomography (ERT), which is a geophysical technique that measures subsurface resistance to a DC electrical current (Hauck and Kneisel, 2008). During ERT measurements, electrical current is transmitted into the ground using two current electrodes and two potential electrodes measure the output voltage which is then recorded (Hilbich et al., 2008; Loke, 1999). An ABEM Terrameter LS profiling system was used with a Wenner electrode array and 1 or 2 m spacing of the electrodes. The length of the ERT surveys range from 40 to 480 m and the range of penetration depths depends on the spacing and length of the array and varied from approximately 6 to 25 m. The field measurements were inverted with RES2DINV software (Loke et al., 2003) using the robust inversion model, which copes best with the rapid changes that occur at the boundaries of frozen and unfrozen materials. Model iterations were stopped when the RMS error fell below 5%, or at the $5^{th}$ iteration, whichever came first. The images presented use a uniform resistivity scale with cold (blue) colours to represent high resistivities and warm (red) colours to represent low resistivities. ERT surveys were conducted where the permafrost patch dimensions were judged the greatest based on the frost probing and visual observations of vegetation and drainage. The typical threshold between frozen and unfrozen soils in the region is 200 Ω m up to 1200 Ω m but the actual value varied from site to site.

The various datasets were combined in order to estimate the boundaries of the permafrost patches at each site. Permafrost patch surface area was calculated based on an assumed elliptical shape, or overlapping ellipses where the boundaries

were more complex. The potential error associated with the use of an ellipse compared to an assumed rectangle is about 27%.

## 2.4 Results

Detailed results are presented from three sites that represent the southeastern part (MP 286), the central (northeast) section (MP 681) and the northwestern end (MP 825) of the transect. Following these three case studies, conditions at the remaining sites are summarized, the functional relationships of the variables are analyzed and a synthesis is developed.

### 2.4.1 MP 286

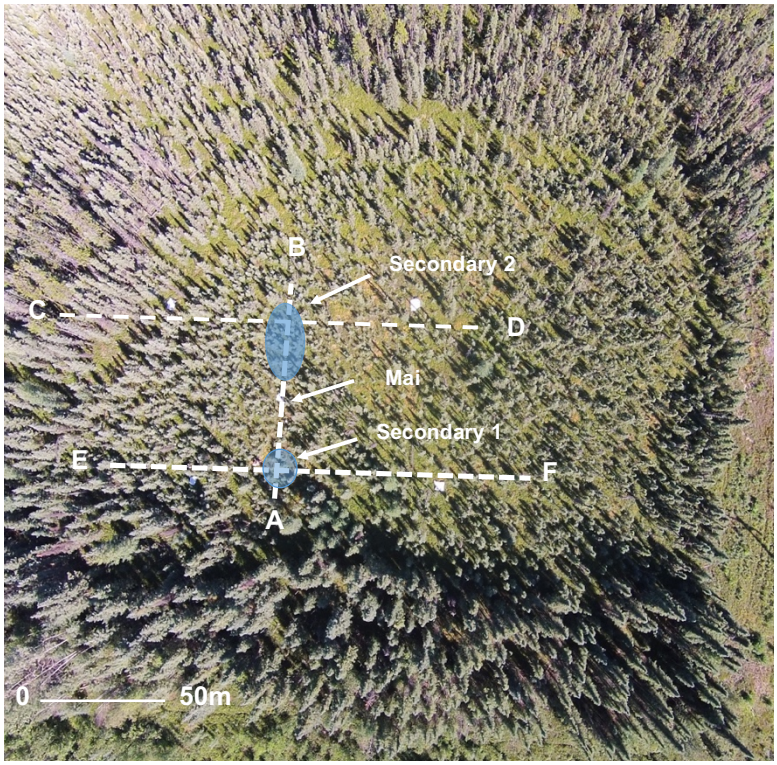


Figure 2.2. Vertical aerial image of MP 286 in August 2014 showing the three ERT transects: the permanent array (A-B), ERT 2 cross-section (C-D,) and ERT 3 cross-section (E-F). The shaded areas represent the interpreted permafrost patches. The main and secondary climate stations and the borehole are marked. Scale is approximate.

MP 286 (Figure 2.2) is located 14 km south of Fort Nelson, BC (see Figure 2.1) at an elevation of 417 m above sea level (asl). The site is in open spruce and tamarack forest with variable tree cover and scattered shrubs (James, 2010). The site exhibits hummocky microtopography with ground cover comprising mosses (including sphagnum), lichens and labrador tea. The mean annual air temperature (MAAT) averaged -0.9°C and varied between a maximum of 0.3°C and a minimum of -2.0°C (Table 2.1). The Mean Annual Ground Surface Temperature (MAGST) at each of the three stations was above 0°C.

The Mean Annual Ground Temperature (MAGT) within the active layer (depth from 0.5 to 1 m) was slightly above 0°C at secondary station 1 (but within the range of error of 0°C) and slightly below 0°C at secondary station 2. Surface offsets averaged 2.3°C at secondary 1 and 3.3°C at secondary 2 while average thermal offsets were -1.3°C and -2.6°C, respectively. Snow depth Days (SDD, cm d) at the site (Table 2.2) varied from a minimum of 2920 cm d to a maximum of 13450 cm d between 2010-2011 and 2013-2014. The winter with the highest SDD value was 2012-2013 with an average of 11140 cm d and the main station had the most snow with an average of 8860 cm d. The historical air photo analysis shows the appearance of a power line cut about 50 m to the south of the site between 1964 and 2002 (Figures 2.3 and 2.4). Although there was no disturbance to the vegetation at the study site, the vegetation clearing may have had an impact on ground thermal conditions in the adjacent undisturbed terrain, altering the permafrost extent over time.

Table 2.1: Climate data for the three study sites along the Alaska Highway corridor (2010-2011 to 2012-2013). Annual averages are for October 1 to September 30 of the years shown. MAGT is at TTOP 100 cm depth. Empty cells represent missing data.

| | | Secondary Station 1 | | Main Station | | | Secondary Station 2 | |
|---|---|---|---|---|---|---|---|---|
| *Site* | *Years* | *MAGST (°C)* | *MAGT (°C)* | *MAGST (°C)* | *MAGT (°C)* | *MAAT (°C)* | *MAGST (°C)* | *MAGT (°C)* |
| *MP 286* | *2010-11* | 1.0 | -0.1 | 1.7 | | -1.2 | 1.8 | -0.2 |
| | *2011-12* | 2.0 | 0.3 | 2.5 | | 0.3 | | |
| | *2012-13* | 1.2 | 0.1 | | | -2.0[a] | 3.0 | -0.2 |
| | *Average* | 1.4 | 0.1 | 2.1 | | -0.9 | 2.4 | -0.2 |
| *MP 681* | *2010-11* | 1.0 | -0.3 | 0.5 | -0.5 | -3.3[b] | 1.4 | 0.9 |
| | *2011-12* | 1.2 | 0.4 | 0.4 | -0.3 | -3.0[c] | 1.4 | 0.4 |
| | *2012-13* | 2.6 | | | 0.0 | -3.7[c] | 2.3 | 1.1 |
| | *Average* | 1.6 | 0.0 | 0.5 | -0.3 | -3.3 | 1.7 | 0.8 |
| *MP 825* | *2010-11* | | | 1.4 | | -1.5[d] | 1.0 | 0.0 |
| | *2011-12* | 2.9 | 1.8 | 1.9 | | -0.2 | | |
| | *2012-13* | 2.9 | 1.4 | 1.3 | | -1.3 | 1.6 | 0.1 |
| | *Average* | 2.9 | 1.6 | 1.5 | -0.1[e] | -1.0 | 1.3 | 0.1 |

[a]Missing data from June 5 to Sept. 30, 2013 estimated by correlation with Fort Nelson Environment Canada station.
[b]Missing data in 2010-2011 estimated through correlation with Watson Lake Environment Canada station and blended with reliable data from MP 681.
[c]Missing data in 2011-2012 and 2012-2013 estimated through correlation with MP 597 station (neighboring site) and blended with reliable data from MP 681.
[d]Missing data from August 1 to August 18, 2011 estimated by correlation with Whitehorse Environment Canada station.
[e]MAGT in 2013-2014 from the borehole at MP 825 (see figure 2.7D)

Table 2.2: Snow covers at three sites along the transect (2010-2011 to 2013-2014). Values were derived from iButton stakes (Lewkowicz 2008) and are expressed as cm d.

| Site | Year | Secondary Station 1 | Main Station | Secondary Station 2 | Average |
|---|---|---|---|---|---|
| *MP 286* | *2010-2011* | 7400 | 8680 | 7930 | 8000 |
| | *2011-2012* | 2920 | 6610 | 5090 | 4870 |
| | *2012-2013* | 9360 | 10630 | 13450 | 11140 |
| | *2013-2014* | 6710 | 9510 | 8790 | 8330 |
| | *Average* | 6590 | 8860 | 8810 | 8090 |
| *MP 681* | *2010-2011* | 8480 | 8160 | 8890 | 8510 |
| | *2011-2012* | 7720 | 7740 | 9690 | 8380 |
| | *2012-2013* | 9570 | 11200 | 10450 | 10400 |
| | *2013-2014* | 7600 | 11670 | 9880 | 9720 |
| | *Average* | 8340 | 9690 | 9730 | 9250 |
| *MP 825* | *2010-2011* | 5500 | 5930 | 5790 | 5740 |
| | *2011-2012* | 5080 | 4970 | 4650 | 4900 |
| | *2012-2013* | 5320 | 3560 | 4740 | 4540 |
| | *2013-2014* | 7550 | 5660 | 4970 | 6060 |
| | *Average* | 5860 | 5030 | 5040 | 5310 |

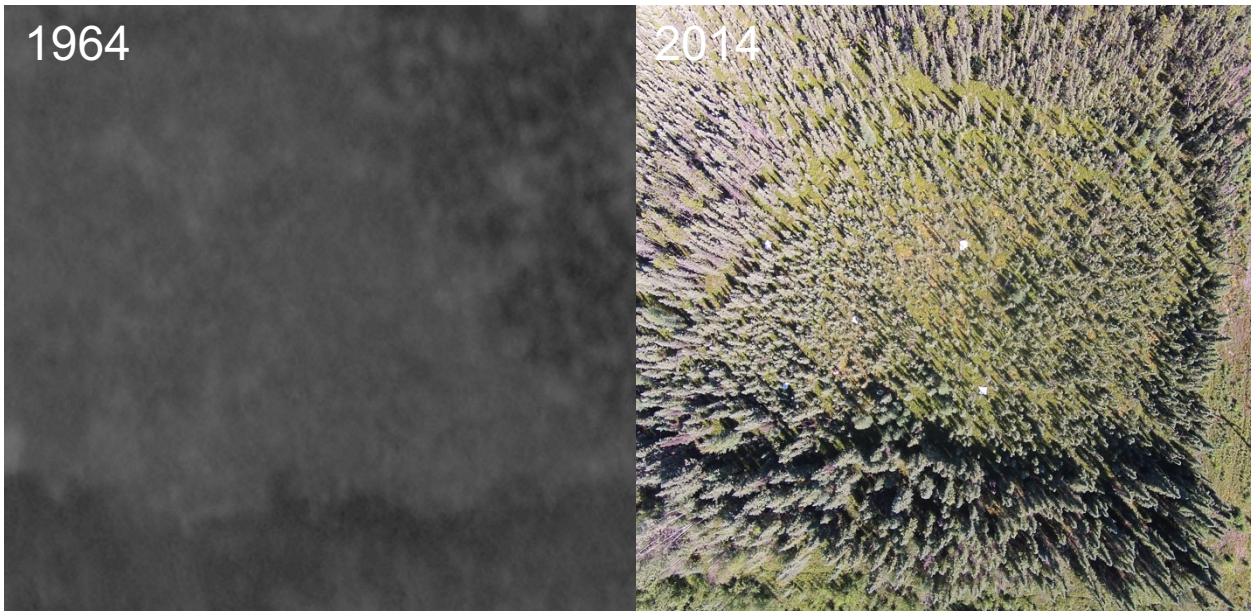


Figure 2.3: MP 286 Historic air photo analysis (A18375-93) from field site in 1964-2014.


Figure 2.4: MP 286 Historic air photo analysis (A18375-93) from field site in 1964-2014. MP 286 satellite imagery from Google Earth Pro from field site in 2002. Dashed square represents site area.

The ERT survey along the 40 m permanent array at MP 286 (Figure 2.5.1) showed considerable variability in the near surface and two bodies with resistivities exceeding 300 Ω m. The layer of lower resistivities immediately below the surface was thin and represented the active layer. The high resistivity bodies were shallow, small and relatively well defined and corresponded to where probing identified a frost table at a depth of less than 120 cm. Cross-sections ERT 2 (Figure 2.5.2) and ERT 3 (Figure 2.5.3) showed similar results, with a single shallow body of higher resistivity. The high resistivites just below the surface at the west end of ERT 2 were interpreted as late-lying seasonal frost due to their thin and shallow nature. It is concluded that two discrete permafrost patches were present at MP 286, varying from 2 to 4 m thick. Secondary station 1 had the lowest average snow cover and the coldest MAGST, but not the coldest ground temperature (Tables 2.1 and 2.2). Soil moisture appeared to be the most important control on permafrost distribution at this site where surface rises of a few centimeters were correlated with the presence of permafrost and vegetation changes between dense and open forest. The large offsets at secondary stations 1 and 2 and the high MAAT suggest that the site is presently out of equilibrium with the climate and that the permafrost patches are no longer ecosystem-protected (Shur and Jorgenson, 2007). Permafrost may have occupied all of the open forest at the site in the past (Figure 2.2), and if so, it has contracted in area and is now degrading.

### 2.4.2 MP 681

MP 681 (Figure 2.6) is located 65 km west of Watson Lake, YT at an elevation of about 850 m asl. The site has an uneven topography with a ground cover of

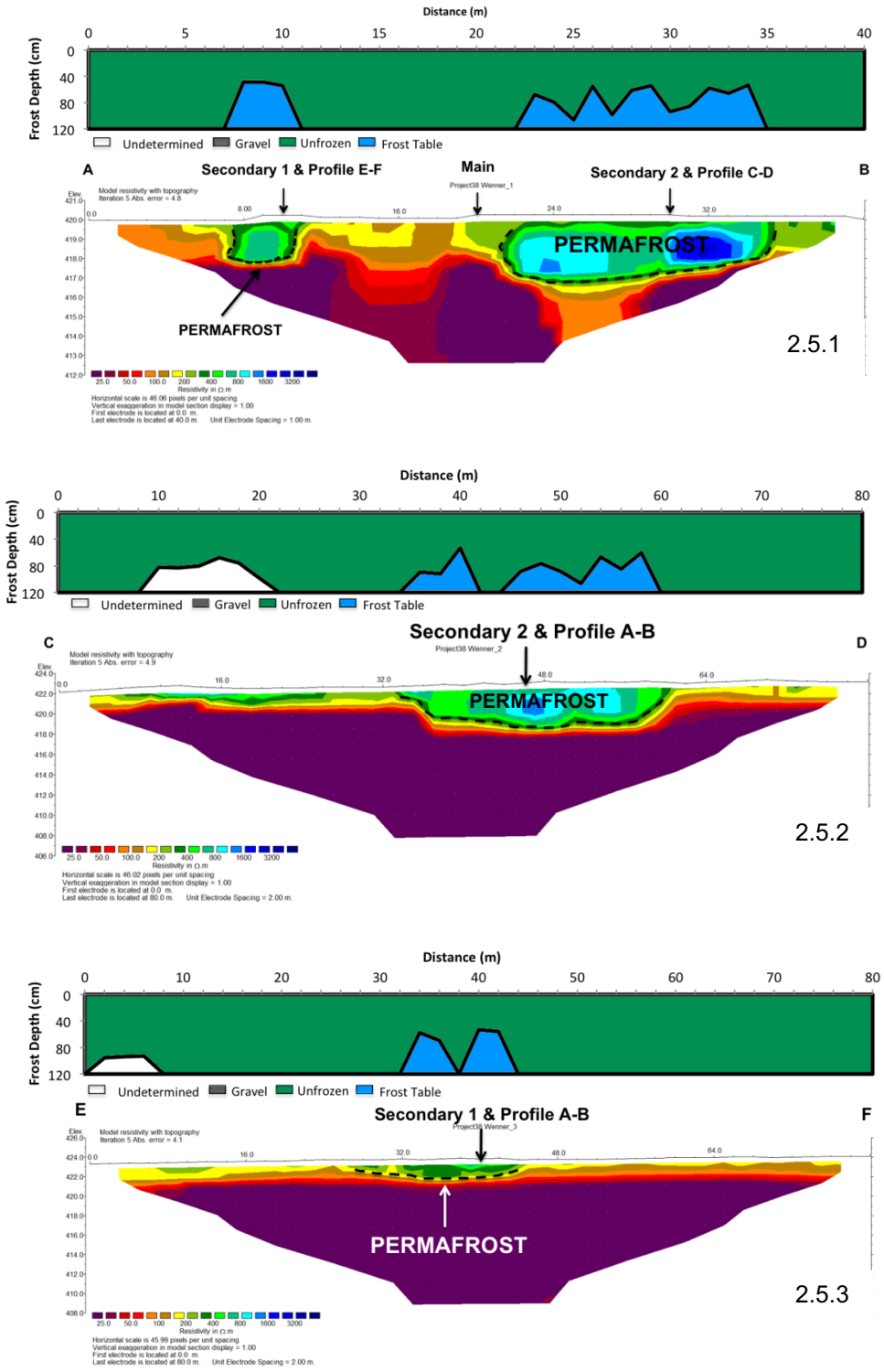


Figure 2.5. Modelled ERT inversion profiles at MP 286 with dashed lines representing inferred permafrost boundaries: 2.5.1 -permanent array; 2.5.2 -ERT 2; 2.5.3 -ERT 3. The frozen/unfrozen boundary is taken to be 300 Ω m at this site. See Appendix B for high-resolution images.

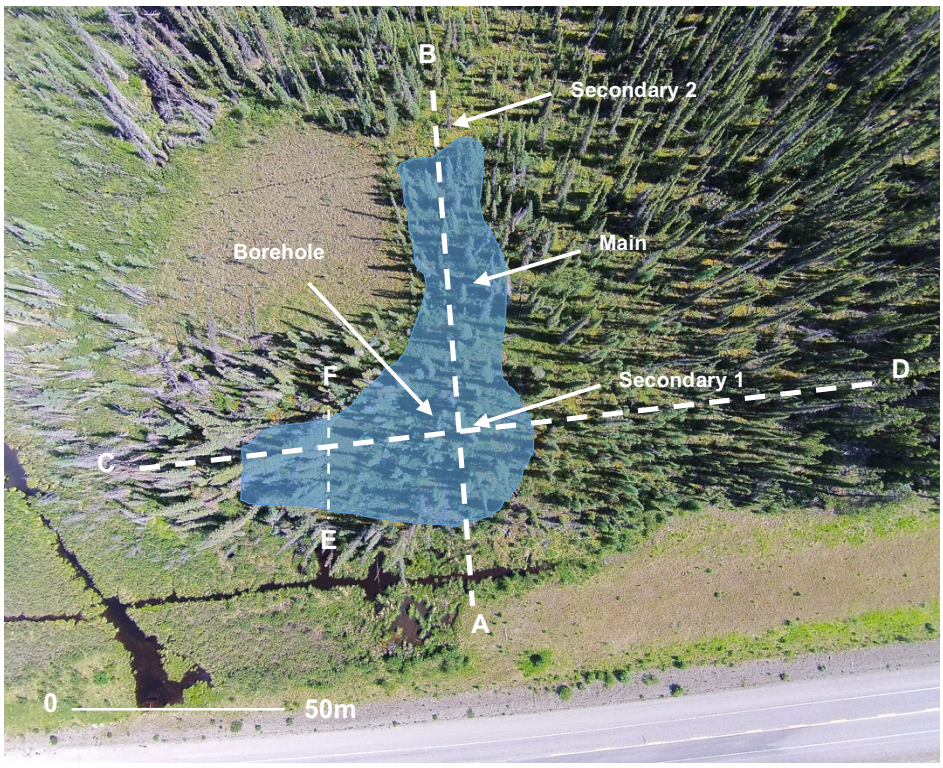


Figure 2.6. Vertical aerial image of MP 681 in August 2014 showing the two ERT transects: the permanent array with extension (A-B) and ERT 2 cross-section (C-D). A frost-probed profile is labelled E-F. The shaded area represents the interpreted permafrost patch. The main and secondary climate stations and the borehole are marked. Scale is approximate.

mosses, lichens, and labrador tea, willow and birch shrubs, with black spruce and tamarack. The soil is moderately cohesive silt, with a thick organic layer (James, 2010). MP 681 is amongst the coldest sites along the transect with a MAAT of -3.3°C and relatively little inter-annual variation (Table 2.1). The MAGST values at the three stations exceeded 0°C in each year with the two secondary stations averaging about 1°C warmer than the main station. MAGT values averaged slightly below 0°C at the main station, 0°C at secondary station 1, and well above 0°C at secondary station 2.

.

The temperature envelope at the borehole (Figure 2.7B, 2.8) indicates an active layer less than 1 m deep with a very shallow depth of zero annual amplitude (~2 m) where the temperature was -0.1°C. Temperatures were -0.2°C at the base of

the borehole at 5 m indicates that permafrost extends to greater depth. The main station at MP 681 had the greatest snow cover with an average of 9730 cm d while secondary station 2 had the least with an average of 8340 cm d (see Table 2.2). The year with the greatest snow cover was 2012-2013 while 2010-2011 had the least.

The ERT permanent array with extension (Figure 2.9.1) showed low resistivities at both ends of the profile where they intersected shallow water bodies. A high resistivity body with values exceeding 800 Ω m was present in the centre extending to a depth of about 8 m and was overlain by a thin discontinuous layer with lower resistivities. ERT 2 cross-profile exhibited low resistivities in a bog near its start (C in Figure 2.9.2). There was a high resistivity body, with values above 800 Ω m in the middle of the profile extending to a maximum depth of about 12 m. This terminated at a small depression and resistivities further along the profile were much lower where the terrain gradually rose. The high resistivity bodies corresponded to locations where a frost table was probed and where the borehole showed the presence of permafrost to >5 m.

Only one patch of permafrost was inferred to be present at MP 681 and it had an irregular shape and a maximum thickness of 12 m. The permafrost boundaries were primarily controlled by drainage, with standing or running water delimiting three sides of the permafrost body while the fourth was marked by a surface depression. The latter was also observable in the vegetation, which became more open with lichens and shrubs dominant. The snowpack was slightly greater in the depression at

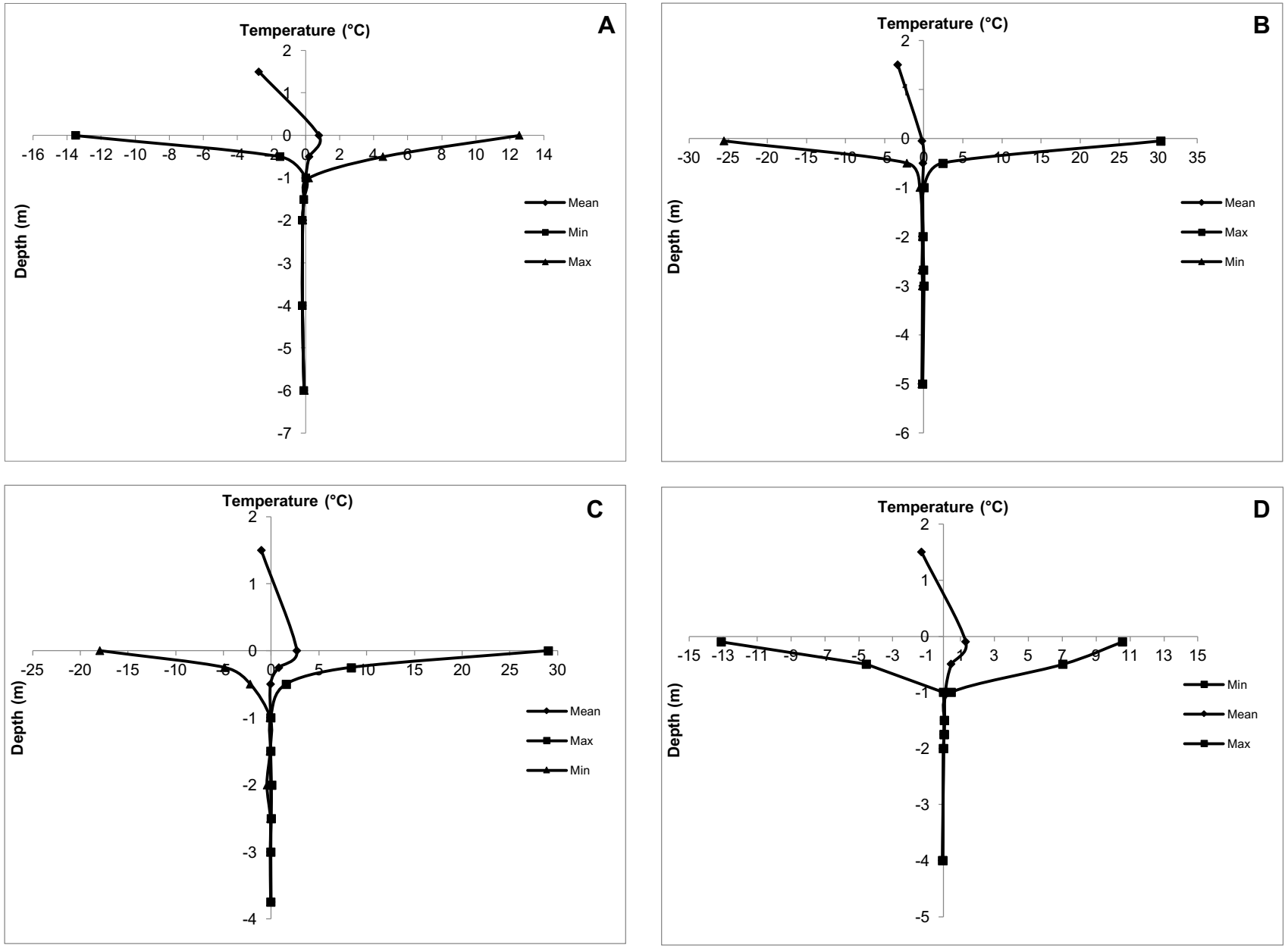


Figure 2.7. A) Temperature envelope for the borehole at MP 178 (2013-2014). The temperature at the base of the borehole at 6 m is -0.1°C. B) Temperature envelope for the borehole at MP 681 (2013-2014). The temperature at the base of the borehole at 5 m is -0.2°C. C) Temperature envelope for borehole at MP 788 (2013-2014). The temperature at the base of the borehole at 3.75 m is -0.1°C. D) Temperature envelope for borehole at MP 825 (2010-2014). A supra-permafrost talik is present between 1 m and 1.75 m where the ground is perennially thawed. The temperature at the base of the borehole at 4 m is -0.05°C.

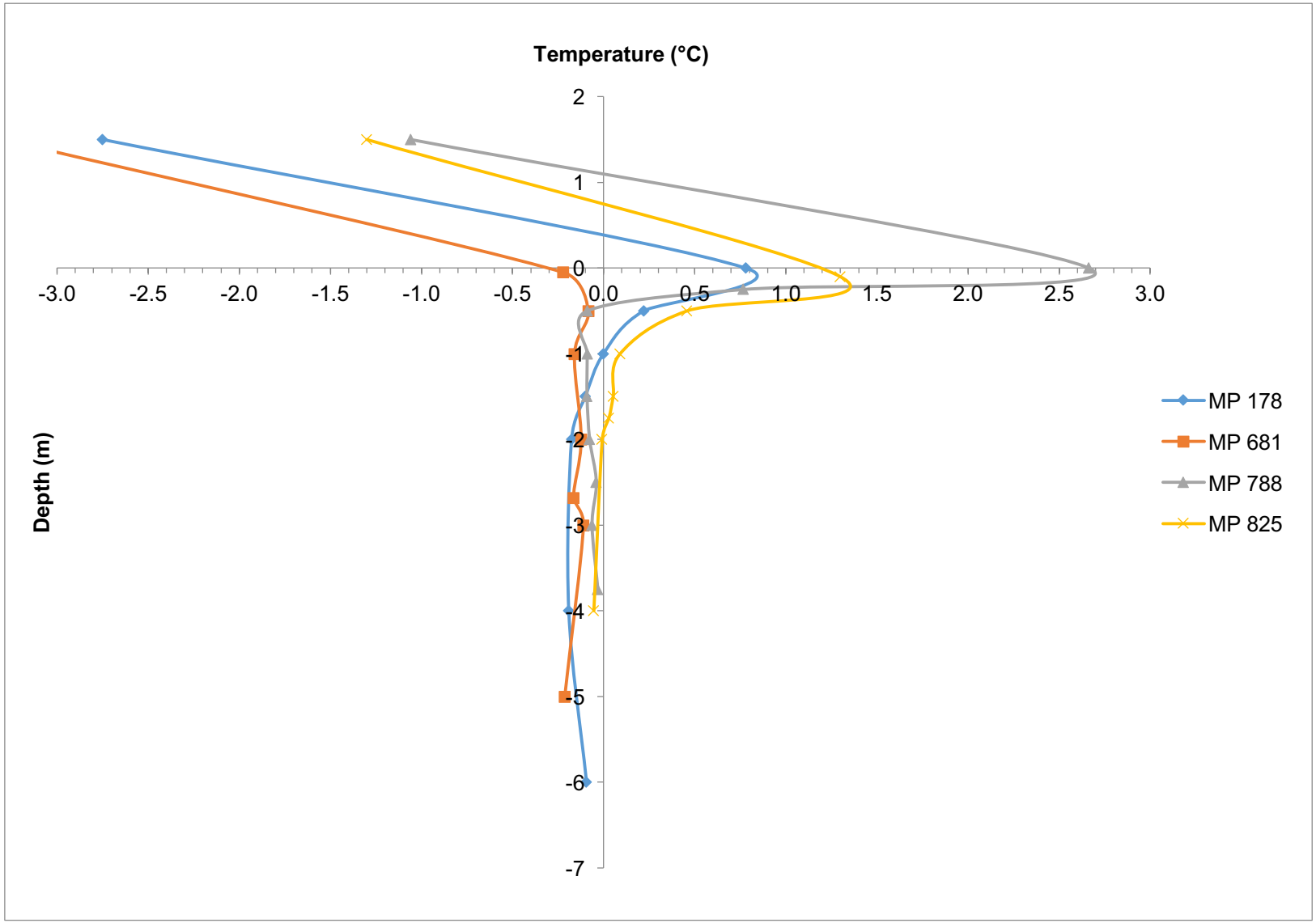


Figure 2.8: Mean air and ground temperatures for boreholes at MP 179 (2013-2014), MP 681 (2013-2014), MP 788 (2013-2014) and MP 825 (2010-2014).

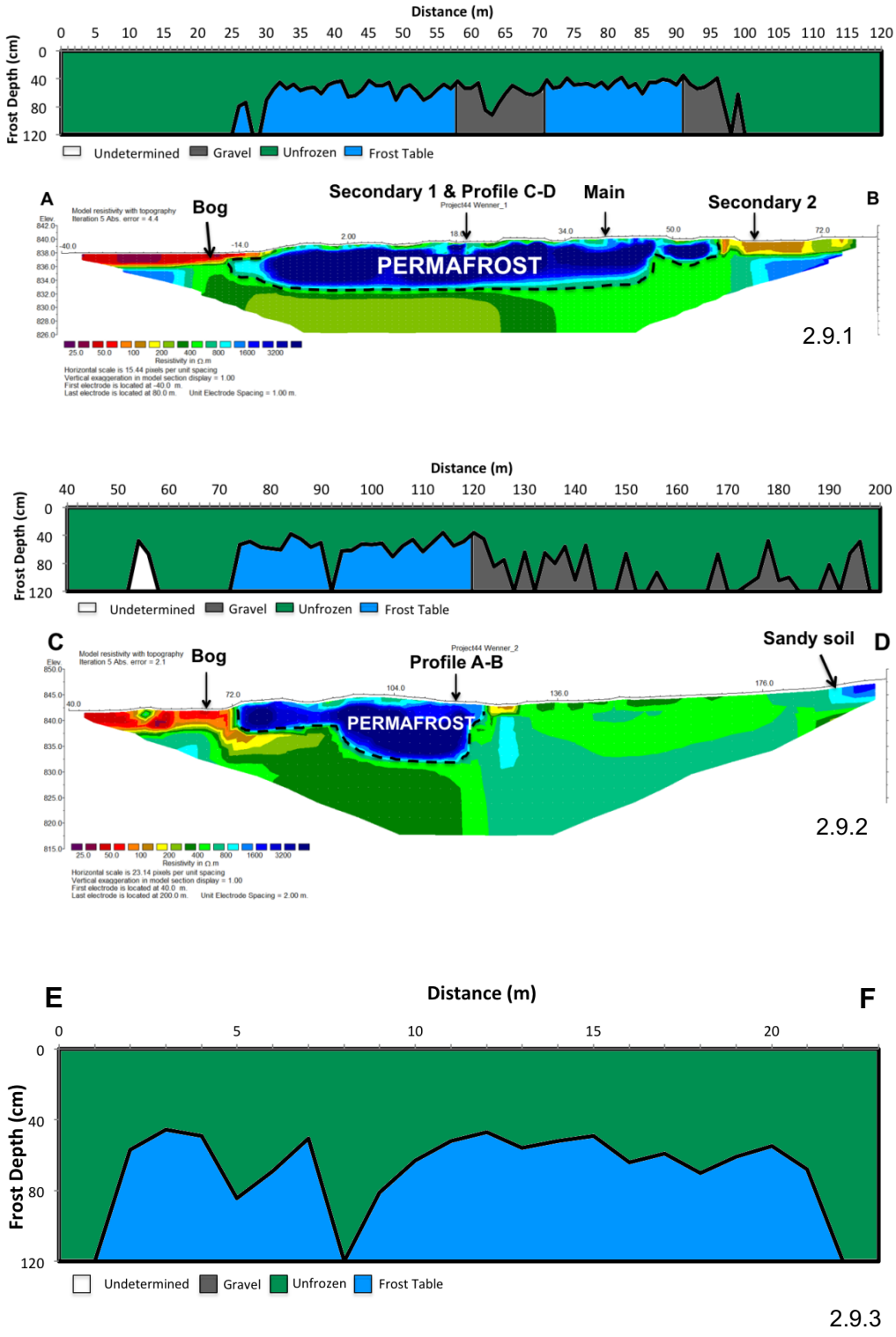


Figure 2.9. Modelled ERT inversion profile at MP 681 with dashed lines representing inferred permafrost boundaries: 2.9.1-permanent array with extension; 2.9.2-ERT 2; 2.9.3 –probed profile (see Figure 2.6). The frozen/unfrozen boundary is taken to be 800 Ω m at this site. See Appendix G for high-resolution images.

secondary station 2 where permafrost was absent and the ground surface temperature was also slightly higher. However, the temperature within the ground was about 1°C warmer than at the secondary 1 and main monitoring sites, so the biggest differences were in the thermal offset and not the surface offset values.

Comparison of the 2014 aerial images with photos taken in 1964 revealed no significant difference in the local setting (Figures 2.10). There was no visual indication of degradation at the site, even though the average apparent resistivity has decreased since 2010 (Lewkowicz et al., 2016).

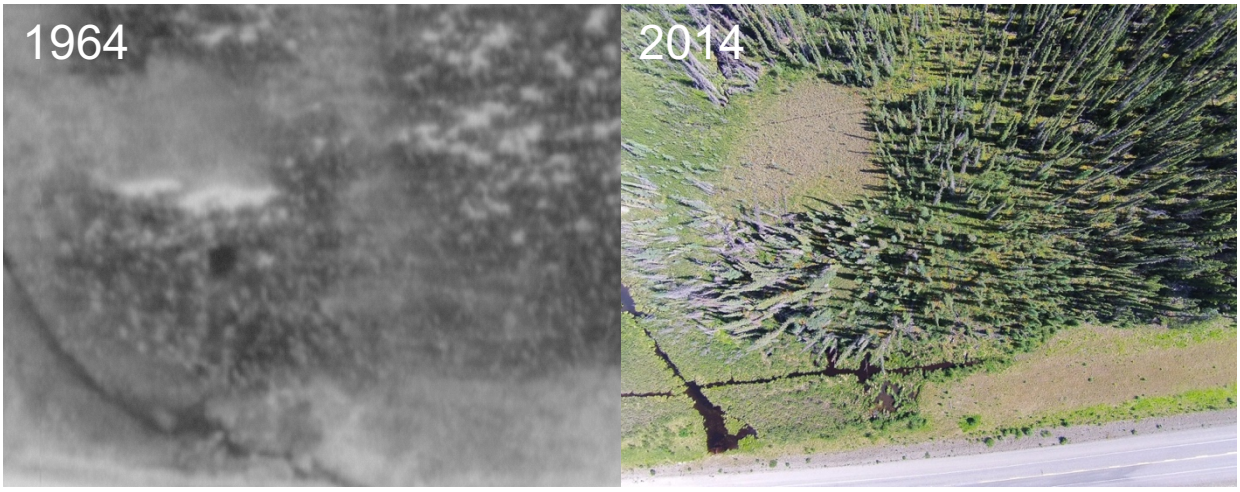


Figure 2.10: Historical air photo analysis (A18390-118) from field site in 1964-2014.

### 2.4.3 MP 825

MP 825 (Figures 2.11 and 2.12) is located approximately 120 km east of Whitehorse, YT at an elevation of 720 m asl. The terrain rises gradually along the fixed array and an undulating surface is superimposed on this trend with a dense forest cover that includes numerous fallen trees. The vegetation comprises black spruce, labrador tea, mosses and shrubs. The soil is cohesive and consists of silt and sand with some gravel (James, 2010).

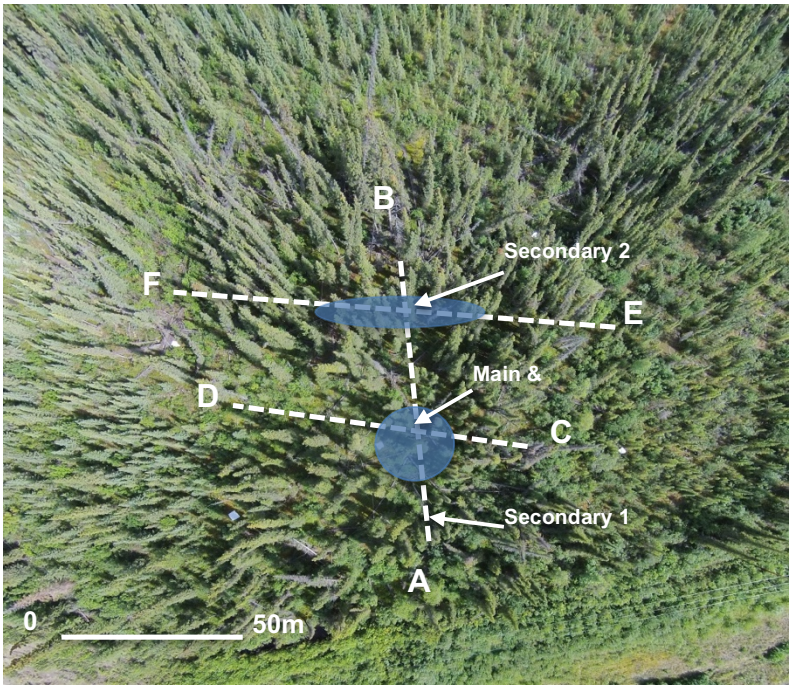


Figure 2.11. Vertical aerial image of MP 825 in August 2014 showing the three ERT transects: the permanent array (A-B), ERT 2 cross-section (C-D,) and ERT 3 cross-section (E-F). The shaded area represents the interpreted permafrost patches. The main and secondary climate stations and the borehole are marked. Scale is approximate.

The MAAT at MP 825 averaged -1.0°C, with a maximum of -0.2°C recorded in 2011-2012 (see Table 2.1). The MAGST at the main station averaged 1.5°C and was almost the same at secondary station 2 (1.3°C) which gave average surface offsets of 2.5°C and 2.3°C respectively. Secondary station 1 was more than one degree warmer at the ground surface, averaging 2.9°C. The MAGT at 1 m depth at the main station was 0.1°C giving a thermal offset of -1.4°C, while the thermal offset averaged -1.2°C at the two secondary stations. The temperature envelope from the MP 825 borehole (Figure 2.7D, 2.8) showed the ground froze and thawed annually to at least 0.5 m, temperatures of just above 0°C to +0.1°C occurred year-round between depths of 1 m and 1.75 m, and the soil remained continuously cryotic at depths of 2 to 4 m (the base of the borehole).

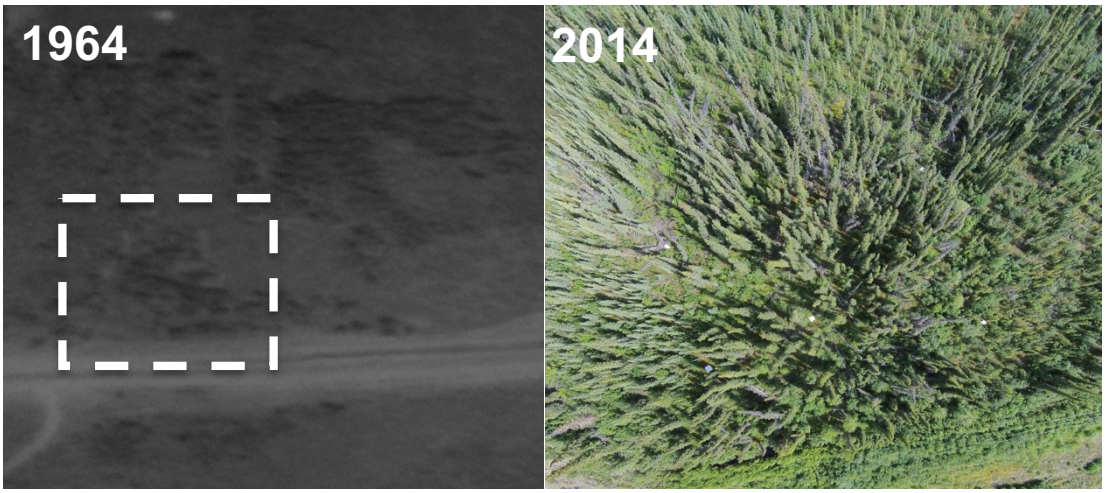


Figure 2.12: Historical air photo analysis (A18404-37) from field site in 1964-2014. Dashed square represents site area.

The three ERT profiles showed discrete bodies of higher resistivity (>300 Ω m) extending from a depth of 1 m to 5-10 m (Figure 2.13). A quasi-continuous low resistivity layer occurred just beneath the surface and lower resistivities also occurred at depth. Probing encountered a frost table at depths of less than 120 cm at locations where the surface low resistivity layer was thin or absent, but not at all locations where the high resistivity layer was apparent at depth.

Two bodies of permafrost were inferred to be present at MP 825 with maximum thicknesses of 9 m and 10 m. The snowpack varies relatively little at the site but was almost always greatest at secondary station 1 where permafrost was absent (see Table 2.2). The vegetation was a good indicator of permafrost distribution at the site as the areas where permafrost was present had larger and visually older trees, often tilted, a thick organic mat and low slope gradients. The neighbouring sites where permafrost was absent were generally drier with a thin organic mat or much wetter with standing or running water. It therefore appears that permafrost body boundaries were controlled by local drainage conditions and topography.

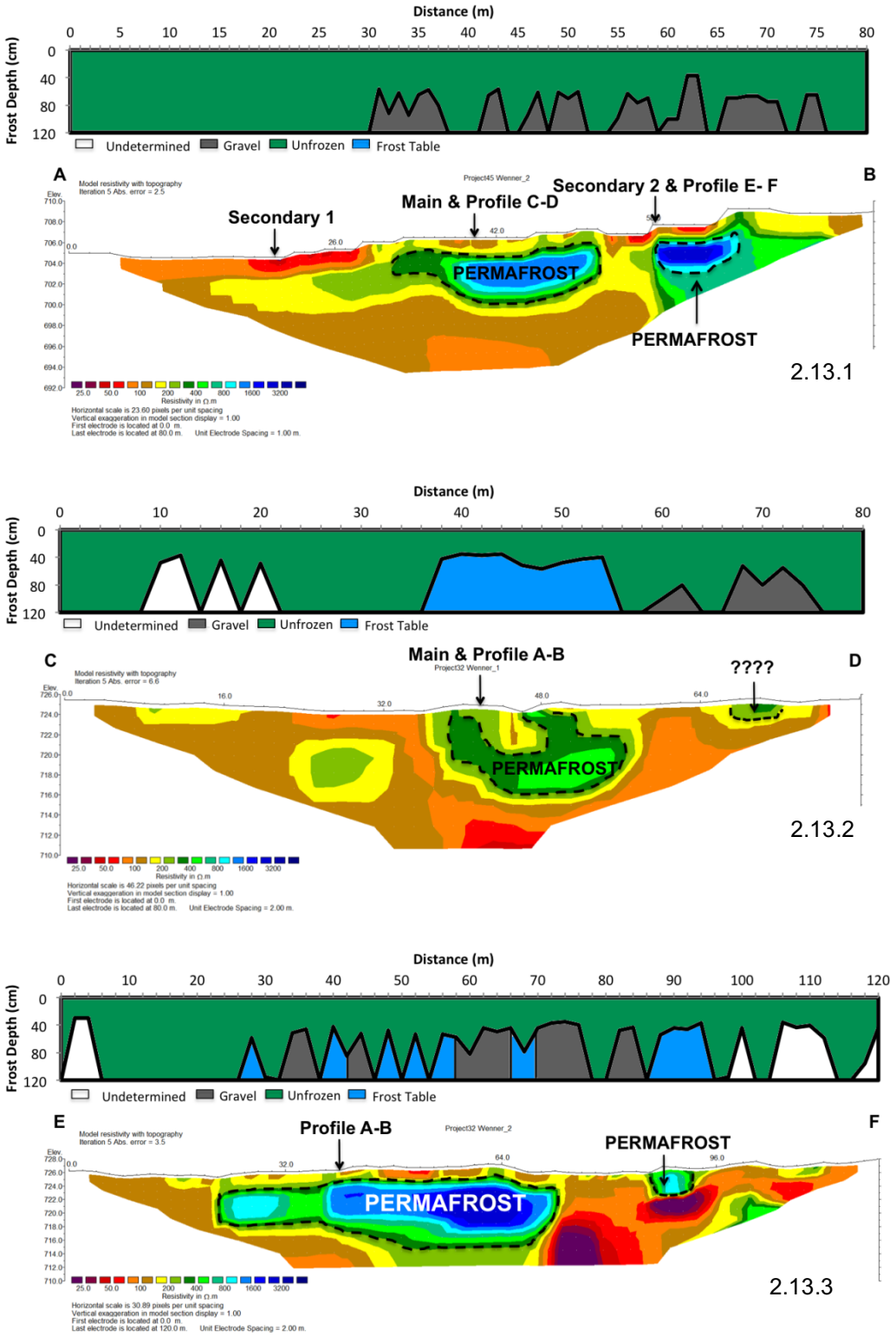


Figure 2.13. Modelled ERT inversion profile at MP 825 with dashed lines representing inferred permafrost boundaries: 2.13.1 -permanent array; 2.13.2 -ERT 2; 2.13.3 -ERT 3. The frozen/unfrozen boundary is taken to be 300 Ω m at this site. See Appendix I for high-resolution images.

There are several indications that the permafrost at MP 825 is degrading, producing a localized thermokarst landscape. First, the surface undulates and a large number of recently fallen trees are present on the slopes of the hummocky mounds. Second, a supra-permafrost talik was present at the borehole for several years even though it refroze 2014-2015 (Lewkowicz et al., 2016). Third, some parts of the permafrost bodies in the ERT profiles are irregular in form (e.g. Figure 2.13.2), with low resistivity layers corresponding to surface depressions, suggesting that thaw settlement has occurred. It is therefore probable that permafrost was previously more widespread at MP 825 and is undergoing degradation, presumably because, as at MP 286, MAAT has risen to values (-1°C over the last 3 years) at which the ecosystem can no longer protect the permafrost.

### 2.4.4 Summary of remaining sites

In this section the results of the entire transect are summarized (Table 2.3).

#### *2.4.4.1 Southeastern end of the transect*

The southeastern section of the transect comprises three sites: MP 178, MP 286 (described above) and MP 341. These sites are characterized by a low electrical resistivity threshold for frozen ground and the smallest permafrost patch surface areas of the transect ranging from 20 $m^2$ to 370 $m^2$ (Table 2.3; Figure 2.14). They are located close to the southern margin of the permafrost zone in this part of western Canada (Figure 2.1), where permafrost is sporadic and patchy.

The local drainage conditions and the vegetation cover restricted the permafrost distribution at MP 178. Several permafrost bodies were present along the ERT

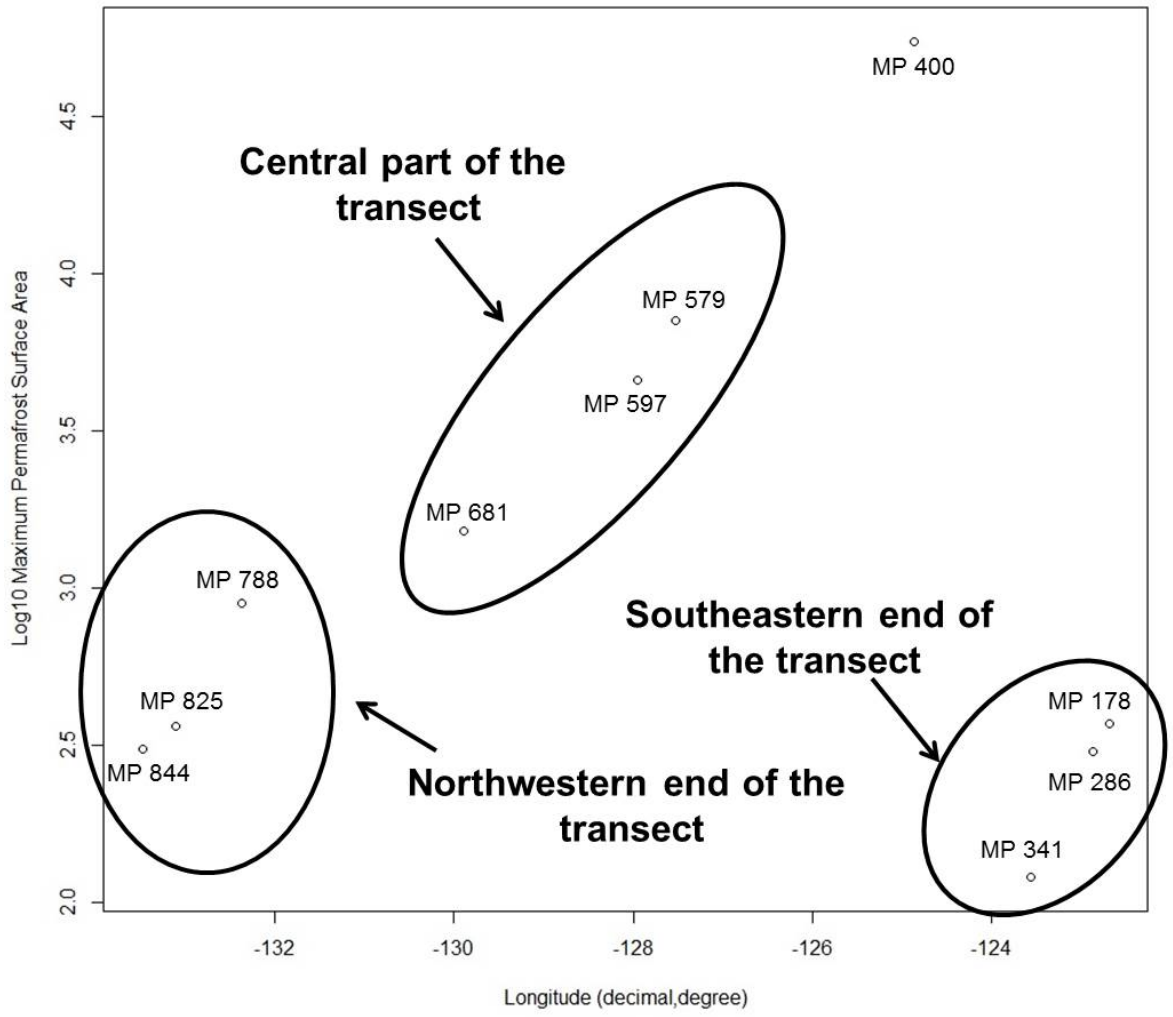


Figure 2.14: Logarithm of maximum permafrost patch size plotted against site longitude.

transects, but these were much smaller than the main body. This site was the highest along the entire transect, had the largest total permafrost surface area at the southern end of the transect (460 $m^2$) and also had the greatest average snow cover (8340 cm d). The average MAGT in the MP 178 borehole was -0.1°C, at 6 m depth (Figure 2.7A, 2.8).

MP 341 had the smallest total permafrost patch area of the transect with 118 $m^2$ and small, shallow and well-constrained permafrost bodies. The climate was similar to

Table 2.3: Summary table of the 10 study sites along the Alaska Highway Corridor, in northern B.C and southern Yukon. Climate data annual averages are calculated from October 1st to September 30th and are from 2010-2011 to 2012-2013. Average Snow Depth Days are from 2010-2011 to 2013-2014 and values were derived from iButton stakes (Lewkowicz, 2008) and are expressed in cm d.

| *MP sites* | **178** | **286** | **341** | **400** | **579** | **597** | **681** | **788** | **825** | **844** |
|---|---|---|---|---|---|---|---|---|---|---|
| *Site elevation (m asl)* | 1098 | 420 | 150 | 1042 | 675 | 672 | 838 | 762 | 706 | 820 |
| *Latitude*[1] | 57.425 | 58.663 | 58.788 | 58.693 | 59.965 | 59.996 | 60.188 | 60.091 | 60.371 | 60.476 |
| *Longitude*[1] | -122.865 | -122.693 | -123.573 | -124.858 | -127.531 | -127.955 | -129.898 | -132.368 | -133.111 | -133.483 |
| *Area of permafrost patch #1 ($m^2$)* | 300 | 370 | 120 | 55000 | 7000 | 4600 | 1500 | 900 | 360 | 310 |
| *Area of permafrost patch #2 ($m^2$)* | 110 | 20 | 75 | n/a | n/a | 78 | n/a | n/a | 300 | n/a |
| *Area of permafrost patch #3 ($m^2$)* | 50 | n/a | n/a | n/a | n/a | n/a | n/a | n/a | 30 | n/a |
| *Total permafrost area ($m^2$)* | 460 | 390 | 190 | 55000 | 7000 | 4700 | 1500 | 900 | 610 | 310 |
| *Max thickness of patch #1 (m)* | 5 | 4 | 3 | 50 | >25 | 12 | 12 | 10 | 9 | 5 |
| *Max thickness patch #2 (m)* | 4 | 2 | 2 | n/a | n/a | 3 | n/a | n/a | 10 | n/a |
| *Max thickness patch #3 (m)* | 2 | n/a | n/a | n/a | n/a | n/a | n/a | n/a | 3 | n/a |
| *# of permafrost bodies* | 3 | 2 | 2 | 1 | 1 | 2 | 1 | 1 | 3 | 1 |
| *Average MAAT (°C)*[3] | -2.1 | -0.9[A] | -1.9[B] | -2.5[C] | -2.5[D] | -2.5 | -3.3[E] | -1.1 | -1.0[F] | -2.0[G] |
| *Average MAGST (°C)*[3] | 0.7 | 2.2 | 2.2 | 1.2 | 2.1 | 1.9 | 0.5 | 2.4 | 1.3 | 1.7 |
| *Average MAGT (°C)*[3] | -0.1 | -0.1 | -0.2 | 0.0 | 0.1 | -0.2 | -0.3 | -0.1 | 0.1 | 0.2 |
| *Average SDD*[4] | 8340 | 8090 | 5910 | 7380 | 9410 | 8490 | 9250 | 6080 | 5310 | 7890 |
| *Surface Offset (°C)* | 2.8 | 3.1 | 4.2 | 3.7 | 4.6 | 4.4 | 3.8 | 3.5 | 2.3 | 3.7 |
| *Thermal Offset (°C)* | -0.8 | -2.3 | -2.4 | -1.2 | -2.0 | -2.2 | -0.8 | -2.4 | -1.2 | -1.5 |
| *Total Offset (°C)* | 2.0 | 0.8 | 1.7 | 2.5 | 2.6 | 2.3 | 3.0 | 1.1 | 1.1 | 2.2 |
| *Permafrost resistivity threshold (Ω m)*[5] | 200 | 300 | 300 | 800 | 800 | 800 | 800 | 800 | 400 | 1200 |
| *Past disturbance*[6] | Yes | Yes | Yes | No | No | No | No | Yes | No | No |

[1] Coordinates are expressed in Decimal Degree format using WGS84 datum. GPS error margin was ± 3m
[2] The permafrost patch sizes were driven from the modeled ERT inversion profiles and frost probing. Permafrost patch surface area was estimated based on an elliptical shape.
[3] Average MAAT, MAGT, MAGST are derived from 2010-2011 to 2012-2013 climate data. MAGT and MAGST averages are based on stations where permafrost was present.
[4] Average SDD represents an average of all three climate stations from 2010-2011 to 2013-2014.
[5] Permafrost boundaries represent the resistivity value chosen to delimit unfrozen and frozen material at each site during the ERT analysis.
[6] Past disturbance analysis is driven from the observation of contemporary and historic air photos of the sites. Yes, means that a disturbance occurred between 1964 and 2015, No means that no major disturbance occurred. Disturbances are considered in a radius of ± 100 m from the sites.
[A] Missing data from June 5 to Sept. 30, 2013 estimated by correlation with Fort Nelson Environment Canada station.
[B] Missing data from April 27 to Sept. 30, 2012, August 18 to Sept. 30 2012 and October 1 to Sept. 30 2012-2013 were estimated by correlation with Fort Nelson Environment Canada station.
[C] 2011-2012 MAAT data acquire via a blended year average with MP 400 data from 2007 to 2014.
[D] MAAT presented are from the neighboring site MP 597, due to serious repeated logger malfunction.
[E] Missing data in 2010-2011 estimated through correlation with Watson Lake Environment Canada station and blended with reliable data from MP 681. Missing data in 2011-2012 and 2012-2013 estimated through correlation with MP 597 station (neighboring site) and blended with reliable data from MP 681
[F] Missing data from August 1 to August 18, 2011 estimated by correlation with Whitehorse Environment Canada station.
[G] Missing data in 2010-2011 and 2011-2012 estimated through correlation with Whitehorse Environment Canada station and blended with reliable data from MP 844

the other sites at this end of the transect with a MAAT of -1.9°C, MAGT of -0.2°C, relatively warm MAGST (2.2°C) and a small thermal and surface offset (total offset 1.7°C).

However, MP 341 had the smallest average number of SDD.

Like MP286, historical air photos indicate that there have been disturbances between 1964 and 2014 in this section of the corridor including alteration of the highway alignment at MP 178 and 341.These changes may have influenced permafrost extent and persistence. The permafrost bodies in the area are probably no longer ecosystem-protected.

#### *2.4.4.2 MP 400*

MP 400 is in a category of its own, with a permafrost patch size more than 10 times larger than the average patch size along the transect (Table 2.3). The site is located within Stone Mountain Provincial Park in Northern BC, and is situated in a mountainous environment. The landscape and environmental settings differ significantly from other field sites. The ERT inversion profiles were challenging to interpret at this site due to high resistivities extending in places to the base of the profile, and the presence of bedrock and dry sandy gravel. The permafrost surface area at MP 400 was based primarily on the ERT results and on the surface vegetation. The area where permafrost was identified consists of hummocky terrain, with a thick organic mat and sparse stunted spruce. The MAAT is relatively cold at -2.5°C and the average SDD stands at 7380 cm d which gives the second most negative MAAT to average SDD ratio along the transect.

#### *2.4.4.3 Central part of the transect*

The middle of the transect comprises MP 579, MP 597 and MP 681 (described above) which are located in the of sporadic discontinuous permafrost zone, close to the boundary with the extensive discontinuous zone. This portion of the transect is characterized by the largest permafrost bodies (Figure 2.14), the highest average SDD and the lowest MAATs (Table 2.3). The largest permafrost body is a peat plateau at MP 579. It is important to note that the climatic data at MP 579 were recorded about 40 m away from the peat plateau where permafrost is absent. Permafrost extent at MP 579 was linked to the vegetation cover and the drainage conditions. At MP 597, the permafrost patch was delimited by a gravelly sand slope, the roadside slope, a stream and a change in ground cover. MP 681 has the largest negative MAAT to average SDD ratio along the transect with MAAT at -3.3°C and average SDD value of 9250. Permafrost at MP 681 was mainly controlled by the drainage condition and the ground cover. Although MAATs were colder in this section than in the rest of the transect, average MAGT values were still very close to 0°C, varying from 0°C to -0.2°C. The permafrost resistivity boundary identified for this section (800 Ω m) was considerably higher than in the southern end of the transect.

#### *2.4.4.4 Northwestern end of the transect*

This end of the transect comprises the sites at MP 788, MP 825 (described above) and MP 844. Permafrost bodies were smaller than in the central part, MAAT varied between -1°C and -2°C and SDD were typically between 5000 and 8000 cm d. MP 788 and MP 825 had hummocky surfaces with a thick organic layer that showed signs of thermokarst and permafrost degradation. MP 844 shows ambiguous electrical

resistivity and MAGT results, as surficial materials were composed of dry gravel, and seasonal frost may have still been present at the time of the surveys. The MP 788 permafrost patch was delimited mainly by drainage and ground cover changes associated with a bog and a gravelly slope. The borehole at MP 788 had a temperature of -0.1°C at 3.75 m depth and large thermal and surface offsets (see Figure 2.7C and 2.8). MP 825 showed signs of permafrost degradation with permafrost patches, present randomly through the site. The permafrost resistivity boundary was set to 1200 Ω m for MP 844 due to the high resistivity values induced by the gravelly soil. The best estimate of the permafrost patch at MP 844 is a depression proximal to the highway, where the forest has lower density and the organic mat is relatively thick. The ERT profiles showed the deepest high resistivity results in comparison to the adjacent locations where high resistivity levels were continuous and restricted to the surficial layer of the ground. The alternative interpretation of the body of frozen ground at MP 844 would be thin, but extensive permafrost, with undetermined boundaries.

### 2.5 Functional analysis of variables

Correlation analyses among the functional variables (permafrost characteristics, location and climate) were undertaken using the 2010-2014 averages (see Table 2.3) and the average for each climate station at the ten field sites in 2010-2014 (see Table 2.5). The aim was to establish if significant correlations exist among the functional variables observed at the sites. The results are presented as correlation scatterplots and coefficients together with an indication of statistical significance at the $p = 0.05$ level.

### 2.5.1 Station averages of 2010-2014

Six of the 55 correlations among the functional variables were significant at the p = 0.05 level or better, but that between latitude and longitude was purely linked to the orientation of the transect and was therefore deemed unimportant (Figure 2.16 and Table 2.4). The relationships between MAGST and MAGT and the temperature offsets need to be carefully considered as the first two are used in the calculation of the offsets.

The $\log_{10}$ – $\log_{10}$ positive correlation between patch surface area and maximum patch thickness was strong ($R^2$ = 0.90, p = 0.000) (Figure 2.15). MAAT was negatively correlated with average SDD ($R^2$ = 0.46, p = 0.030), and was also negatively correlated with total offset ($R^2$ = 0.96, p = 0.000).

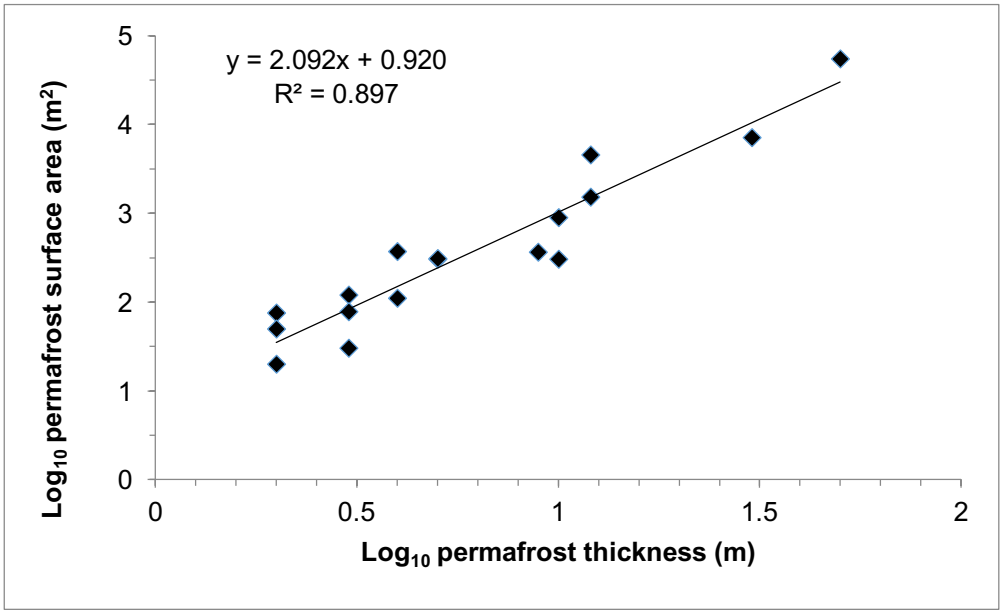


Figure 2.15: Scatterplot of $\text{Log}_{10}$ permafrost thickness vs. $\text{Log}_{10}$ permafrost surface area. All permafrost patches are included (n = 17). Linear regression equation is displayed next to the $R^2$. The black line represents the least squares linear regression line for this log-log relationship. Note: areas shown are based on ellipses and could be up to 27% higher if patch areas are rectangular.


Figure 2.16: Correlation matrix for site variables (2010-2014). Surface_Area represents the $Log_{10}$ of the maximum patch size at each site ($m^2$). Max_thickness represents the $Log_{10}$ of the maximum permafrost thickness at each site.

Table 2.4: Correlation matrix between functional variables (2010-2014). Values are in r (correlation coefficient). Significant variables are in bold font. Significance legend: p= 0.0001*** 0.001** 0.01* 0.05".

| | $Log_{10}$ Max Permafrost Surface Area | $Log_{10}$ Max Permafrost Thickness | Latitude | Longitude | MAAT | MAGST | MAGT | Average SDD | Average Surface Offset | Average Thermal Offset | Average Total Offset |
|---|---|---|---|---|---|---|---|---|---|---|---|
| $Log_{10}$ Max Permafrost Surface Area | | **0.95**$^{***}$ | 0.09 | 0.05 | -0.50 | -0.12 | 0.06 | 0.41 | 0.42 | 0.12 | 0.55 |
| $Log_{10}$ Max Permafrost Thickness | | | 0.21 | -0.12 | -0.46 | -0.17 | 0.19 | 0.32 | 0.32 | 0.22 | 0.53 |
| Latitude | | | | **-0.89**$^{**}$ | -0.05 | 0.20 | 0.26 | -0.01 | 0.23 | -0.14 | 0.12 |
| Longitude | | | | | -0.09 | -0.01 | -0.40 | 0.21 | 0.10 | -0.10 | -0.01 |
| MAAT | | | | | | 0.53 | 0.31 | **-0.68**$^{"}$ | -0.60 | -0.43 | **-0.98**$^{***}$ |
| MAGST | | | | | | | 0.16 | -0.23 | 0.37 | **-0.97**$^{***}$ | -0.51 |
| MAGT | | | | | | | | -0.14 | -0.20 | 0.09 | -0.12 |
| Average SDD | | | | | | | | | 0.50 | 0.17 | **0.68**$^{"}$ |
| Average Surface Offset | | | | | | | | | | -0.44 | 0.59 |
| Average Thermal Offset | | | | | | | | | | | 0.46 |
| Average Total Offset | | | | | | | | | | | |

MAGST was negatively correlated with the average thermal offset ($R^2$ = 0.94, p = 0.000) and average SDD was positively correlated with the average total offset ($R^2$ = 0.46, p = 0.032).

### 2.5.2 All climate stations 2010-2014

A larger sample (n=30) was established by calculating functional variables and permafrost thickness for each of the site stations (Table 2.5). This was done in order to increase the potential of finding significant trends along the transect.

Eleven of the 21 correlations among functional variable at each climate stations were significant at the p = 0.05 level or better. However, the significance of the correlation between $Log_{10}$ permafrost thickness and MAGT (at TTOP) should be disregarded because its distribution does not follow the normality requirement and is probably subject to autocorrelation (Table 2.6 and Figure 2.17). Average SDD is negatively correlated with MAGST ($R^2$ = 0.16, p = 0.030), positively correlated with average thermal offset ($R^2$ = 0.17, p = 0.023) and positively correlated with average total offset ($R^2$ = 0.33, p = 0.001).

MAGST is positively correlated with average surface offset ($R^2$ = 0.29, p = 0.002) and negatively correlated with the average thermal offset ($R^2$ = 0.50, p = 0.000). MAGT is positively correlated with average thermal offset ($R^2$= 0.18, p= 0.020) and positively correlated with average offset ($R^2$= 0.21, p= 0.010). Average surface offset is negatively correlated with average thermal offset ($R^2$= 0.22, p= 0.009) and positively correlated with average total offset ($R^2$= 0.34, p= 0.001). Average thermal offset is positively correlated with total offset ($R^2$= 0.20, p= 0.013).

Table 2.5: Table of all functional variables calculated for 2010-2014 for each of the three climatic stations at the ten field sites. Sites where permafrost thickness could not be inferred due to the limited ERT penetration depth have been marked >25.

| Site | Station | Permafrost thickness (m) | SDD (cm d) | MAGST (°C) | MAGT (°C) | Surface Offset (°C) | Thermal Offset (°C) | Total Offset (°C) |
|---|---|---|---|---|---|---|---|---|
| **MP 178** | Secondary 1 | 0 | 8440 | 1.2 | 0.8 | 3.3 | -0.4 | 2.9 |
| | Main | 0 | 9470 | 0.2 | -0.1 | 2.3 | -0.3 | 2.0 |
| | Secondary 2 | 1 | 7120 | 0.7 | -0.1 | 2.8 | -0.8 | 2.0 |
| **MP 286** | Secondary 1 | 2 | 6590 | 1.4 | 0.1 | 2.3 | -1.3 | 1.0 |
| | Main | 0 | 8860 | 2.1 | 2.1 | 3.0 | 0.0 | 3.0 |
| | Secondary 2 | 2.5 | 8810 | 2.4 | -0.2 | 3.3 | -2.6 | 0.7 |
| **MP 341** | Secondary 1 | 1 | 6400 | 2.1 | 0.1 | 4.0 | -2.1 | 2.0 |
| | Main | 0 | 6340 | 2.2 | -0.1 | 4.1 | -2.3 | 1.8 |
| | Secondary 2 | 2 | 4990 | 2.2 | -0.2 | 4.1 | -2.4 | 1.7 |
| **MP 400** | Secondary 1 | >25 | 7060 | 2.7 | 0.1 | 5.2 | -2.6 | 2.6 |
| | Main | 12 | 7830 | 1.4 | 0.1 | 3.9 | -1.3 | 2.6 |
| | Secondary 2 | 12 | 7240 | 1.2 | -0.0 | 3.7 | -1.2 | 2.5 |
| **MP 579** | Secondary 1 | 0 | 9000 | 1.8 | 0.4 | 4.3 | -1.4 | 2.9 |
| | Main | 0 | 9220 | 0.6 | 0.5 | 3.1 | -0.1 | 3.0 |
| | Secondary 2 | 0 | 10030 | 2.1 | 0.1 | 4.6 | -2.0 | 2.6 |
| **MP 597** | Secondary 1 | 5 | 7990 | 2.2 | -0.1 | 4.7 | -2.2 | 2.4 |
| | Main | >25 | 9080 | 1.2 | 0.2 | 3.7 | -1.0 | 2.7 |
| | Secondary 2 | 7 | 8410 | 1.9 | -0.3 | 4.4 | -2.2 | 2.3 |
| **MP 681** | Secondary 1 | 6 | 9690 | 1.6 | 0 | 4.9 | -1.6 | 3.3 |
| | Main | 6 | 9730 | 0.5 | -0.3 | 3.8 | -0.8 | 3.0 |
| | Secondary 2 | 0 | 8340 | 2.1 | 0.6 | 5.4 | -1.5 | 3.9 |
| **MP 788** | Secondary 1 | 0 | 5690 | 3.5 | 1.3 | 4.6 | -2.2 | 2.4 |
| | Main | 9 | 4820 | 2.4 | -0.1 | 3.5 | -2.5 | 1.0 |
| | Secondary 2 | 7 | 7730 | 2.3 | -0.1 | 3.4 | -2.4 | 1.0 |
| **MP 825** | Secondary 1 | 0 | 5860 | 2.9 | 1.6 | 3.9 | -1.3 | 2.6 |
| | Main | 5 | 5030 | 1.5 | -0.2 | 2.5 | -1.7 | 0.8 |
| | Secondary 2 | 3 | 5030 | 1.3 | -0.3 | 2.3 | -1.6 | 0.7 |
| **MP 844** | Secondary 1 | 0 | 8350 | 1.7 | 0.2 | 3.7 | -1.5 | 2.2 |
| | Main | 6 | 8170 | 1.7 | 0.2 | 3.7 | -1.5 | 2.2 |
| | Secondary 2 | 0 | 7150 | 1.3 | 0.6 | 3.3 | -0.7 | 2.6 |

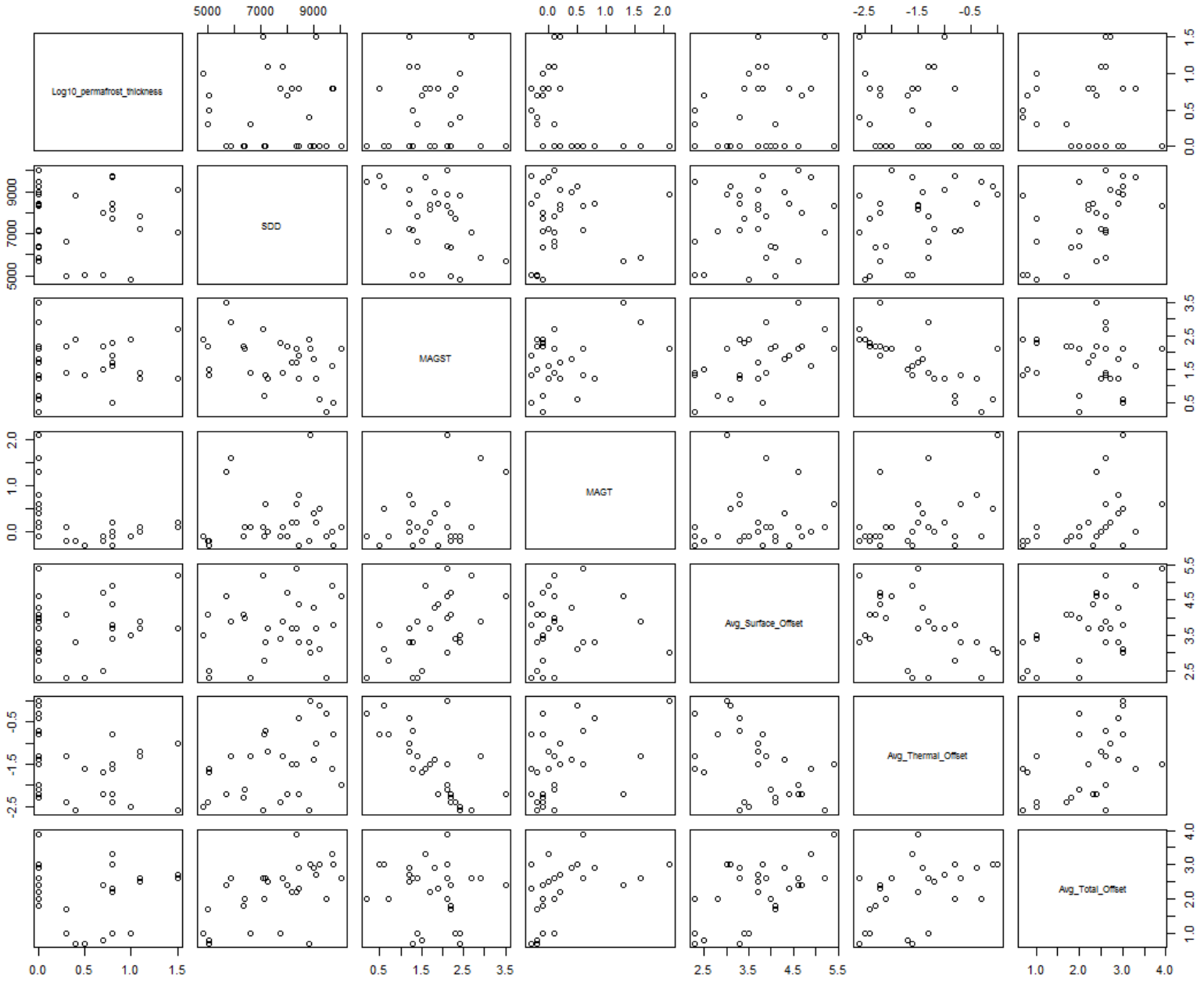


Figure 2.17: Correlation matrix for station variables (2010-2014). Log10_permafrost_thickness represents the $Log_{10}$ of the permafrost thickness inferred for each station from the ERT profiles.

Table 2.6: Correlation coefficient matrix (r values) between station variables (2010-2014). Significant variables are in bold font. Significance legend: p= 0.0001*** 0.001** 0.01* 0.05".

| | $Log_{10}$ permafrost thickness | SDD | MAGST | MAGT | Surface Offset | Thermal Offset | Total Offset |
|---|---|---|---|---|---|---|---|
| $Log_{10}$ permafrost thickness | | -0.02 | -0.01 | -0.42[a] | 0.17 | -0.30 | -0.11 |
| SDD | | | **-0.40**" | 0.04 | 0.19 | **0.41**" | **0.57**** |
| MAGST | | | | 0.34 | **0.54**** | **-0.71***** | -0.10 |
| MAGT | | | | | 0.07 | **0.42**" | **0.46*** |
| Surface Offset | | | | | | **-0.47*** | **0.58**** |
| Thermal Offset | | | | | | | **0.45*** |
| Total Offset | | | | | | | |

[a] Note: Relationship has a high enough correlation coefficient to reach the p = 0.05 significance level but does not meet distribution requirements for valid statistical testing (see Figure 2.16).

## 2.6 Discussion

### 2.6.1 Functional relationship between variables and current state of permafrost

The only significant correlation observed with regards to permafrost body dimensions was between $\log_{10}$ permafrost patch area and $\log_{10}$ maximum thickness which were strongly positively correlated (Figure 2.16).

Extrapolating from this relation, a permafrost body 100 m thick, which might be near the boundary between the extensive discontinuous and continuous zones, would have an area of 0.285 $km^2$. Permafrost 500 m thick, which represents conditions in parts of the Canadian Arctic Archipelago (see Heginbottom et al., 1995) and well within the continuous permafrost zone, is predicted to have an area of approximately 13.5 $km^2$. This suggests that the relationship does not hold beyond the thicknesses measured along the transect and that the line may flatten out near the northern margin of extensive discontinuous permafrost. The relationship may also be affected by spatial variation in geothermal heat flow expressed as differing geothermal gradients. Geothermal heat flow is known to vary from <50 to >100 $mW/m^2$ and geothermal gradients range from 20 to 40 mK/m in the region traversed by the study transect (Figures 5.2 and 5.4 in Grasby et al. 2012). However, available maps are too coarse to determine if the sites themselves are affected by this range.

None of the air and ground climate variables was significantly correlated with the permafrost surface area and permafrost thickness, which was unexpected.

MAAT was significantly negatively correlated with average SDD showing that the coldest part of the transect also experienced the most snow. MAAT was negatively correlated with the total offset which is logical considering the very narrow range of

TTOP temperatures. A significant relationship was expected between MAAT and permafrost patch size, but was not present.

MAGST was negatively correlated with the thermal offset for the sites as a whole and for the individual stations. Under equilibrium conditions, the thermal offset depends on the ratio of frozen to unfrozen thermal conductivity of the active layer materials so in principle, there is no reason why there should be a correlation with MAGST. However, this result would be expected for locations with permafrost bodies which are out of equilibrium with the current climate, as the apparent thermal offset is then a product of permafrost persistence, and not the cause. MAGST was also positively correlated to surface offset for the individual stations, a logical relationship given the limited range in MAAT and the inclusion of stations with and without permafrost. A significant relationship between MAGST and total offset was expected, given the former's correlation with both surface and thermal offset, but was not present.

MAGT was positively correlated with thermal offset for the station data, which was expected because ground temperatures rise as the thermal offset gets smaller (less negative). MAGT was also positively correlated with total offset for the station data, but not with surface offset. A significant relationship between MAGT and permafrost thickness was expected, but was not present for site data. The correlation for the station data was higher but the distribution of data did not permit statistical testing.

Average SDD was significantly negatively correlated with MAGST for station data. Given that higher amounts of snow normally relate to warmer ground

temperatures a positive correlation would be expected. This result apparently underlines that some of the highest SDD values are found in the coldest parts of the transect. Average SDD was significantly positively correlated with the thermal offset (i.e. greater snow is associated with a less negative thermal offset) for the station data. This likely reflects the influence of SDD on MAGST and the relationship between MAAT and SDD. Average SDD was significantly positively correlated with total offset for both site and station data. This was expected given its influence on MAGST and its spatial relationship with MAAT along the transect. A significant relationship between SDD and the surface offset was expected given its importance in energy transfer between the air and ground surface during winter months, but was not present in either the site or station datasets.

The surface offset was negatively correlated with the thermal offset in the station data. Theoretically, these are independent variables under equilibrium conditions, but the data show that the bigger the surface offset, the more negative the thermal offset. This probably relates to the presence of permafrost anchoring the ground temperature below 0°C which means that a large thermal offset corresponds to a high MAGST and thus a large surface offset given limited MAAT range. Surface offset in the station dataset was also positively correlated with total offset while the latter was negatively correlated with thermal offset. These results would be expected based on the derivation of the three parameters.

Permafrost patch boundaries at individual sites were influenced negatively or positively by vegetation (e.g. by changes in the organic mat), topography (e.g. by the presence of surface depressions), surficial material (e.g. by the presence of gravel) and

drainage (e.g. by the presence of flowing or standing water). These results conform to observations made in many previous studies (e.g. Brown, 1970) and so were expected.

The field observations and the analyses of functional relationships lead to an important question: to what degree is the permafrost along the transect in equilibrium? There are three possible answers to this question: (1) permafrost is in quasi-equilibrium at all sites; (2) permafrost is in a transient (out of equilibrium) state at all sites; and (3) sites along the transect can be either in quasi-equilibrium or in a transient state depending on their local conditions. The permafrost found along the transect most likely dates from the Little Ice Age (Halsey et al., 1995; Heginbottom et al., 1995; Zhang et al., 2006) but it may not have been formed simultaneously at all sites nor reached the same temperatures by the start of the 20$^{th}$ Century warming and the thickest permafrost patches, such as MP 400, might have formed prior to the Little Ice Age. Sites therefore have different starting points, which would create a heterogeneous distribution of permafrost change rates under a warming climate (Halsey et al. 1995, Vitt et al. 2000; Zhang et al., 2005; Zhang et al., 2006). Each specific location would have then reached its current climatic conditions according to different time-scales and these would have influenced heterogeneously the current thermal state at each individual site (Zhang et al., 2005; Zhang et al., 2006).

Lewkowicz et al. (2016) calculated the changes in average apparent resistivity for the permanent electrode arrays at the ten sites examined in this thesis for the period 2010 to 2015. Most showed a distinct downward trend in apparent resistivities indicating progressive change from frozen to unfrozen soil water. Tilted and fallen trees are present at MP 825 and MP 788, a talik was present at MP 825 (although it refroze in

2014-2015) and aerial photos suggest that there might have been enlargement of water bodies adjacent to MP 178, MP 579, MP 681 and MP 788 but this is hard to assess conclusively due to the low quality of the images. The absence of significant relationships between permafrost patch size (area and thickness) and the air and ground climatic variables suggests a time dependent, asynchronous evolution of permafrost and climatic conditions at the sites. For example, the low variability in MAGT (-0.3°C to 0.2°C) in contrast to that of MAAT (-0.9°C to -3.3°C) suggests that changes in MAGT have stalled at the point of thaw which may have been reached at different times at the individual study sites. The negative correlation between MAGST and the thermal offset indicates that the size of the latter is largely being controlled by the ground surface temperature as the persistence of permafrost anchors temperatures within the ground close to 0°C. The observed MAGTs suggest that the positive net ground heat flux is being used as latent heat as unfrozen moisture contents gradually increase (James et al., 2013). The evidence, therefore, is that permafrost is degrading at the study sites. Some sites may be less advanced in terms of degradation, with only warming accompanied by internal changes in unfrozen moisture content, while others have changed in terms of area and form.

The absence of significant correlations between the functional variables and permafrost patch size indicates that it would be difficult or impossible to use climatic variables to accurately estimate permafrost characteristics patch size near the southern margin of the discontinuous zone. Upscaling assuming equilibrium conditions would not produce an accurate representation of the present permafrost distribution, because all the evidence is that permafrost is degrading along the transect. The use of a transient

permafrost model would be necessary in order to adequately incorporate the influence of time on the current permafrost distribution (Riseborough et al., 2008; Zhang, 2013; Zhang et al., 2003; Zhang et al., 2006)

### 2.6.2 Conceptual model of permafrost patch size distribution and evolution

The observation made during this research were synthesized as a conceptual model that aims to explain the permafrost patch size variability along the transect and the evolution of permafrost bodies at the field sites. The model was developed in the context of the literature, but it is anchored with observations from the study transect and may not apply outside this region.

The conceptual model is founded on three key assumptions. First, the permafrost bodies are in a transient state relative to their local environmental conditions. This implies that the local ecosystem protection (Shur and Jorgenson, 2007) is no longer sufficient to conserve permafrost in the face of a warming climate, and that the permafrost will degrade entirely over the long-term, even if the climate were to cease warming. Second, it is assumed that drainage acts as the main positive feedback for permafrost degradation at the sites (Jorgenson et al., 2010). Thaw of permafrost causes surface settlement which promotes ponding of water in low-lying areas, thus accelerating the thermal degradation of permafrost at those locations (Jorgenson et al., 2010). Drainage has the potential to create new degradation fronts on a permafrost body, so that its degradation is not limited to the boundaries of the permafrost patch (Jorgenson et al., 2010). The third assumption is that permafrost patches in the isolated and sporadic discontinuous zones experience three-dimensional degradation, with vertical as well as lateral thaw (McClymont et al., 2013).

The conceptual model comprises six evolutionary stages (Figure 2.18).

Stage 1 represents a permafrost body in quasi-equilibrium with its local environment. The permafrost body occupies the entire area favourable to permafrost (e.g.: a peat plateau) and shows no signs of degradation. None of the sites along the transect appear to be a stage 1 permafrost body.

In stage 2, the permafrost body has retained all or most of its mass, but is no longer in equilibrium with the environment. For example, it may be thawing internally with a slow, progressive increase in unfrozen moisture as ground temperatures approach 0°C, or it may start to be subject to lateral thaw. Examples of this stage are MP 681 (Figure 2.19A) and MP 400, both of which have a unitary permafrost body that occupies an area of homogeneous environmental conditions with boundaries associated with local controls that prevent permafrost presence. The progressive

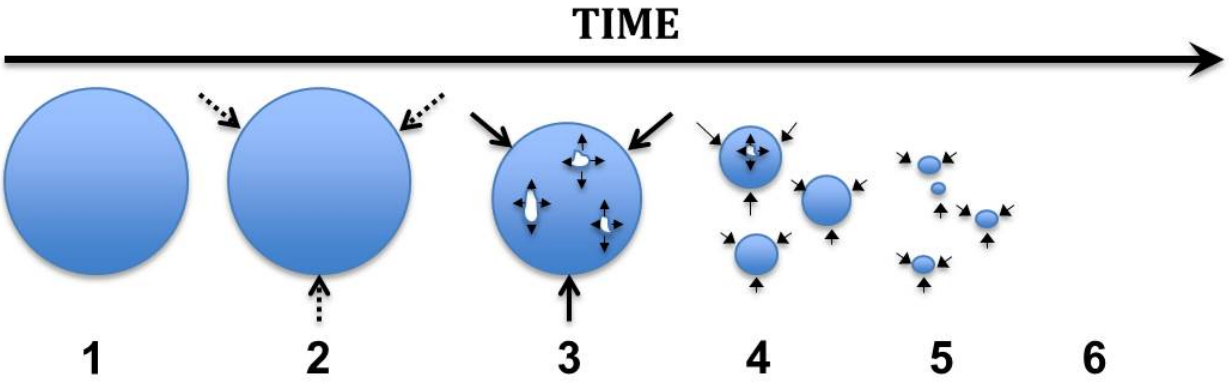


Figure 2.18. Conceptual model of permafrost patch size and evolution from a unitary permafrost body in quasi-equilibrium with the local environment through to complete degradation of permafrost Shaded circles represent permafrost bodies. Dashed black arrows represent lateral degradation and/or internal degradation. Black arrows represent direction of degradation. White shapes represent areas of thaw generated by drainage conditions at the site. Arrows size does not reflect the magnitude of the degradation.

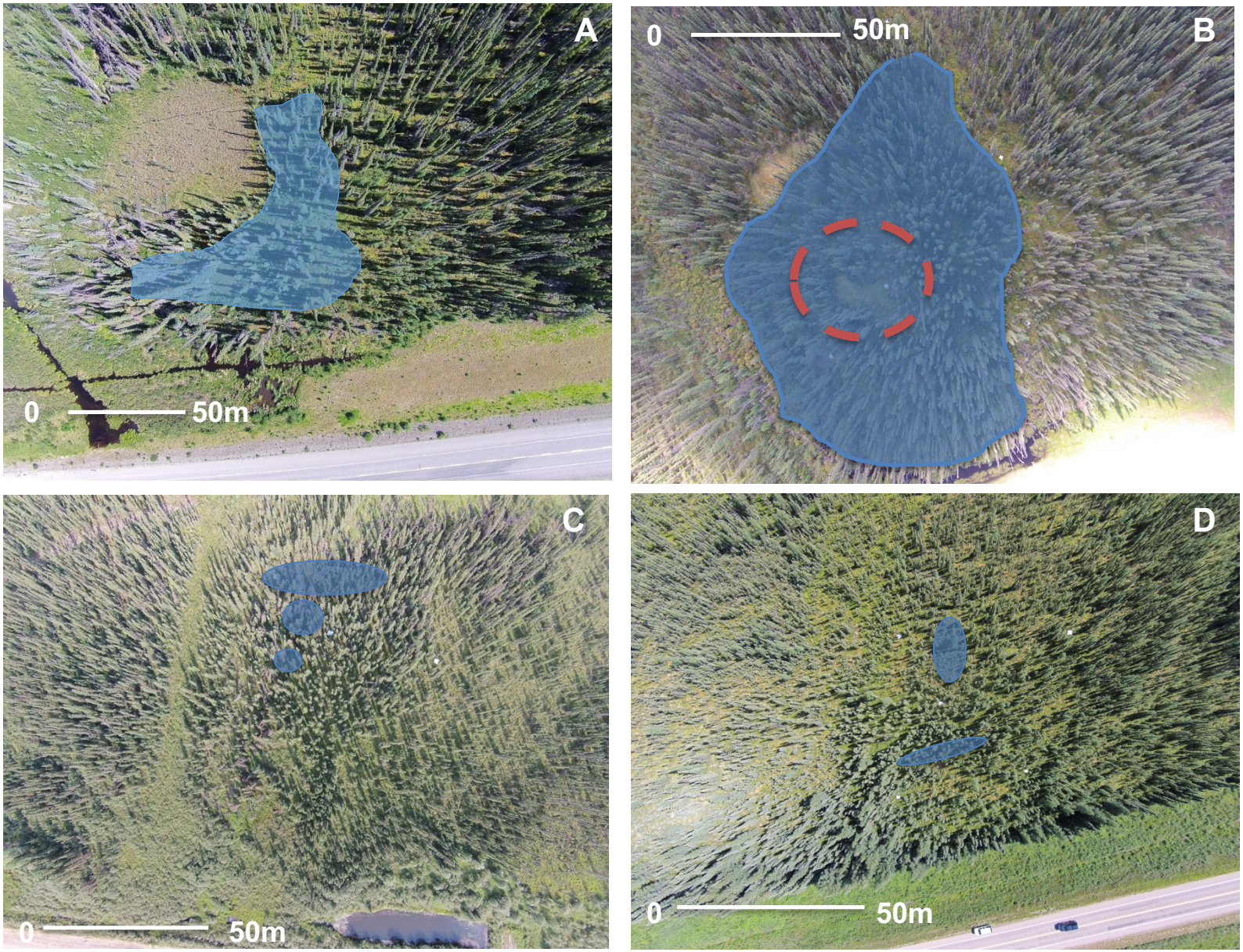


Figure 2.19: Site examples of degradation stages in the conceptual model (Figure 2.18). A - Stage 2: MP 681; B - Stage 3: MP 597; C - Stage 4: MP 178; D - Stage 5: MP 341 permafrost patch. Shaded areas represent permafrost patch extent. Dashed red circle represents an area of standing water. All aerial images from 2014. Scale is approximate.

decrease in average apparent resistivities at the sites from 2010 to 2015 (Lewkowicz et al., 2016) indicates that unfrozen moisture contents are increasing.

Stage 3 represents a permafrost body subject to three-dimensional thaw. This stage is characterized by the beginning of positive feedback from the local drainage conditions enhanced by the developing microtopography. New degradation fronts are then formed on the permafrost body. This stage encompasses the majority of the sites in the central (northeast) of the transect with MP 579, MP 597 and MP 788 falling into this category. For example, the thick permafrost patch at MP 579 is situated on a peat plateau that is constrained by the surrounding standing water (Figure 2.19B). However, a new degradation front has started in the middle of the patch due to drainage conditions.

Stage 4 is marked by the breakdown of the initial unitary permafrost body into several smaller patches of permafrost. Changes in drainage can potentially start new degradation fronts on the remaining permafrost patches. In this stage, the remaining permafrost bodies are still relatively thick and close to each other, distinguishing the stage from its successors. MP 178 and MP 825 are categorized as stage 4 sites due to the size of the permafrost patches, their thickness, spatial distribution and evidence of degradation on the remaining bodies (Figure 2.19C; Appendices A and H).

Stage 5 is the final stage in which permafrost patches are still present. The remaining permafrost bodies are small, shallow and especially vulnerable to disturbance. MP 286, MP 341 and MP 844 are examples of this stage, with permafrost patches persisting only because of lags between current climate conditions and

environmental settings and the reaction of the ground (Figure 2.19D).

Stage 6 represents the complete disappearance of permafrost patches at locations where they could be found in the past. James et al. (2013) showed that this had occurred at almost half of the permafrost sites along the transect examined by Roger Brown in 1964 (Brown, 1967).

The break-down of a single permafrost body into smaller permafrost patches has also been observed on peat plateaus near Fort Simpson N.W.T (Quinton et al., 2009). There, the peat plateau was disaggregated by water causing thermal degradation. In northern Québec, the degradation of a lithalsa was initiated following the loss of ground cover and was enhanced by standing water (Beck et al., 2015; Calmels et al., 2008). The rapid degradation of palsas in peatland, influenced by adjacent flowing water, change in precipitation and fluctuating water levels, was observed in northern Québec and described as a one-way, self-organizing process (Thibault and Payette, 2009; Vallée and Payette, 2007; Payette et al., 2004). No other examples are known in the literature that deal with progressive change in permafrost patch size. The conceptual model of Brown (1970) (Figure 1.1) provides a static cross-sectional view of the discontinuous permafrost zones and was produced at a time when climate was stable or had cooled for several decades. In comparison, Figure 2.19 recognizes that climate warming represents a crucial factor that is resulting in changes to permafrost distribution and contiguity at a multi-decadal time scale. Brown's (1970) figure needs to be reconceptualized in terms of patch size and thickness (which have been shown to be proportional), in the vertical location of permafrost bodies (no isolated bodies at depth), and in the thickness of the active layer (generally less than 1 m).

## 2.7 Conclusions

The following conclusions were reached from the geophysical surveys, aerial image interpretations, climate data analyses and statistical analyses.

(1) Permafrost patches examined at the ten study sites varied in area from 10 to 50 000 $m^2$. There was a strong log-log relationship between patch area and permafrost thickness.

(2) There were no statistically significant relationships between climatic parameters and permafrost patch area or thickness. The absence of links indicates that the current permafrost conditions are lagged relative to climate, probably by varying amounts of time.

(3) The boundaries of permafrost patches related to drainage, microtopography, soils, ground cover and disturbances. These factors have long been recognized as controls on permafrost distribution in areas of discontinuous permafrost.

(4) Observations suggest that the permafrost along the transect is in the process of degrading. However, there were geographic differences among the sites, which can be divided into three main groups: the southeast sites have numerous small permafrost bodies higher MAATs and small total offsets; the central (northeast) sites have larger, unitary permafrost bodies, the largest SDD values, lower MAATs and large total offsets; the northwest sites have relatively moderate MAATs, average to small total offsets and numerous but moderately-sized permafrost bodies.

(5) A conceptual model of permafrost patch size evolution through time was

proposed for the isolated patches and sporadic discontinuous permafrost zones traversed by the study transect. It portrays progressive changes to a single body of quasi-equilibrium permafrost that is subject to climate warming. The permafrost body gradually warms, then breaks down spatially with new degradation fronts created by local standing or running water, and finally degrades entirely.

(6) Permafrost patch size along the transect appears to be linked to the original extent of the permafrost body under quasi-equilibrium conditions, local environmental controls on permafrost boundaries, and the time since the permafrost became unsustainable due to insufficient ecosystem protection under a warming climate. This highlights the need to take time into consideration for regional modelling in the discontinuous zones, and hence the importance of using transient rather than equilibrium models to characterize permafrost in the region.

# Chapter 3: DISCUSSION AND CONCLUSIONS

## 3.1 Discussion

### 3.1.1 Research limitations

Since the results were discussed in section 2.6, this part of the thesis is focused on the limitation of the research and future suggested work.

A number of factors represented limitations to the research. The main challenge in the computation of the transect statistics was the small sample size. In the event that certain elements of the sample were biased, the true picture of the conditions observed along the transect may have been missed.

Ambiguous results sometimes caused complex interpretations of the ERT inversion profiles, but field observations of the local environment at the sites helped in understanding the results. ERT is a labour-intensive method that requires significant electrical power which can prove challenging in the context of fieldwork in remote areas. A maximum of three ERT transects were undertaken at each site in order to respect the time schedule and the energy demands of the equipment. Therefore, the estimated permafrost patch surface area is based on elliptical shapes, which could have resulted in an unknown degree of error in the patch size value. Frost-probing results could have also differed depending on the force administered by the operator on the frost probe and is also limited by the probe length and the soil type.

With annual variability of the active layer thickness, equipment malfunction, human errors and impact of the natural environment (e.g. animals or water damaging the equipment), temperature data sets were incomplete. This issue was addressed by infilling data series through correlation with a neighbouring station, blended year

calculations, creation of averages when possible and by careful screening the data used. An additional problem at MP 579 was that air and ground climate data were from the original ERT array, whereas the permafrost patch was located on an adjacent peat plateau. Therefore, the ground temperature data do not properly represent conditions where permafrost is present at this site.

The potential influence of the snowpack on ground temperatures was represented using Snow Depth Days (cm d) which incorporates both depth and duration. A comparison with maximum snow depth, however, showed a high correlation between the two indices (Appendix N). Therefore, maximum snow depth could also have been used. Neither produced significant correlations with the permafrost patch parameters.

The use of the UAV was challenging in certain circumstances. High winds, rain, trees and poor visibility prevented or complicated its operation. The UAV's software calculated elevation relative to the take-off point which was often on higher ground in order to have an uncompelled view. Therefore the altitude shown was not the true distance from the ground, resulting in an approximate and variable scale across the image.

### 3.1.2 Future work

Several possibilities exist for research to improve our understanding of permafrost patch size and dynamics in the isolated patches and sporadic discontinuous permafrost zones.

Increasing the sample size by investigating more sites in the region, would

improve the chances of obtaining statistically significant correlations and reduce the possible influence of bias from outliers in the current small sample.

An important question that was not addressed in this this research concerned spacing between sites with permafrost patches. The conceptual model follows the break-down of a unitary patch, but does not include how far away the next patch is to be found. This is a significant topic for validating our present conceptualization of permafrost distribution in space (Brown, 1970). This might be possible using airborne electromagnetic surveys (Minsley et al., 2012; Pastick et al., 2013) or as new tools are developed, with satellite-based remote sensing data (Zhang, 2013).

Three-dimensional thermal modeling of permafrost evolution through time would be the next logical step to validate the conceptual model advanced in this thesis (McClymont et al, 2013). Multiple boreholes equipped with thermistor cables would be needed in order to validate model predictions. Intensive surveying of sites using multiple ERT transects to obtain high resolution and three-dimensional ERT surveys could potentially generate important information on the local controls influencing permafrost patch size (Loke, 2011). A more physically rigorous model of the development of patch size through time could then be developed and applied to the permafrost in the study area.

The creation of high-resolution DEMs (Bemis et al., 2014), to better understand the local drainage conditions and the establishment of a rigorous moisture content monitoring plan at multiple points of the sites would also help understand how the drainage affects permafrost (Jorgenson et al., 2010; Quinton et al. 2009).

The installation of a control station at the study sites in a different environmental setting than where permafrost is present could provide useful information on local controls and spatial variability, especially where the permafrost bodies are large and occupy the entire area that is favourable for permafrost.

### 3.2 Summary and conclusions

This research aimed to initiate an evaluation of permafrost patch size in the sporadic discontinuous and isolated patches permafrost zones of northern BC and southern Yukon. The context of the project was the ongoing challenge of upscaling from point measurements (such as ground temperature measured in boreholes) to regional permafrost models. The primary objective was to improve our understanding of spatial trends in permafrost patch size and the variables that influence it. In addition, the goal was to compare results with Roger Brown's (1970) conceptual model of permafrost thickness and continuity.

A total of 28 ERT profiles were obtained at ten field sites located between Fort St. John and Whitehorse. These sites were selected and previously examined and equipped with climate stations and permanent ERT arrays (Brown, 1970; James et al., 2010; Lewkowicz et al., 2011; Miceli, 2012). Four years of climate data (2010-2014) were compiled, and correlation analyses were performed among the derived functional variables. An unmanned air vehicle was used to obtain near vertical aerial photos in 2014 and these were compared to 1964 air photos of the field sites.

Following these analyses, the following conclusions were reached:

(1) Permafrost patches examined at the ten study sites varied in area from 10 to

50 000 $m^2$. There was a strong log-log relationship between patch area and permafrost thickness.

(2) There were no statistically significant relationships between climatic parameters and permafrost patch area or thickness. The absence of links indicates that the current permafrost conditions are lagged relative to climate, probably by varying amounts of time.

(3) The boundaries of permafrost patches related to drainage, microtopography, soils, ground cover and disturbances. These factors have long been recognized as controls on permafrost distribution in areas of discontinuous permafrost.

(4) Observations suggest that the permafrost along the transect is in the process of degrading. However, there were geographic differences among the sites, which can be divided into three main groups: the southeast sites have numerous small permafrost bodies higher MAATs and small total offsets; the central (northeast) sites have larger, unitary permafrost bodies, the largest SDD values, lower MAATs and large total offsets; the northwest sites have relatively moderate MAATs, average to small total offsets and numerous but moderately-sized permafrost bodies.

(5) A conceptual model of permafrost patch size evolution through time was proposed for the isolated patches and sporadic discontinuous permafrost zones traversed by the study transect. It portrays the progressive changes to a single body of quasi-equilibrium permafrost that is subject to climate warming. The permafrost body gradually warms, then breaks down spatially with new degradation fronts created by local standing or running water, and finally degrades entirely.

(6) Permafrost patch size along the transect appears to be linked to the original extent of the permafrost body under quasi-equilibrium conditions, local environmental controls on permafrost boundaries, and the time since the permafrost became unsustainable due to insufficient ecosystem protection under a warming climate. This highlights the need to take time into consideration for regional modelling in the discontinuous zones, and hence the need to use transient rather than equilibrium models to characterize permafrost in the region.

Spatial trends in permafrost patch spacing were not addressed in this thesis and remain an important gap in our collective understanding of permafrost distribution in the isolated patches and sporadic discontinuous permafrost zones. Airborne electromagnetic surveys could be used to address this question. Thermal modelling of permafrost patches along the transect would also be an important step forward to understanding permafrost evolution. Therefore, multiple future research possibilities exist to further enhance our understanding of permafrost patch distribution and evolution in the study area.

# REFERENCES

AMAP (2012*) Arctic Climate Issue 2011: Change in Arctic Snow, Water, Ice and Permafrost: SWIPA 2011 Overview Report*. Arctic Monitoring and Assessment Programme (AMAP), Oslo, xi + 97 pp.

Bemis S.P., S. Micklethwaite et al. ((2014) Ground-based and UAV-based photogrammetry: a multi-scale, high-resolution mapping tool for structural geology and paleoseismology. *Journal of Structural Geology* **69**: 163-178.

Bindoff, N.L., P.A. Stott et al. (2013) Detection and Attribution of Climate Change: from Global to Regional. In: Climate Change 2013: *The Physical Science Basis. Contribution of Working Group I to the Fifth Assessment Report of the Intergovernmental Panel on Climate Change* [Stocker, T.F., D. Qin, G.-K. Plattner, M. Tignor, S.K. Allen, J. Boschung, A. Nauels, Y. Xia, V. Bex and P.M. Midgley (eds.)]. Cambridge University Press, Cambridge, United Kingdom and New York, NY, USA.

Brown, R.J.E. (1967*) Permafrost Investigations in British Columbia and Yukon Territory*. Ottawa: National Research Council of Canada, Division of Building Research: 55.

Brown, R. J. E. (1970) *Permafrost in Canada: Its Influence on Northern Development*. University of Toronto Press, Toronto: 234.

Brown, R.J.E. and T.L. Péwé (1973*) Distribution of permafrost in North America and its relationship to the environment: A review, 1963–1973*. In Proceedings of the 2nd International Conference on Permafrost, Yakutsk, USSR, North American contribution. National Academy of Science, Washington, DC; 71–100.

Brown, J., O.J. Ferrians, et al. (2001*) Circum-Arctic map of permafrost and ground ice conditions*. Boulder, CO: National Snow and Ice Data Center. Digital media.

Burn, C. R. (1998) The response (1958–1997) of permafrost and near-surface ground temperatures to forest fire, Takhini River valley, southern Yukon Territory. *Canadian Journal of Earth Sciences*. **35**: 184–199.

Calmels F., M. Allard and G. Delisle (2008) Development and decay of lithalsa in Northern Québec: A geomorphological history. *Geomorphology* **97**: 287-299.

Cheng G. (2004) Influences of local factors on permafrost occurrence and their implications of Quinghai-Xizang Railway design. *Science in China Series D: Earth Sciences* **47**(8): 704-709.

Church M. and J., M. Ryder (2010) *Chapter 2: Physiography of British Columbia*. Pike, R.G., T.E. Redding, R.D. Moore, R.D. Winker and K.D. Bladon (editors). 2010. Compendium of forest hydrology and geomorphology in British Columbia. B.C. Min. For. Range, For. Sci. Prog., Victoria, B.C. and FORREX Forum for Research and Extension in Natural Resources, Kamloops, B.C. Land Manag. Handb. 66. www.for.gov.bc.ca/hfd/pubs/Docs/Lmh/Lmh66.htm

DJI (2014) Phantom 2 Vision+: Retrieved (05/28/14) http://www.dji.com/product/phantom-2-vision-plus/spec

Duk-Rodkin, A. (2004) *Glacial History, In: Ecoregions of the Yukon Territory: Biophysical properties of Yukon landscapes*, C.A.S. Smith, J.C. Meikle and C.F. Roots (eds.), Agriculture and Agri-Food Canada, PARC Technical Bulletin No. 04-01, Summerland, British Columbia, p. 24-26.".

Environment Canada (2016a): Retrieved (01/03/16), *Protected Areas, by Ecological Region*. https://www.ec.gc.ca/indicateurs-indicators/default.asp?lang=en&n=A1570B00

Environment Canada (2016b): Retrieved (01/03/16), *Canadian Climate Data*. http://climate.weather.gc.ca/advanceSearch/searchHistoricData_e.html#stnNameTab.

Fisher, D., E. Osterberg et al. (2008) The Mt Logan Holocene-Late Wisconsinan isotope record: tropical Pacific-Yukon connections. *The Holocene* **18**(5): 667-677.

French, H. M. (2007) *The periglacial environment*. Chichester, England; Hoboken, NJ, John Wiley and Sons: 478.

Gajewski K., J., Bunbury et al. (2014) Paleoenvironmental studies in southwestern Yukon. *Arctic* **67**(1): 58-70.

Goodrich, L. E. (1982) The influence of snow cover on the ground thermal regime. *Canadian Geotechnical journal* **19**: 421-432.

Grasby, S.E., D.M. Allen, et al. (2011) Geothermal Energy Resource Potential of Canada, *Geological Survey of Canada*, Open File **6914**, 322.

Halsey, L.A., D.H. Vitt and C. Zoltai (1995) Disequilibrium response of permafrost in boreal continental western Canada to climate change. *Climate Change* **30**(1): 57-73.

Hartmann, D.L., A.M.G. Klein Tank et al. (2013) Observations: Atmosphere and Surface. In: Climate Change 2013: *The Physical Science Basis. Contribution of Working Group I to the Fifth Assessment Report of the Intergovernmental Panel on Climate Change* [Stocker, T.F., D. Qin, G.-K. Plattner, M. Tignor, S.K. Allen, J. Boschung, A. Nauels, Y. Xia, V. Bex and P.M. Midgley (eds.)]. Cambridge University Press, Cambridge, United Kingdom and New York, NY, USA.

Hauck, C. (2002) Frozen ground monitoring using DC resistivity tomography. *Geophysical Research Letter* **29**(21): 2016.

Hauck, C. and C. Kneisel (2008) *Applied Geophysics in Periglacial Environments*, Cambridge University Press: 240.

Hauck, C., D.V. Mühll, et al. (2003) Using DC resistivity tomography to detect and characterize mountain permafrost. *Geophysical Prospecting* **51**(4): 273–284.

Heginbottom, J. A., M. A. Dubreuil, et al. (1995*) Canada -- Permafrost in National Atlas of Canada*, 5th edition, Plate 2.1 (MCR 4177).

Hilbich, C., C. Hauck, et al. (2008) Monitoring mountain permafrost evolution using electrical resistivity tomography: A 7-year study of seasonal, annual, and long-term variations at Schilthorn, Swiss Alps. *Journal of Geophysical Research* **113**(F1): F01S90.

Hilbich C., Marescot, et al. (2009) Applicability of electrical resistivity tomography monitoring to coarse blocky and ice-rich permafrost landforms. *Permafrost and Periglacial Processes* **20**: 269-284.

(IPCC) Intergovernmental Panel on Climate Change, (2013) *Climate Change 2013: Summary for policymakers and the physical science basis.* Contribution of Working Groups I to the Fifth Assessment Report of the Intergovernmental Panel on Climate Change. Principal authors: Stocker, F.S., Qin, D., Plattner, G.K., Tignor, M.M.B., Allen, S.K., Boschung, J., Nauels, A., Xia, Y., Bex, V., Midgley, P.M. IPCC, Geneva, Switzerland, p.1552.

James, M. (2010) *Historic Change in Permafrost Distribution in Northern British Columbia and Southern Yukon Territory, Canada*. M.Sc., University of Ottawa.

James, M., A. Lewkowicz, et al. (2013) Multi-decadal degradation and persistence of permafrost in the Alaska Highway corridor, northwest Canada. *Environmental Research Letters* **8**, 045013: 10.

Jorgenson, M.T., V., Romanovsky, et al. (2010) Resilience and vulnerability of permafrost to climate change. *Canadian Journal of Forest Research* **40**(7): 1219-1236.

Kaab, A. (2008) Remote sensing of permafrost-related problems and hazads. *Permafrost and Periglacial Processes* **19**: 107-136.

Kneisel, C., C. Hauck, et al. (2000) Permafrost below the Timberline Confirmed and Characterized by Geoelectrical Resistivity Measurements, Bever Valley, Eastern Swiss Alps. *Permafrost and Periglacial Processes* **11**(4): 295-304.

Kneisel, C., C. Hauck, et al. (2008) Advances in geophysical methods for permafrost investigations. *Permafrost and Periglacial Processes* **19**(2): 157–178.

Lewkowicz, A. G. (2008) Evaluation of miniature temperature-loggers to monitor snowpack evolution at mountain permafrost sites, northwestern Canada. *Permafrost and Periglacial Processes* **19**(3): 323–331.

Lewkowicz, A.G., O. Bellehumeur-Genier et al. (2016) Change in discontinuous permafrost in the Alaska Highway corridor examined by repeated electrical resistivity tomography and ground temperature monitoring, northwest Canada. *XI International Conference on Permafrost (Abstract)*, Postdam Germany, June 20-24 2016.

Lewkowicz, A. G., B. Etzelmüller, et al. (2011) Characteristics of discontinuous permafrost based on ground temperature measurements and electrical resistivity tomography, southern Yukon, Canada. *Permafrost and Periglacial Processes* **22**(4): 320–342.

Loke, M. H. (1999) *Electrical imaging surveys for environmental and engineering studies: A practical guide to 2-D and 3-D surveys*. Malaysia: 61.

Loke, M. H. (2011) *Tutorial: 2-D and 3-D electrical imaging surveys*: 128.

Loke, M.H., Acworth, I. and Dahlin, T. (2003) A comparison of smooth and blocky inversion methods in 2D electrical imaging surveys. *Exploration Geophysics* **34**: 182-187.

McClymont, A.F., M., Hayashi et al. (2013) Geophysical imaging and thermal modeling of subsurface morphology and thaw evolution of discontinuous permafrost.

*Journal of Geophysical Research* **118**: 1826-1837.

Miceli, M. (2012) *Seasonal cycling in electrical resistivities at ten thin permafrost sites, Southern Yukon and Northern British Columbia.* M.Sc., University of Ottawa.

Minsley, B.J., J.D. Abraham et al. (2012) Airborne electromagnetic imaging of discontinuous permafrost. *Geophysical Research Letters* **39**: L02503, doi:10.1029/2011GL050079.

Muller, S. W. (1943*) Permafrost or permanently frozen ground and related engineering problems*. Special Report, Strategic Engineering Study, Intelligence Branch, Office, Chief of Engineers, no. 62, 136 pp. Second printing, 1945, 230.

Pastick N.J., M. T. Jorgenson et al. (2013) Extending airborne electromagnetic surveys for regional active layer and permafrost mapping with remote sensing and ancillary data, Yukon Flats ecoregion, Central Alaska. *Permafrost and Periglacial Processes* **24**: 184-199.

Payette, S., Delwaide et al. (2004) Accelerated thawing of subarctic peatland permafrost over the last 50 years. *Geophysical Research Letters*, **31**(L18208).

Quinton W.L., M. Hayashi and L.E. Chasmer (2009) Peatland Hydrology of Discontinuous Permafrost in the Northwest Territories: Overview and Synthesis. *Canadian Water Resources Journal* **43**(4): 311-328.

Riseborough D., N., Shiklomanov, et al. (2008) Recent Advances in Permafrost Modelling. *Permafrost and Periglacial Processes* **19**: 137-156.

Romanovsky, V. E., S. L. Smith, and H. H. Christiansen (2010) Permafrost thermal state in the polar Northern Hemisphere during the International Polar Year 2007–2009: A Synthesis. *Permafrost and Periglacial Process* **21**: 106–116.

Rowe, J. S. (1972*) Forest regions of Canada*. Ottawa, Information Canada: 172.

Schaefer, K., T. J. Zhang, and al. (2011) Amount and timing of permafrost carbon

release in response to climate warming. *Tellus B*. **63**:165–180.

Schuur, E.A.G., A.D. McGuire et al. (2015) Climate change and the permafrost carbon feedback. *Nature* **520**: 171-179/

Schuur, E. A. G., J. G. Vogel, et al. (2009) The effect of permafrost thaw on old carbon release and net carbon exchange from tundra. *Nature* **459**: 556–559.

Shur, Y.L., K.M. Hinkel, et al. (2005) The Transient Layer: Implications for Geocryology and Climate-Change Science. *Permafrost and Periglacial Processes* **16**: 5–17.

Shur, Y. L. and M. T. Jorgenson (2007) Patterns of permafrost formation and degradation in relation to climate and ecosystems. *Permafrost and Periglacial Processes* **18**(1): 7–19.

Smith, M. W. and D. W. Riseborough (1996) Permafrost monitoring and detection of climate change. *Permafrost and Periglacial Processes* **7**(4): 301–309.

Smith, M. W. and D. W. Riseborough (2002) Climate and the limits of permafrost: a zonal analysis. *Permafrost and Periglacial Processes* **13**(1): 1–15.

Smith, S. (2004) *Soils, In: Ecoregions of the Yukon Territory: Biophysical properties of Yukon landscapes, landscapes*, C.A.S. Smith, J.C. Meikle and C.F. Roots (eds.), Agriculture and Agri-Food Canada, PARC Technical Bulletin No. 04-01, Summerland, British Columbia, p. 35-38.

Smith, S. L., V. E. Romanovsky, et al. (2010) Thermal state of permafrost in North America: a contribution to the international polar year. *Permafrost and Periglacial Processes* **21**(2): 117–135.

Taylor, E., B. Taylors et al. (1997) *The Climates of British Columbia and Yukon*. Responding to global climate change in British Columbia and Yukon: Volume I of the Canada Country Study: Climate impacts and adaptation. E. Taylor and B. Taylor. Ottawa, Canada Communication Group INC.

Thibault, S., and Payette, S. (2009) Recent permafrost degradation in bogs of the James Bay area northern Quebec, Canada. *Permafrost and Periglacial Processes*, **20**: 383-389.

Throop, J., A. G. Lewkowicz, et al. (2012) Climate and ground temperature relations at sites across the continuous and discontinuous permafrost zones, northern Canada. *Canadian Journal of Earth Sciences* **49**: 865–876.

Vallée, S., and Payette, S. (2007) Collapse of permafrost mounds along a subarctic river over the last 100 years (northern Québec). *Geomorphology*, **90**: 162-170.

Vaughan, D.G., J.C. Comiso et al. (2013) Observations: Cryosphere. In: Climate Change 2013: *The Physical Science Basis. Contribution of Working Group I to the Fifth Assessment Report of the Intergovernmental Panel on Climate Change* [Stocker, T.F., D. Qin, G.-K. Plattner, M. Tignor, S.K. Allen, J. Boschung, A. Nauels, Y. Xia, V. Bex and P.M. Midgley (eds.)]. Cambridge University Press, Cambridge, United Kingdom and New York, NY, USA.

Viau, A.E., K. Gajweski et al. (2008) Low and high frequency climate variability in Eastern Beringia during the past 25 000 years. *Canadian Journal of Earth Sciences* **45**: 1425-1453.

Viit D.H., L.A. Halsey et al. (1994) The Bog Landforms of Continental Western Canada in Relation to Climate and Permafrost Patterns. *Arctic and Alpine Research* **26**(1): 1-13.

Vitt, D.H., L.A. Halsey et al. (2000) The changing landscape of Canada's western boreal forest: current dynamics of permafrost. *Canadian Journal of Forest Research* **30**: 283-287.

Vonder Mühll, D., Hauck, C., and Gubler, H. (2002) Mapping of mountain permafrost using geophysical methods. *Progress in Physical Geography* **26**(4): 643-660.

Wahl H.E., D.B. Fraser, et al. (1987) *Climate of Yukon*. Environment Canada, Ottawa: 321.

Williams, P. J. and M. W. Smith (1989) *The Frozen Earth: Fundamentals of Geocryology*. Cambridge, Cambridge University Press.

Zhang, T. (2005) Influence of the seasonal snow cover on the ground thermal regime: An overview. *Reviews of Geophysics* **43**(4): RG4002.

Zhang, Y. (2013) Spatio-Temporal features of permafrost thaw projected from long-term high-resolution modeling for a region in the Hudson Bay Lowlands in Canada. *Journal of Geophysical Research: Earth Surface* **118**: 542-552.

Zhang, Y., W. Chen and J. Cihlar (2003) A process-based model for quantifying the impact of climate change on permafrost thermal regimes. *Journal of Geophysical Research* **108**: D22, 4695.

Zhang, Y., W. Chen and D.W. Riseborough (2006) Temporal and spatial changes of permafrost in Canada since the end of the Little Ice Age. *Journal of Geophysical Research* **111**: D22103.

Zhang, Y., W. Chen and al. (2005) Soil temperature in Canada during the twentieth century: Complex responses to atmospheric climate change. *Journal of Geophysical Reseach* **110**: D03112.

Zimov, S. A., E. A. G. Schuur, and F. S. Chapin (2006) Permafrost and the global carbon budget. *Science* **312**: 1612–1613.

# APPENDICES

## Appendix A: MP 178

Table A1: Coordinates of the ERT lines at MP 178.

| | Transect starts | | Transect ends | |
|---|---|---|---|---|
| ERT Transect | Latitude | Longitude | Latitude | Longitude |
| Permanent array (A-B) | 57.42554 | -122.86577 | 57.42538 | -122.86516 |
| ERT 1 (C-D) | 57.42545 | -122.86500 | 57.42552 | -122.86699 |
| ERT 2 (E-F) | 57.42546 | -122.86524 | 57.42475 | -122.86523 |

Table A2: Annual Snow Depth Days values (SDD) (cm d) calculated for each station at MP 178.

| Year | Main (SDD) | Sub 1 (SDD) | Sub 2 (SDD) | Average |
|---|---|---|---|---|
| 2010-2011 | 11100 | 10540 | 10170 | 10600 |
| 2011-2012 | 4640 | 4800 | 4130 | 4520 |
| 2012-2013 | 14500 | 11950 | 9410 | 11950 |
| 2013-2014 | 7620 | 6450 | 4770 | 6280 |
| Average | 9470 | 8440 | 7120 | 8340 |

Table A3: Air and ground temperatures (°C) at MP 178. Missing data are represented as blank cells.

| | | Main station | | | | Sub 1 | | | | Sub 2 | | | |
|---|---|---|---|---|---|---|---|---|---|---|---|---|---|
| Years | MAAT | MAGST 1 | MAGST 2 | MAGT 40 cm | MAGT 90 cm | MAGST 1 | MAGST 2 | MAGT 40 cm | MAGT 90 cm | MAGST 1 | MAGST 2 | MAGT 40 cm | MAGT 90 cm |
| 2010-2011 | -2.7 | 0.6 | 0.0 | | | 0.8 | 1.1 | 0.4 | 0.1 | 0.5 | 0.5 | 0.3 | -0.1 |
| 2011-2012 | -1.0 | 0.6 | -1.0 | 0.2 | 0.1 | 1.1 | 1.3 | 1.6 | 1.0 | 0.9 | 0.7 | 0.6 | -0.1 |
| 2012-2013 | -2.8 | -0.5 | -0.4 | 0.1 | -0.3 | 1.7 | 1.7 | 3.2 | 1.2 | 0.8 | 0.8 | 0.9 | -0.1 |
| Average | -2.2 | 0.2 | -0.5 | 0.2 | -0.1 | 1.2 | 1.4 | 1.7 | 0.8 | 0.7 | 0.7 | 0.6 | -0.1 |

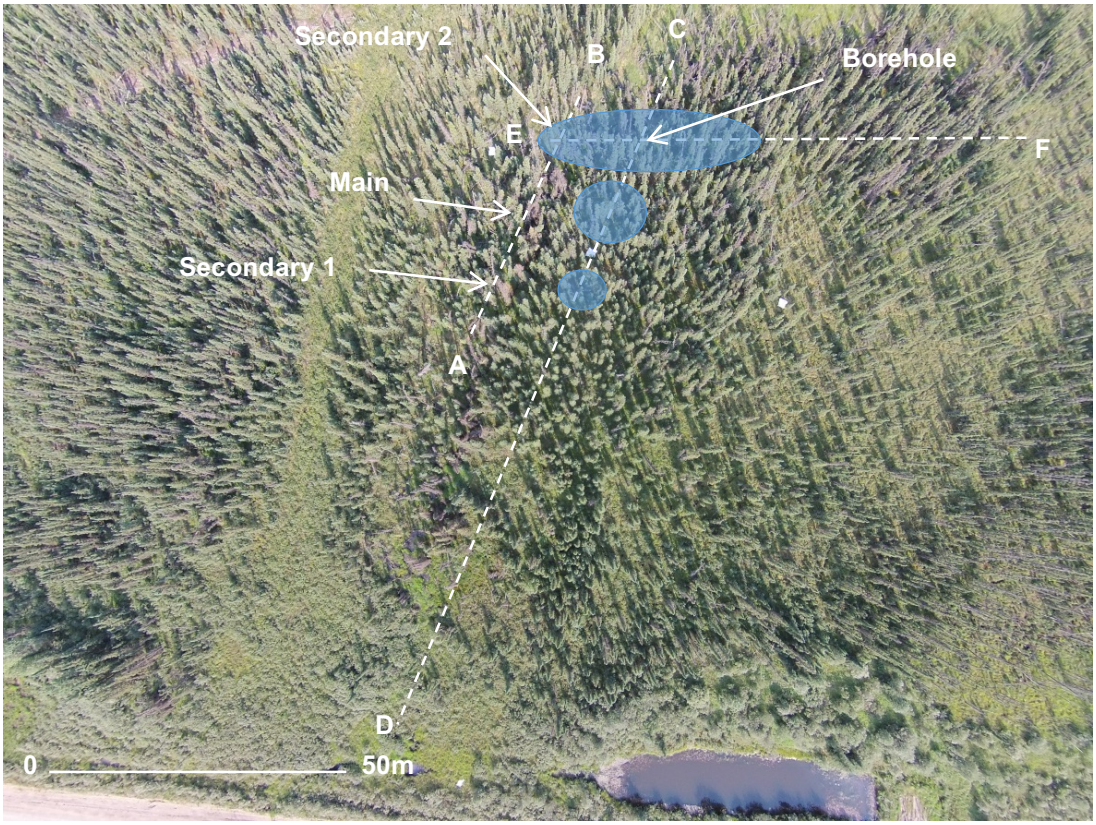


Figure A1: Air photo for MP 178 in 2014. Shaded ellipses represent permafrost patches; dashed lines represent ERT transects and climate monitoring instruments locations are marked. The scale is approximate.

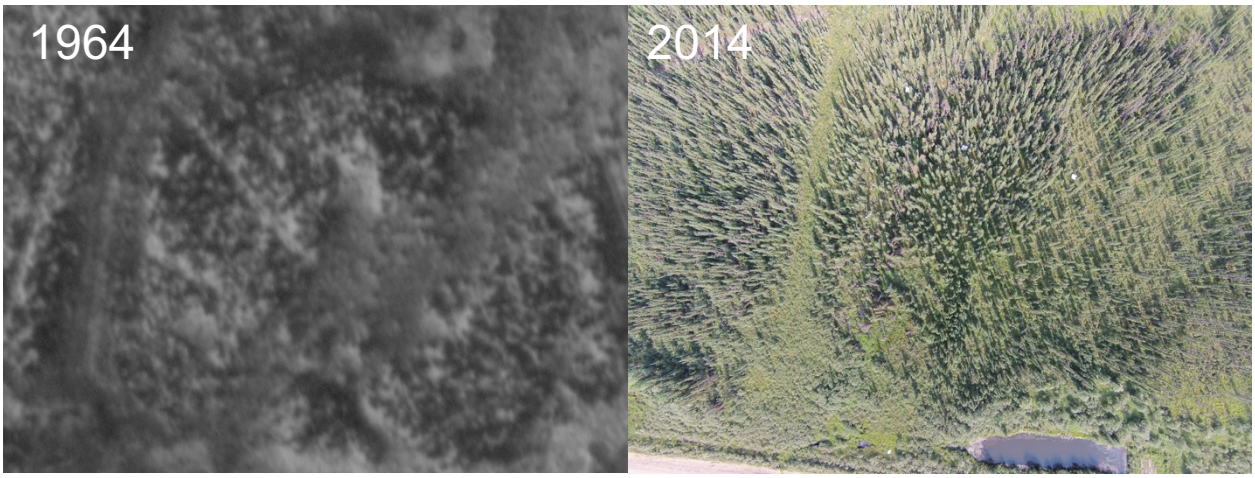


Figure A2: Historic air photo analyses for MP 178 (close-up) in 1964 and 2014.


Figure A3: MP 178 Historic air photo analysis from field site in 1964-2011. MP 178 satellite imagery from Google Earth Pro from field site in 2011. Dashed square represents site area.

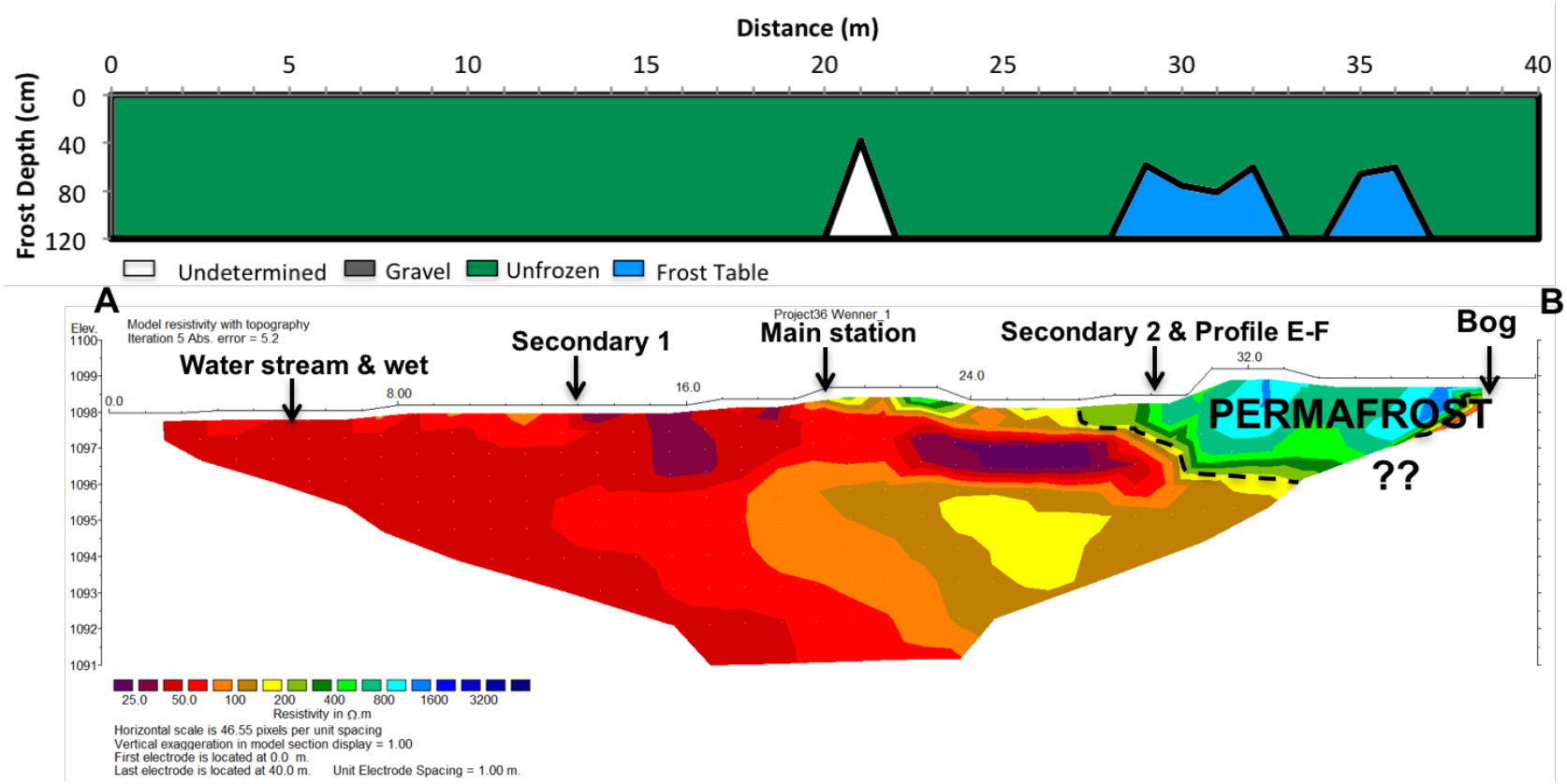


Figure A4: Modelled ERT inversion profile at MP 178 for the permanent array, with dashed lines representing inferred permafrost. The frozen/unfrozen boundary is taken to be 200 Ω m at this site.

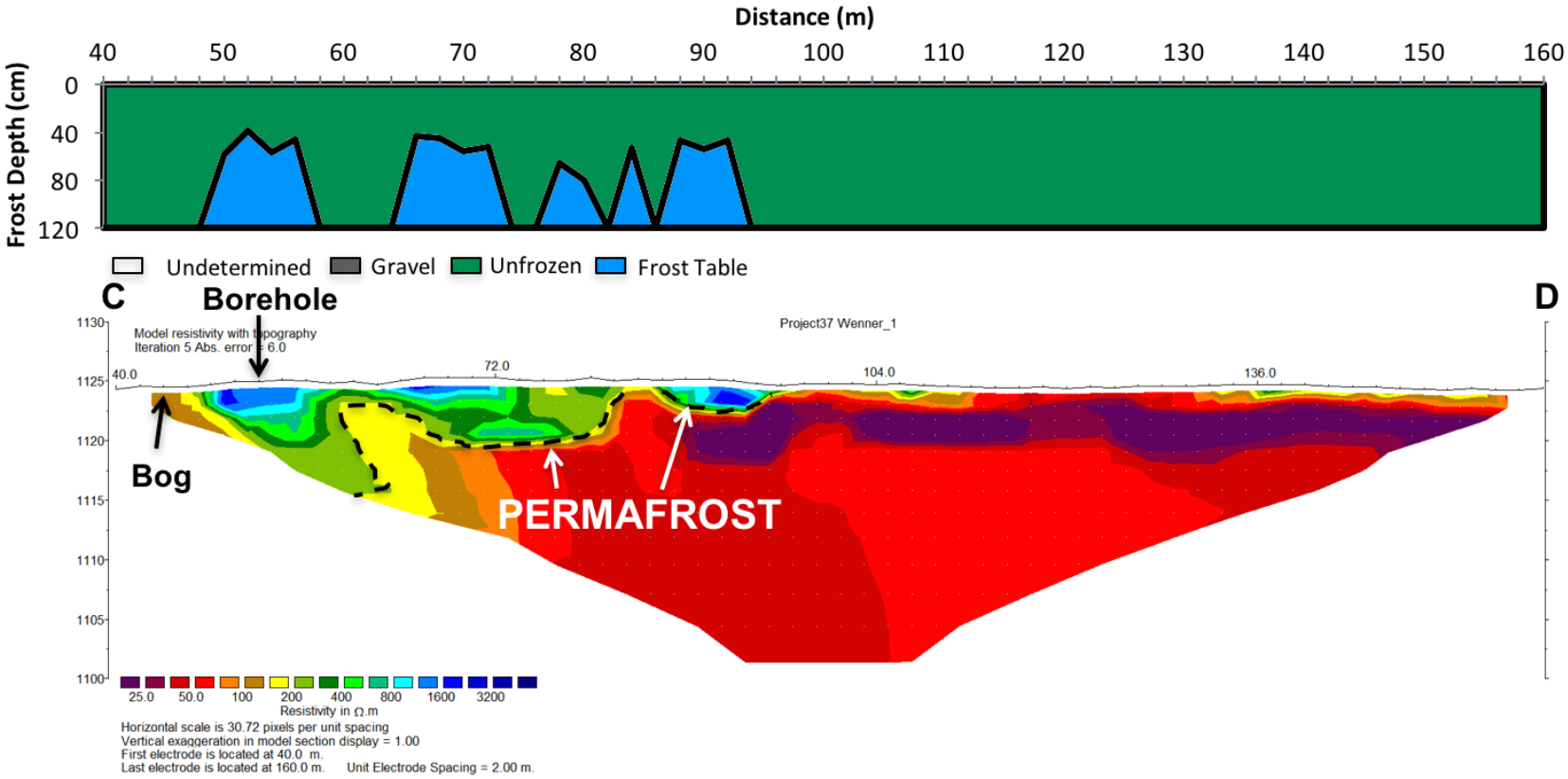


Figure A5: Modelled ERT inversion profile at MP 178 for ERT 1, with dashed lines representing inferred permafrost. The frozen/unfrozen boundary is taken to be 200 Ω m at this site.

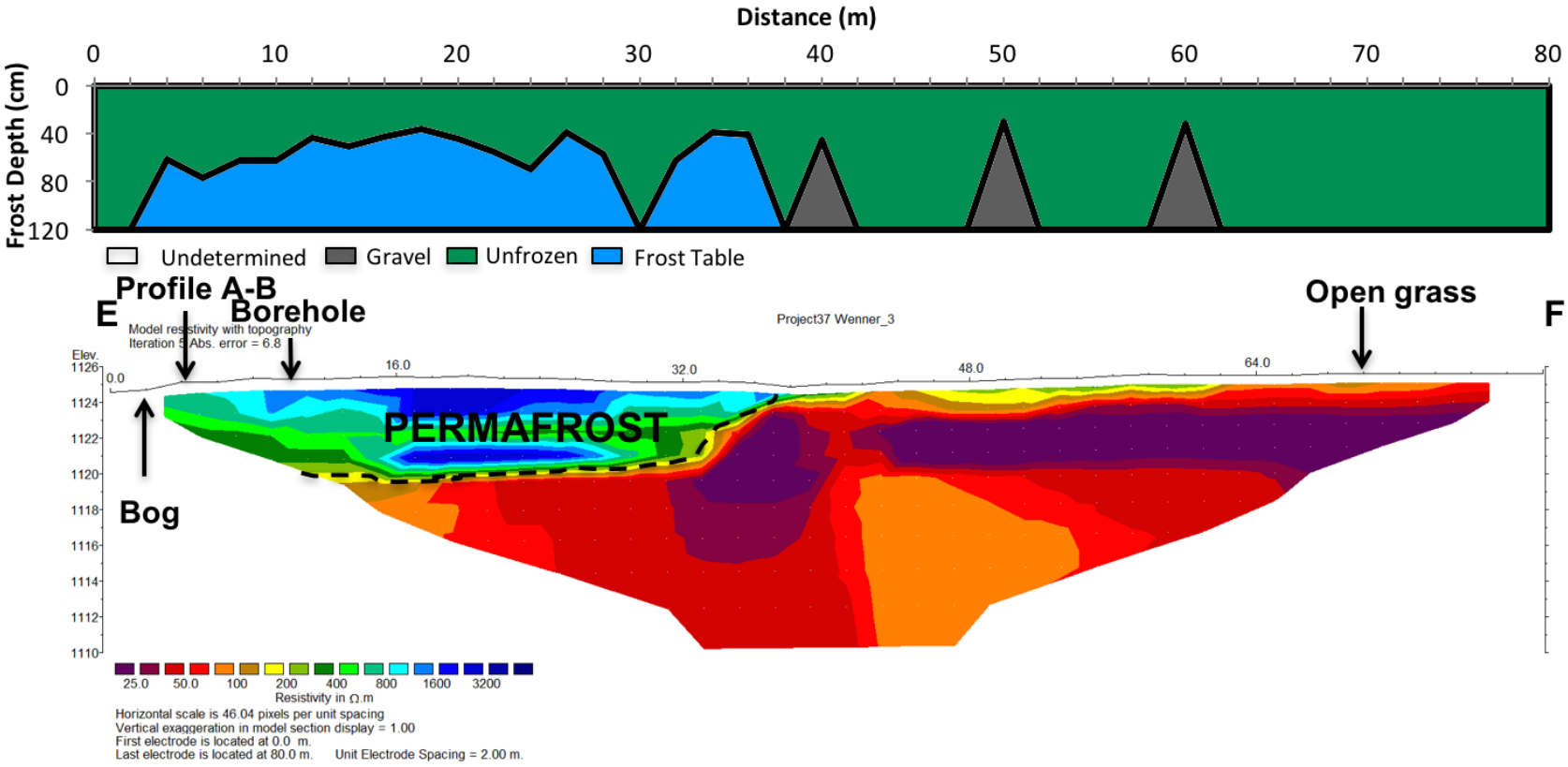


Figure A6: Modelled ERT inversion profile at MP 178 for ERT 2, with dashed lines representing inferred permafrost. The frozen/unfrozen boundary is taken to be 200 Ω m at this site.

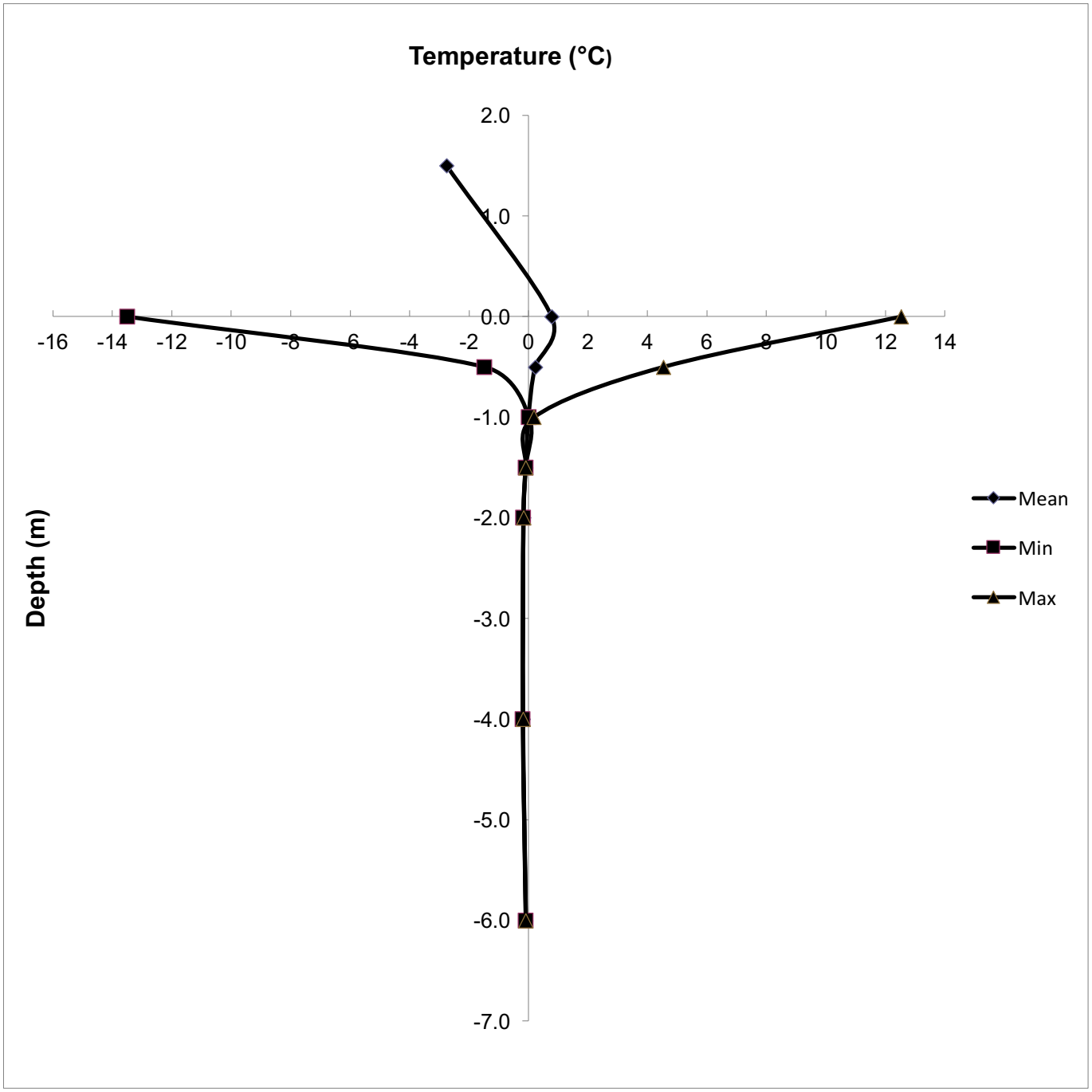


Figure A7: Temperature envelope for the borehole at MP 178 (2013-2014). The temperature at the base of the borehole at 6 m is -0.1°C.

## Appendix B: MP 286

Table B1: Coordinates of the ERT lines at MP 286.

| | Transect starts | | Transect ends | |
|---|---|---|---|---|
| | Latitude | Longitude | Latitude | Longitude |
| Permanent array (A-B) | 58.66328 | -122.69361 | 58.66346 | -122.69294 |
| ERT 1 (C-D) | 58.66372 | -122.69313 | 58.66309 | -122.69278 |
| ERT 2 (E-F) | 58.66365 | -122.6936 | 58.66298 | -122.69314 |

Table B2: Annual Snow Depth Days values (SDD) (cm d) calculated for each station at MP 286.

| Year | Main (SDD) | Sub 1 (SDD) | Sub 2 (SDD) | Average |
|---|---|---|---|---|
| 2010-2011 | 8680 | 7400 | 7930 | 8000 |
| 2011-2012 | 6610 | 2920 | 5090 | 4870 |
| 2012-2013 | 10630 | 9360 | 13450 | 11140 |
| 2013-2014 | 9510 | 6710 | 8790 | 8330 |
| Average | 8860 | 6590 | 8810 | 8090 |

Table B3: Air and ground temperatures (°C) at MP 286. Missing data are represented as blank cells.

| | Main | | Sub 1 | | | | Sub 2 | | | |
|---|---|---|---|---|---|---|---|---|---|---|
| Years | MAAT | MAGST | MAGST 1 | MAGST 2 | MAGT 50 cm | MAGT 100 cm | MAGST 1 | MAGST 2 | MAGT 50 cm | MAGT 100 cm |
| 2010-2011 | -1.2 | 1.7 | 1.5 | 1.0 | 0.1 | -0.1 | 2.5 | 1.8 | 0.1 | -0.2 |
| 2011-2012 | 0.3 | 2.5 | 1.6 | 2.0 | 0.4 | 0.3 | 2.7 | | 1.5 | |
| 2012-2013 | -2.0[A] | | 3.3 | 1.2 | 2.6 | 0.1 | 0.4 | 3.0 | 0.2 | -0.2 |
| Average | -0.9 | 2.1 | 2.1 | 1.4 | 1.0 | 0.1 | 1.8 | 2.4 | 0.6 | -0.2 |

[A] Missing data from June 5 to Sept. 30, 2013 estimated by correlation with Fort Nelson Environment Canada station.

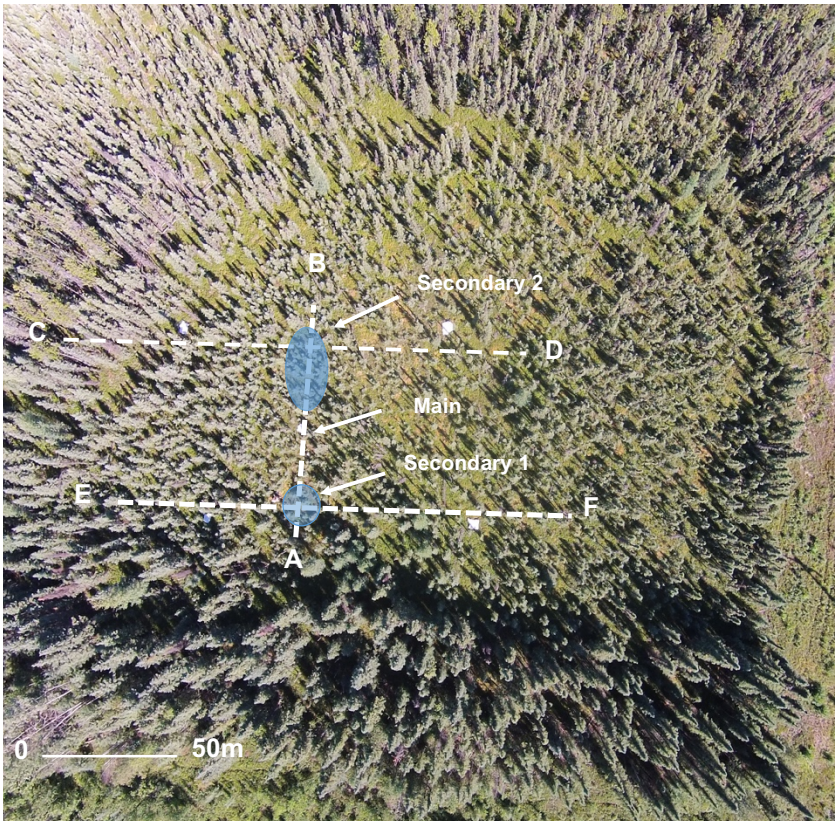


Figure B1: Air photo for MP 286 in 2014. Shaded ellipses represent permafrost patches; dashed lines represent ERT transects and climate monitoring instruments locations are marked. The scale is approximate.

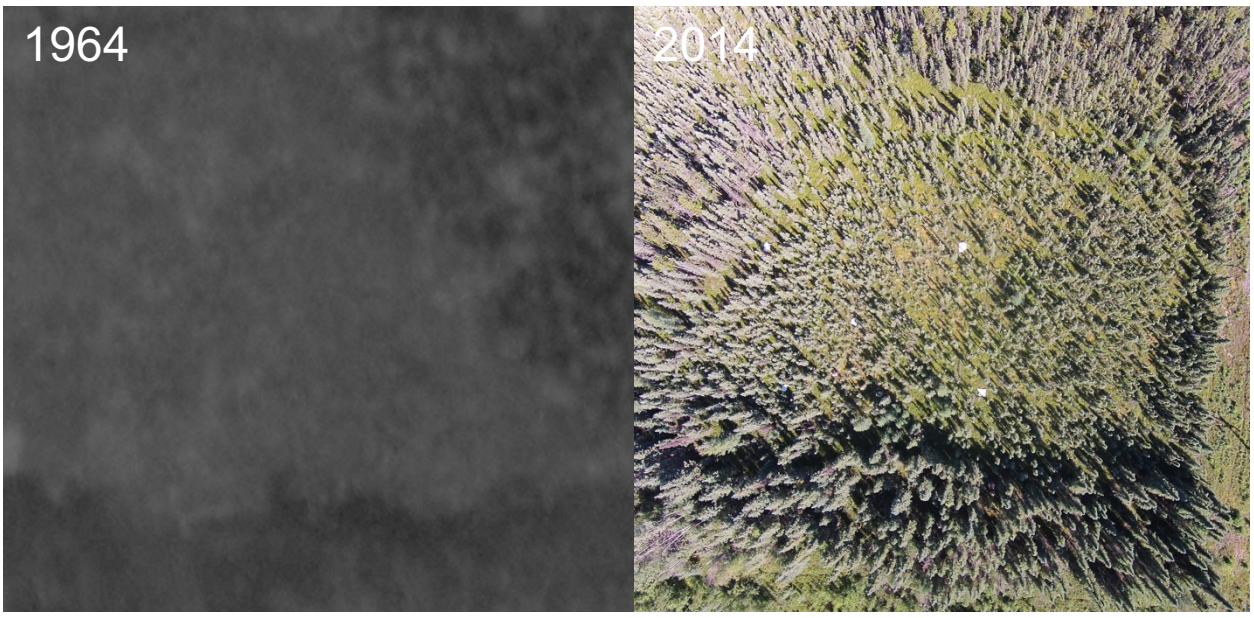


Figure B2: Air photo for MP 286 in 1964 (Small scale).


Figure B3: MP 286 Historic air photo analysis from field site in 1964-2014. MP 286 satellite imagery from Google Earth Pro from field site in 2002. Dashed square represents site area.

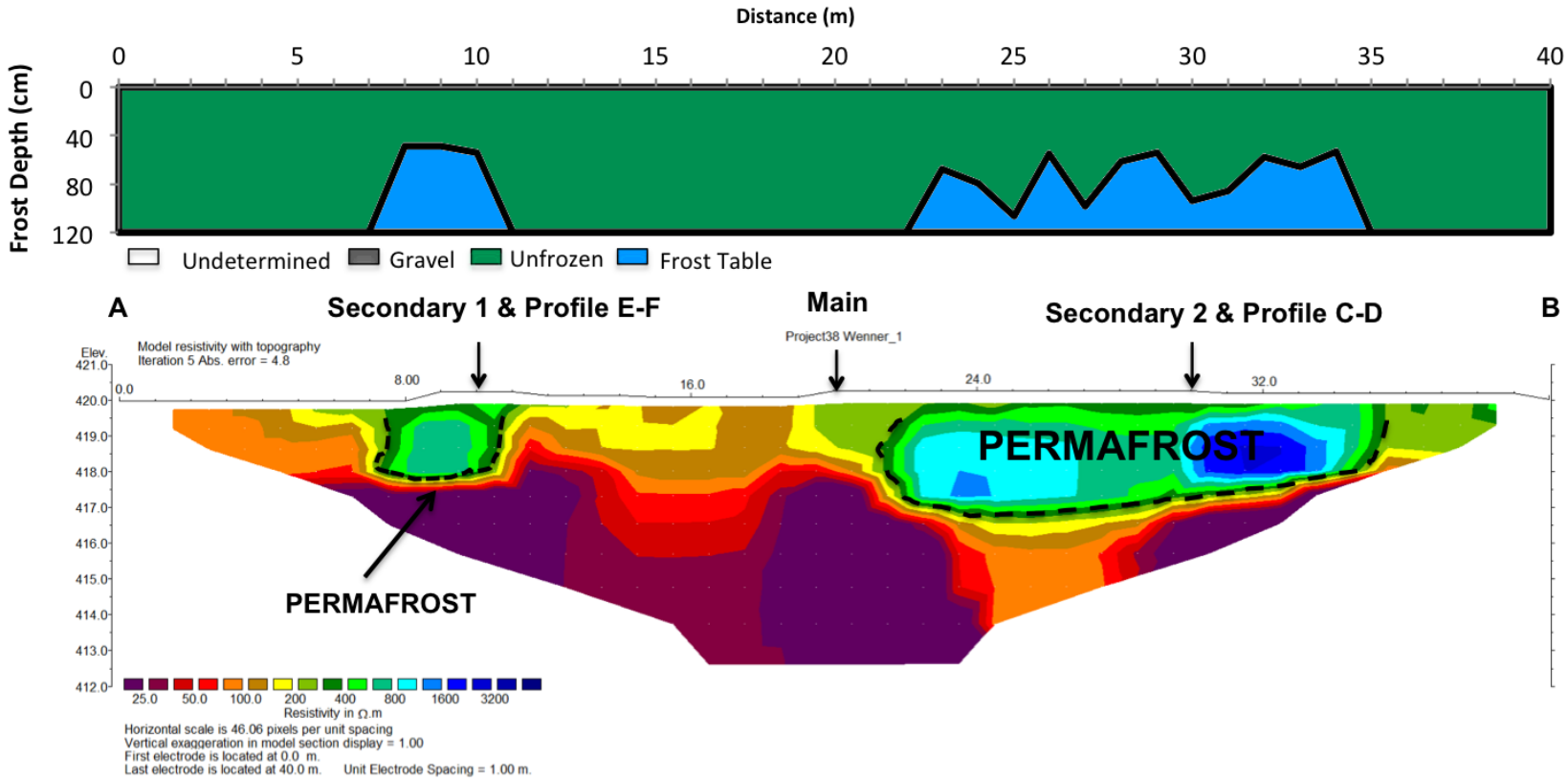


Figure B4: Modelled ERT inversion profile at MP 286 for the permanent array, with dashed lines representing inferred permafrost. The frozen/unfrozen boundary is taken to be 300 Ω m at this site.

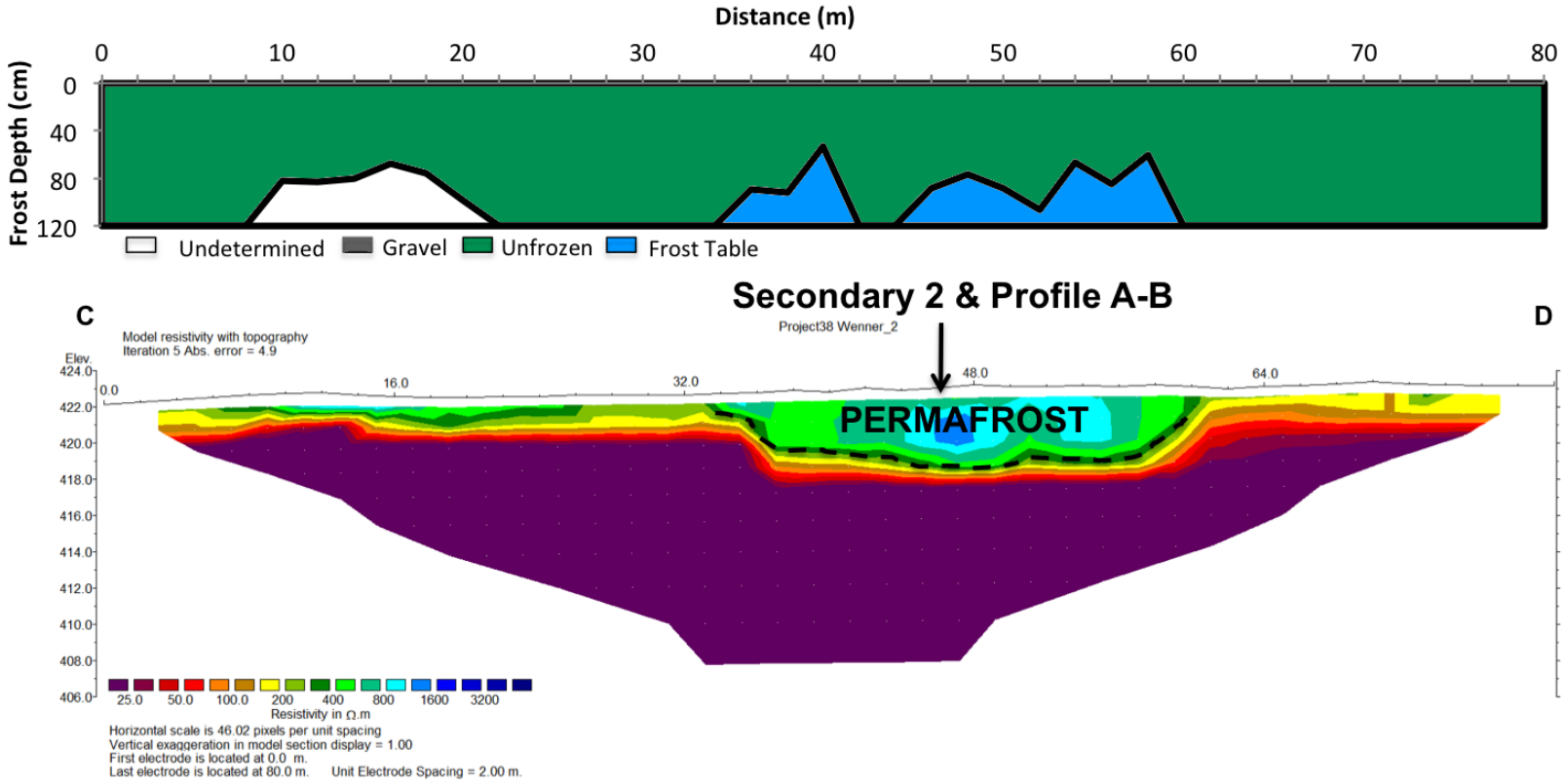


Figure B5: Modelled ERT inversion profile at MP 286 for ERT 1, with dashed lines representing inferred permafrost. The frozen/unfrozen boundary is taken to be 300 Ω m at this site.

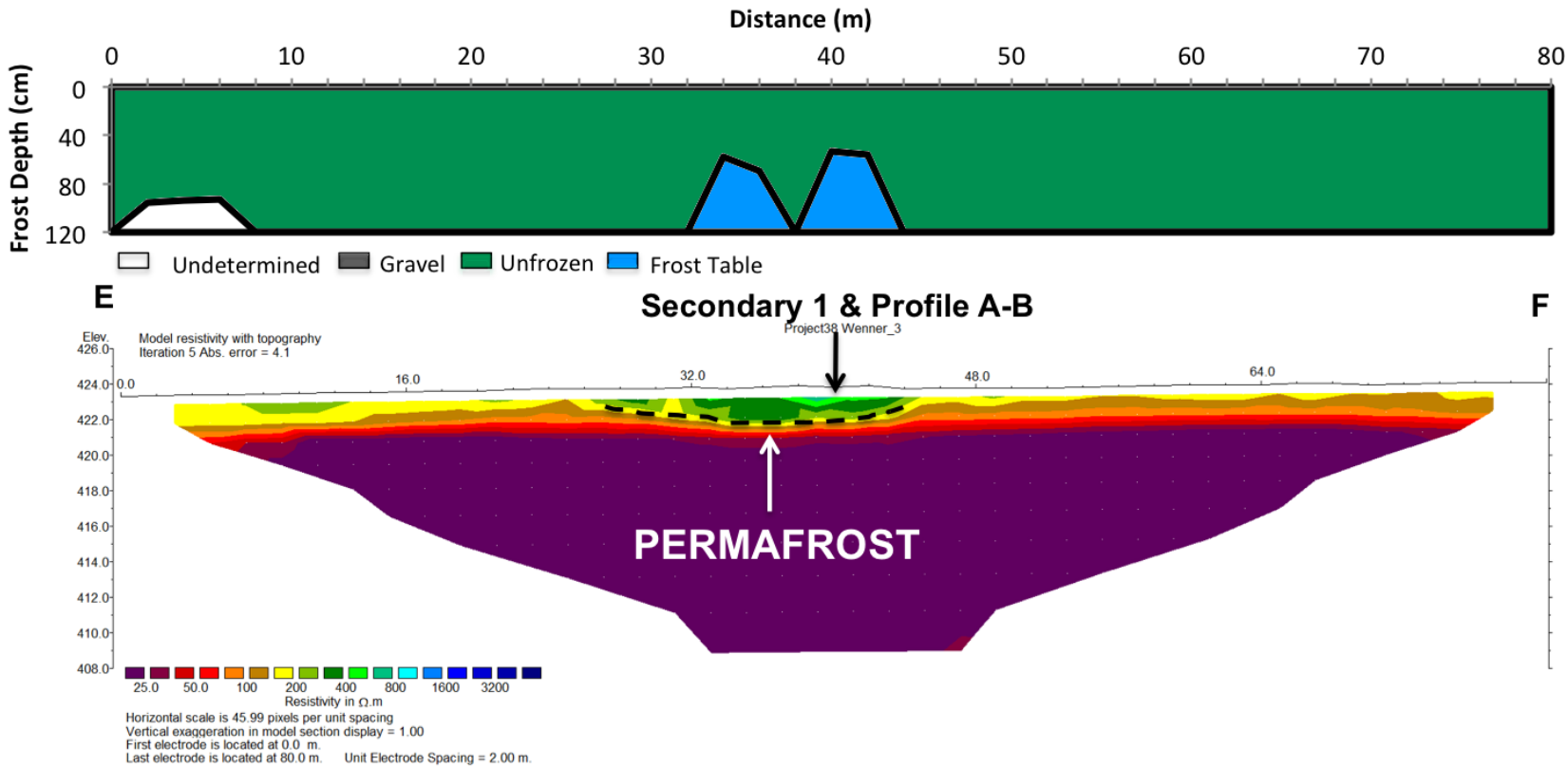


Figure B6: Modelled ERT inversion profile at MP 286 for ERT 2, with dashed lines representing inferred permafrost. The frozen/unfrozen boundary is taken to be 300 Ω m at this site.

## Appendix C: MP 341

Table C1: Coordinates of the ERT lines at MP 341.

| | Transect starts | | Transect ends | |
|---|---|---|---|---|
| ERT transect | Latitude | Longitude | Latitude | Longitude |
| Permanent array (A-B) | 58.78837 | -123.57322 | 58.78807 | -123.57283 |
| ERT 1 (C-D) | 58.78798 | -123.57332 | 58.78867 | -123.57320 |
| ERT 2 (E-F) | 58.78801 | -123.57324 | 58.78833 | -123.57204 |

Table C2: Annual Snow Depth Days values (SDD) (cm d) calculated for each station at MP 341.

| Years | Main (SDD) | Sub 1 (SDD) | Sub 2 (SDD) | Average |
|---|---|---|---|---|
| 2010-2011 | 6130 | 6840 | 5850 | 6270 |
| 2011-2012 | 4740 | 2820 | 3540 | 3700 |
| 2012-2013 | 6200 | 7600 | 5130 | 6310 |
| 2013-2014 | 8300 | 8340 | 5420 | 7350 |
| Average | 6340 | 6400 | 4990 | 5910 |

Table C3: Air and ground temperatures (°C) at MP 341. Missing data are represented as blank cells.

| | | Main | | | Sub 1 | | | | Sub 2 | | | |
|---|---|---|---|---|---|---|---|---|---|---|---|---|
| Years | MAAT | MAGST 1 | MAGT 50 cm | MAGT 100 cm | MAGST 1 | MAGST 2 | MAGT 50 cm | MAGT 100 cm | MAGST 1 | MAGST 2 | MAGT 50 cm | MAGT 100 cm |
| 2010-2011 | -2.3 | 2.3 | -0.1 | -0.1 | 1.6 | 2.2 | 0.5 | 0.2 | 1.9 | 1.8 | -0.2 | -0.2 |
| 2011-2012 | -0.7[A] | 2.6 | | | 2.2 | | | 0.1 | 2.5 | 2.4 | -0.2 | -0.2 |
| 2012-2013 | -2.8[B] | 1.7 | | | 2.5 | | | -0.1 | 2.3 | 2.8 | 0.6 | -0.2 |
| Average | -1.9 | 2.2 | -0.1 | -0.1 | 2.1 | 2.2 | 0.5 | 0.1 | 2.2 | 2.3 | 0.1 | -0.2 |

[A] Missing data from April 27 to Sept. 30, 2012 and August 18 to Sept. 30 2012 were estimated by correlation with Fort Nelson Environment Canada station.

[B] October 1 to Sept. 30 2012-2013 were estimated by correlation with Fort Nelson Environment Canada station.

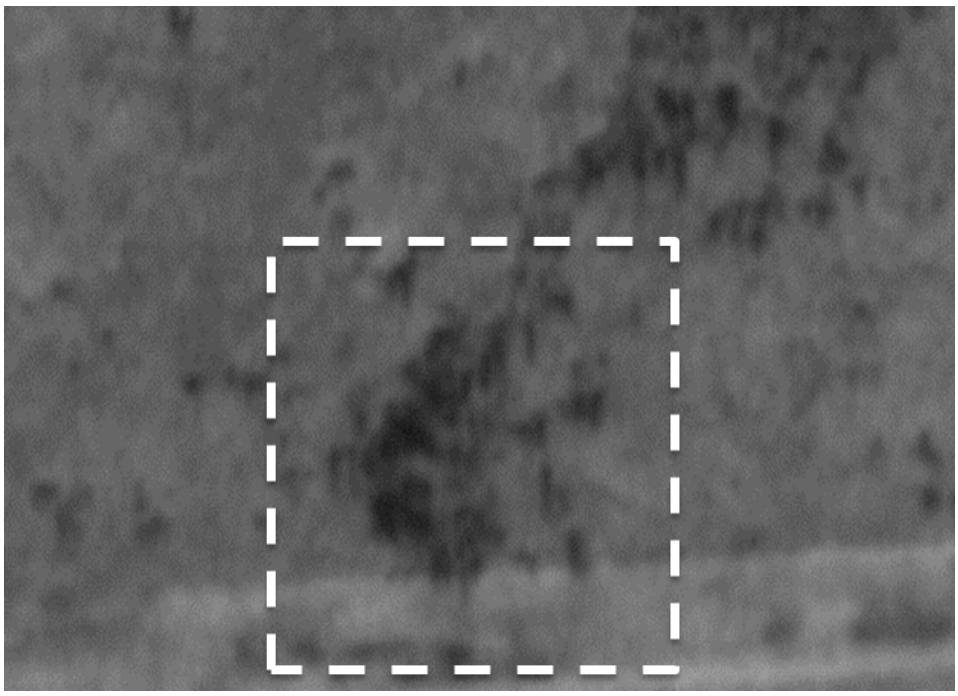

Figure C1: Air photo for MP 341 in 1964. Dashed square represents the study area.

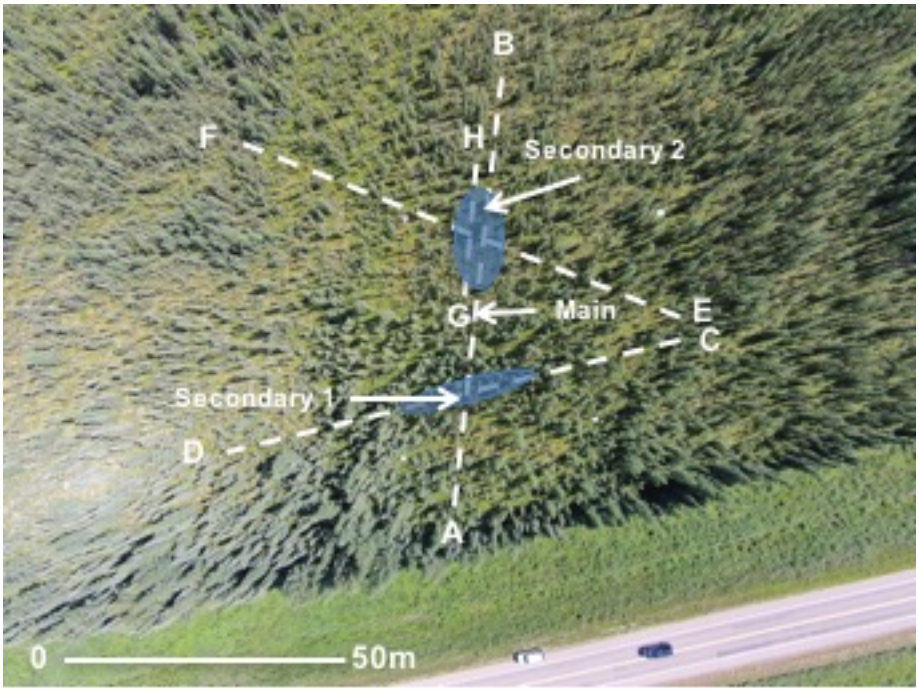


Figure C2: Air photo for MP 341 in 2014. Shaded ellipses represent permafrost patches; dashed lines represent ERT transects and climate monitoring instruments locations are marked. The scale is approximate.

Figure C3: Air photo for MP 341 in 1964 (Larger scale). Dashed square represents the study area.


Figure C4: Satellite imagery from Google Earth Pro, Landsat, of MP 341 in 2005. Dashed square represents study area

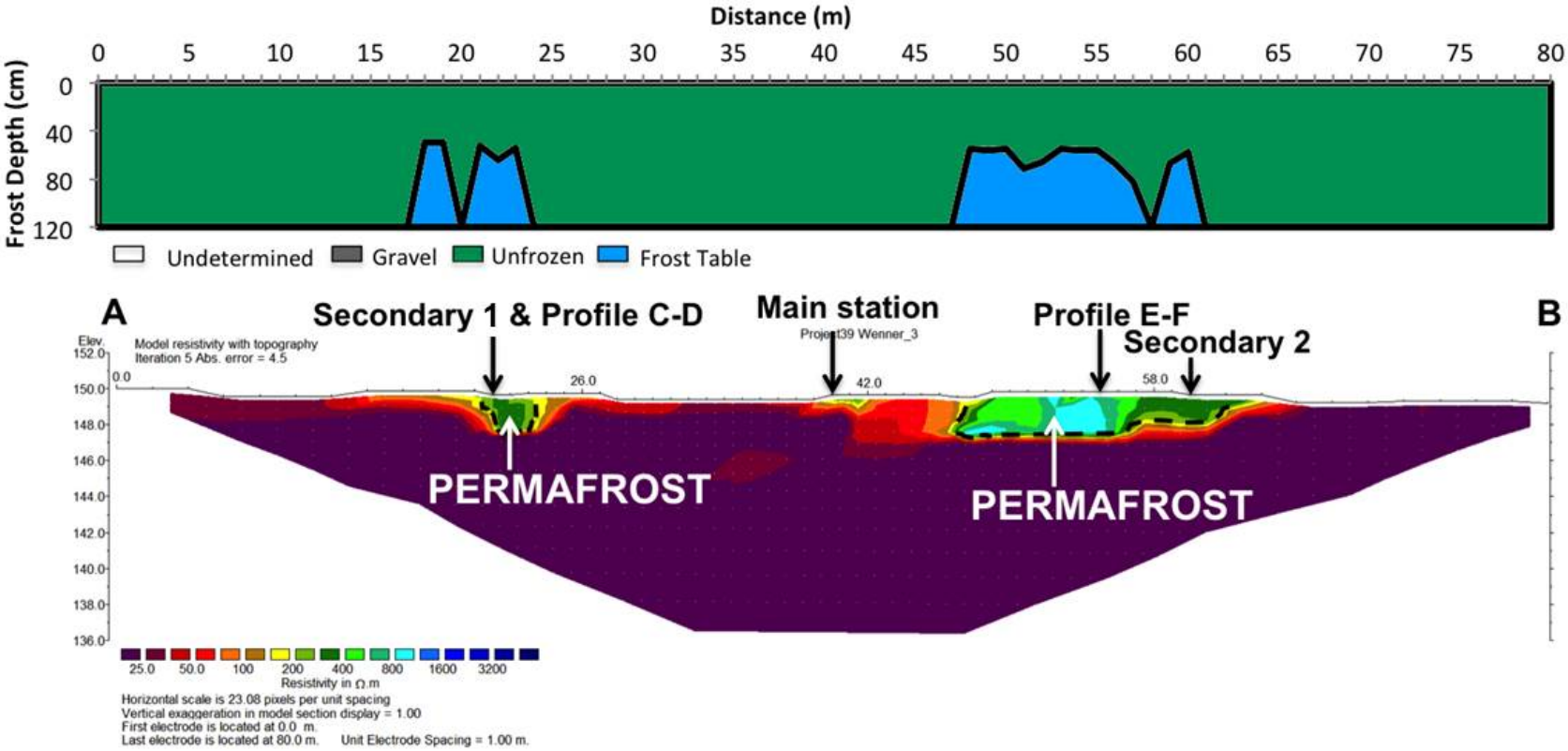


Figure C5: Modelled ERT inversion profile at MP 341 for the permanent array, with dashed lines representing inferred permafrost. The frozen/unfrozen boundary is taken to be 300 Ω m at this site.

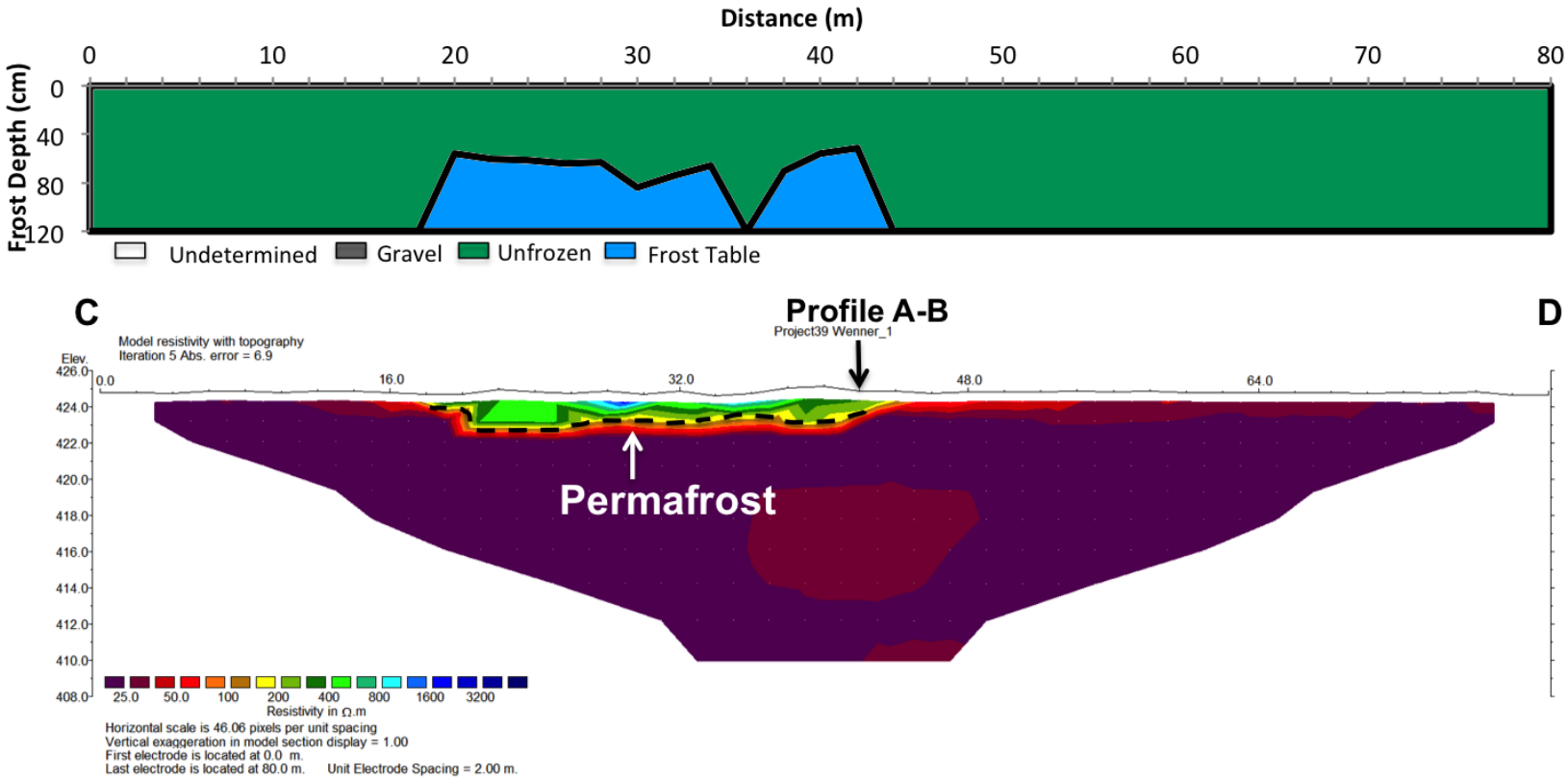


Figure C6: Modelled ERT inversion profile at MP341 for the ERT 1, with dashed lines representing inferred permafrost. The frozen/unfrozen boundary is taken to be 300 Ω m at this site.

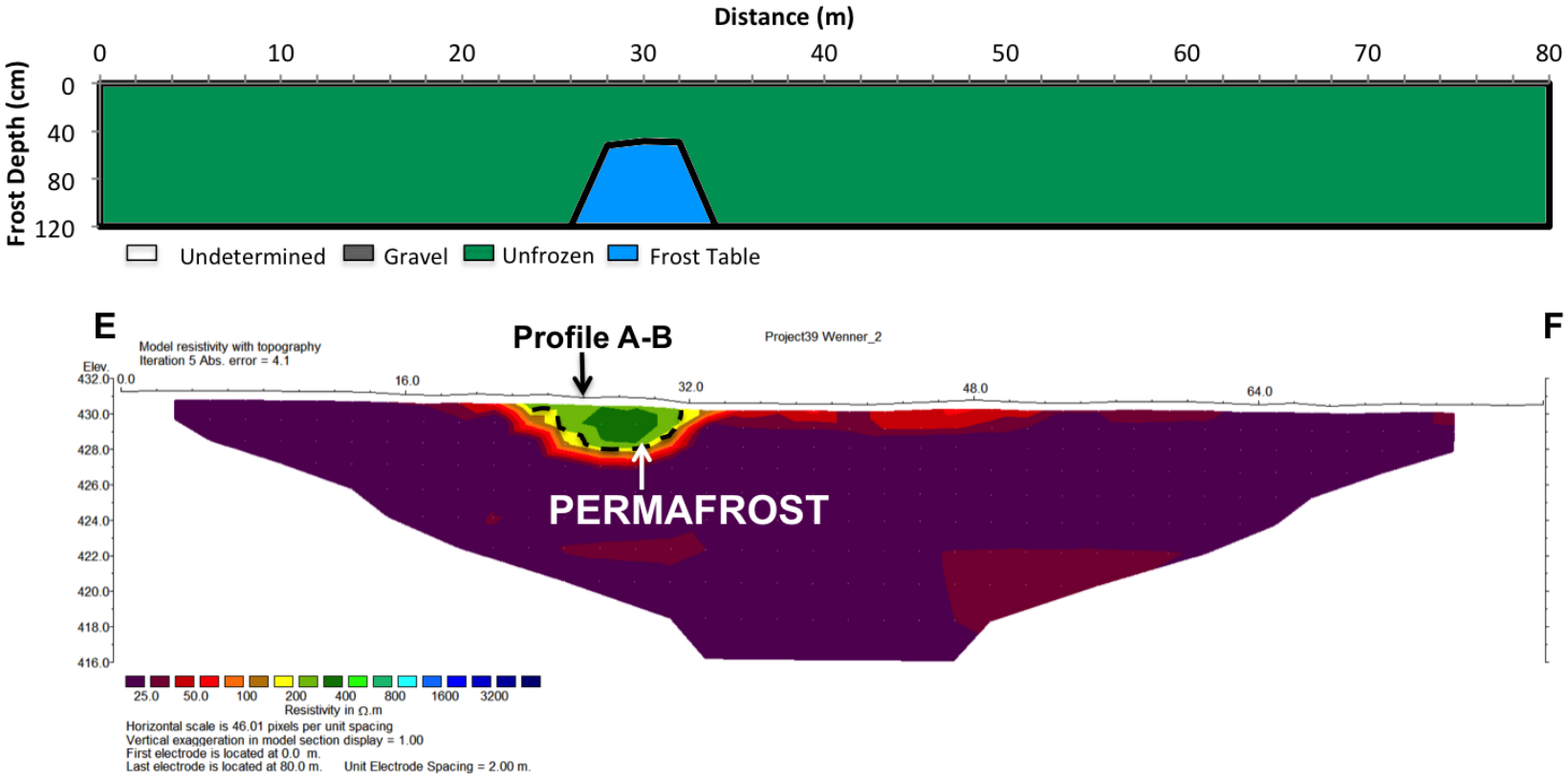


Figure C7: Modelled ERT inversion profile at MP 341 for the ERT 2, with dashed lines representing inferred permafrost. The frozen/unfrozen boundary is taken to be 300 Ω m at this site.

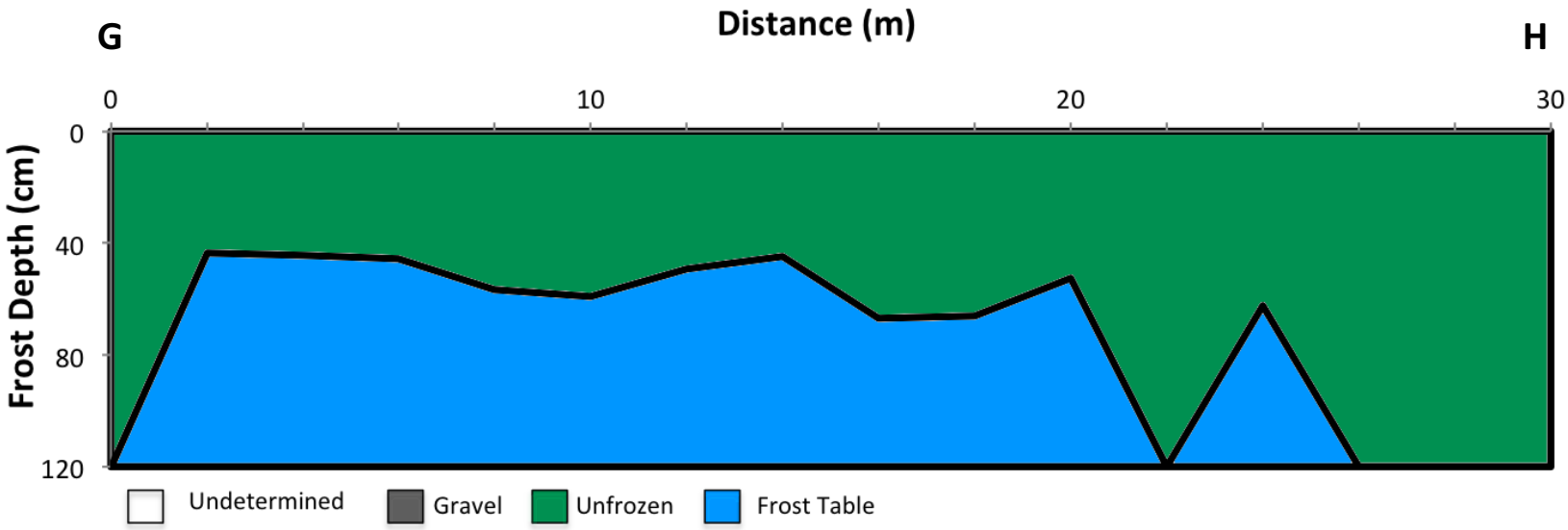


Figure C8: Frost probing survey at MP 341 next to secondary station 2

## Appendix D: MP 400

Table D1: Coordinates of the ERT lines at MP 400.

| | Transect starts | | Transect ends | |
|---|---|---|---|---|
| ERT transect | Latitude | Longitude | Latitude | Longitude |
| ERT 1 (C-D) | 58.69524 | -124.86328 | 58.69215 | -124.85773 |
| Permanent array (A-B) | 58.69344 | -124.85891 | 58.69309 | -124.85963 |

Table D2: Annual Snow Depth Days values (SDD) (cm d) calculated for each station at MP 400.

| Years | Main (SDD) | Sub 1 (SDD) | Sub 2 (SDD) | Average |
|---|---|---|---|---|
| 2010-2011 | 8900 | 8250 | 8460 | 8540 |
| 2011-2012 | 4580 | 4680 | 2520 | 3920 |
| 2012-2013 | 5160 | 7090 | 8500 | 6920 |
| 2013-2014 | 12700 | 8200 | 9490 | 10130 |
| Average | 7830 | 7060 | 7240 | 7380 |

Table D3: Air and ground temperatures (°C) at MP 400. Missing data are represented as blank cells.

| | | | Main | | | | | | Sub 1 | | | Sub 2 | | |
|---|---|---|---|---|---|---|---|---|---|---|---|---|---|---|
| Years | MAAT | MAGST | MAGT 10 cm | MAGT 25 cm | MAGT 40 cm | MAGT 50 cm | MAGST 1 | MAGST 2 | MAGT 50 cm | MAGT 100 cm | MAGST 1 | MAGST 2 | MAGT 50 cm | MAGT 100 cm |
| 2010-2011 | -2.7 | 1.4 | 1.9 | 1.2 | 0.4 | -0.1 | 2.5 | 2.5 | 0.3 | 0.1 | 0.9 | | | -0.1 |
| 2011-2012 | -2.1[A] | | | | | | 2.8 | 2.9 | 0.5 | 0.0 | 1.2 | | | 0.0 |
| 2012-2013 | -2.6 | 0.3 | 2.0 | 1.2 | 0.3 | 0.3 | 3.0 | 3.0 | 1.1 | 0.3 | 1.3 | 1.1 | 0.2 | 0.1 |
| Average | -2.5 | 1.4 | 2.0 | 1.2 | 0.3 | 0.1 | 2.7 | 2.8 | 0.7 | 0.1 | 1.2 | 1.1 | 0.2 | 0.0 |

[A] MAAT 2011-2012 data derived from a blended year average of MP 400 data from 2007 to 2014.


Figure D1: MP 400 Historic air photo analysis from field site in 1964-2013. MP 400 satellite imagery from Google Earth Pro from field site in 2013.

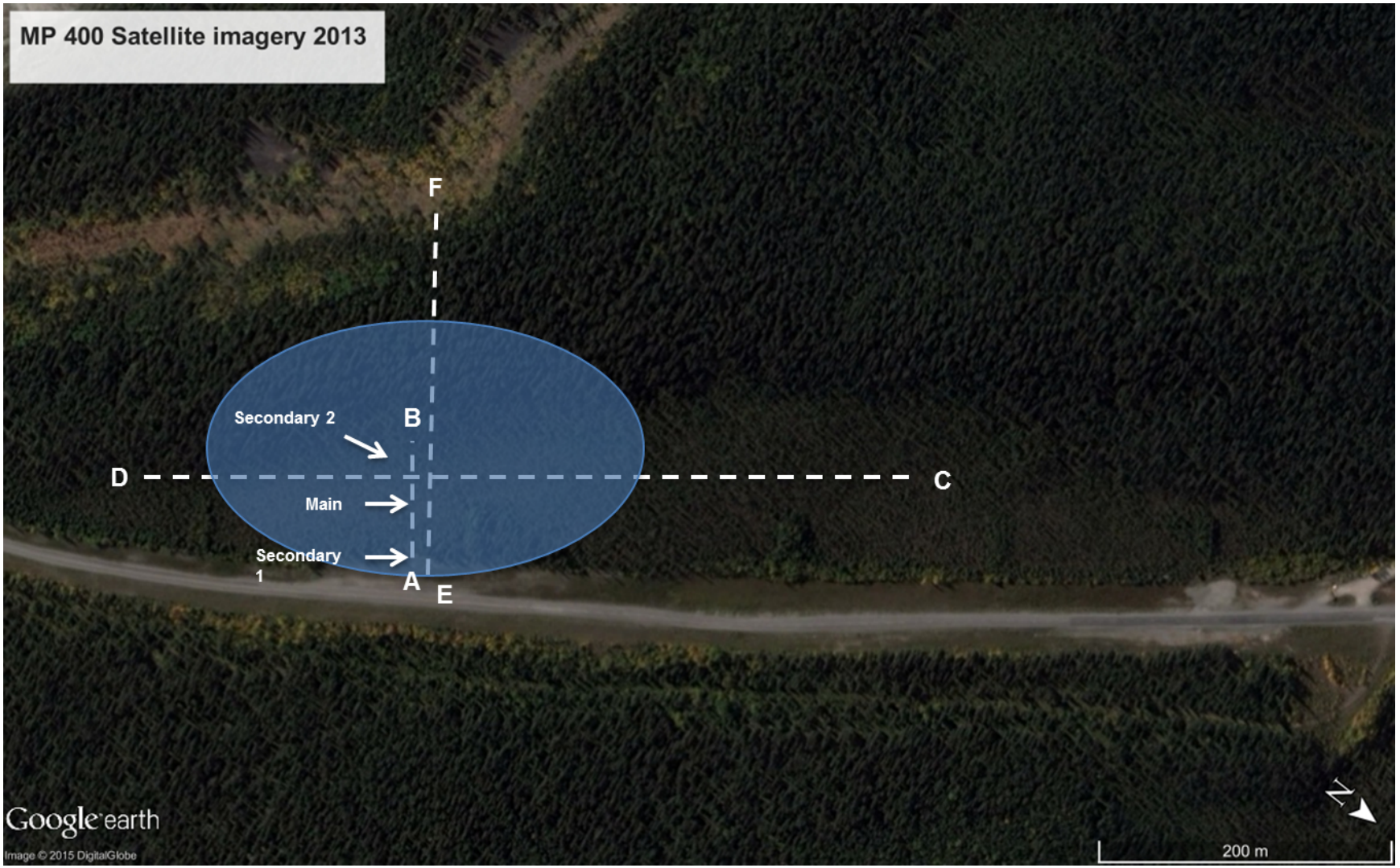


Figure D2: Satellite imagery from Google Earth, DigitalGlobe, in 2013. Shaded ellipses represent permafrost patches; dashed lines represent ERT transects and climate monitoring instruments locations are marked. Image is rotated 90°.

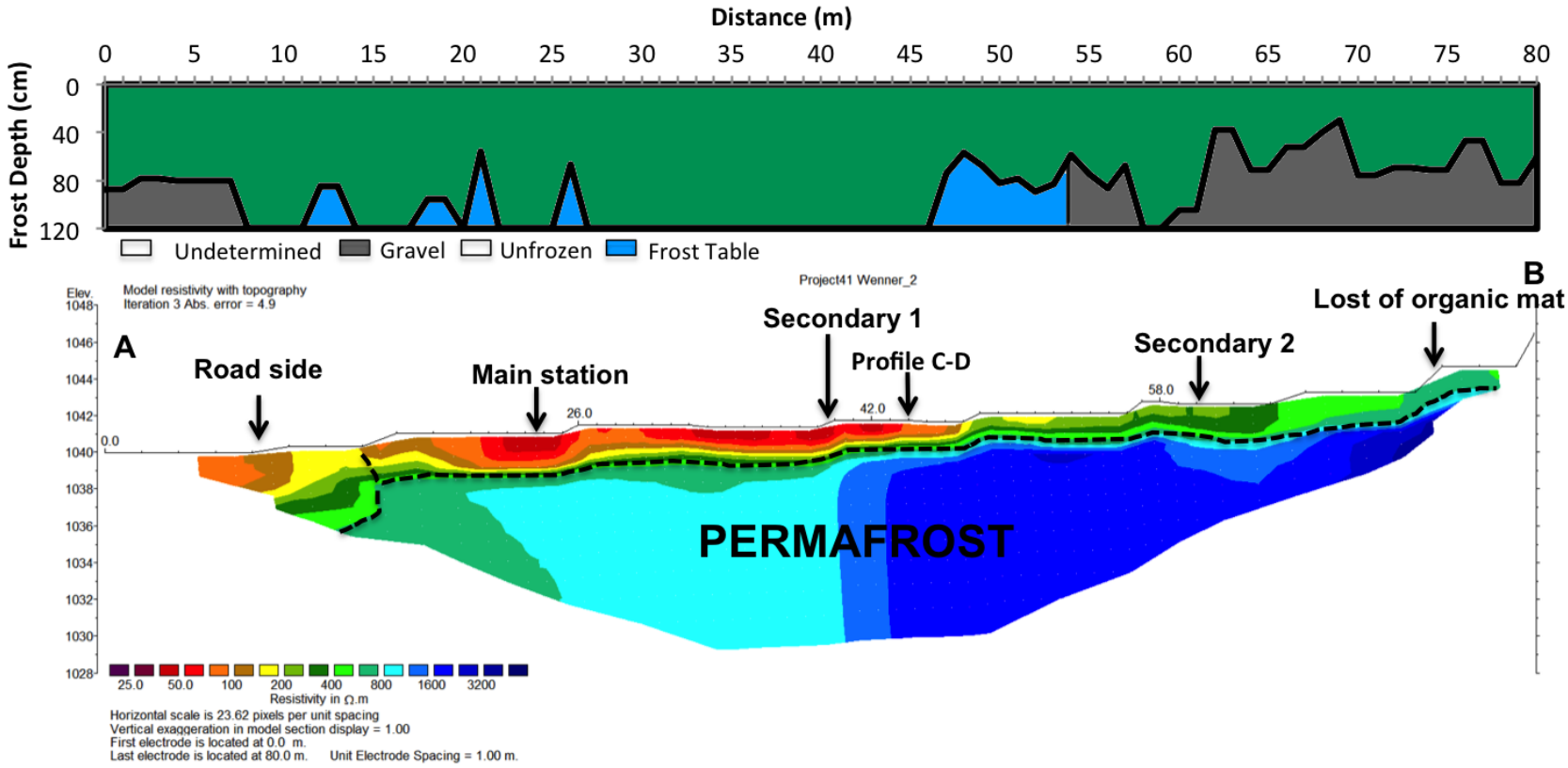


Figure D3: Modelled ERT inversion profile at MP 400 for the permanent array, with dashed lines representing inferred permafrost. The frozen/unfrozen boundary is taken to be 800 Ω m at this site.

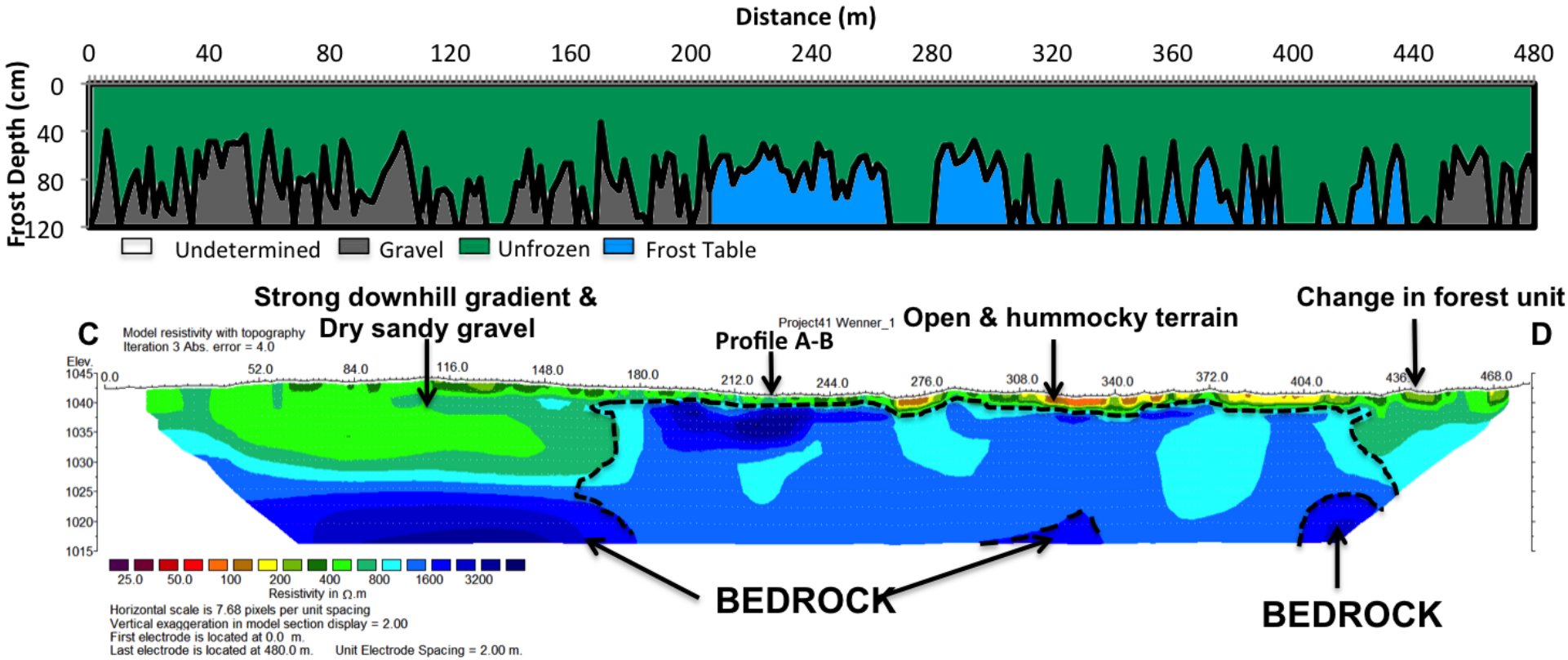


Figure D4: Modelled ERT inversion profile at MP 400 for the ERT 1, with dashed lines representing inferred permafrost. The frozen/unfrozen boundary is taken to be 800 Ω m at this site.

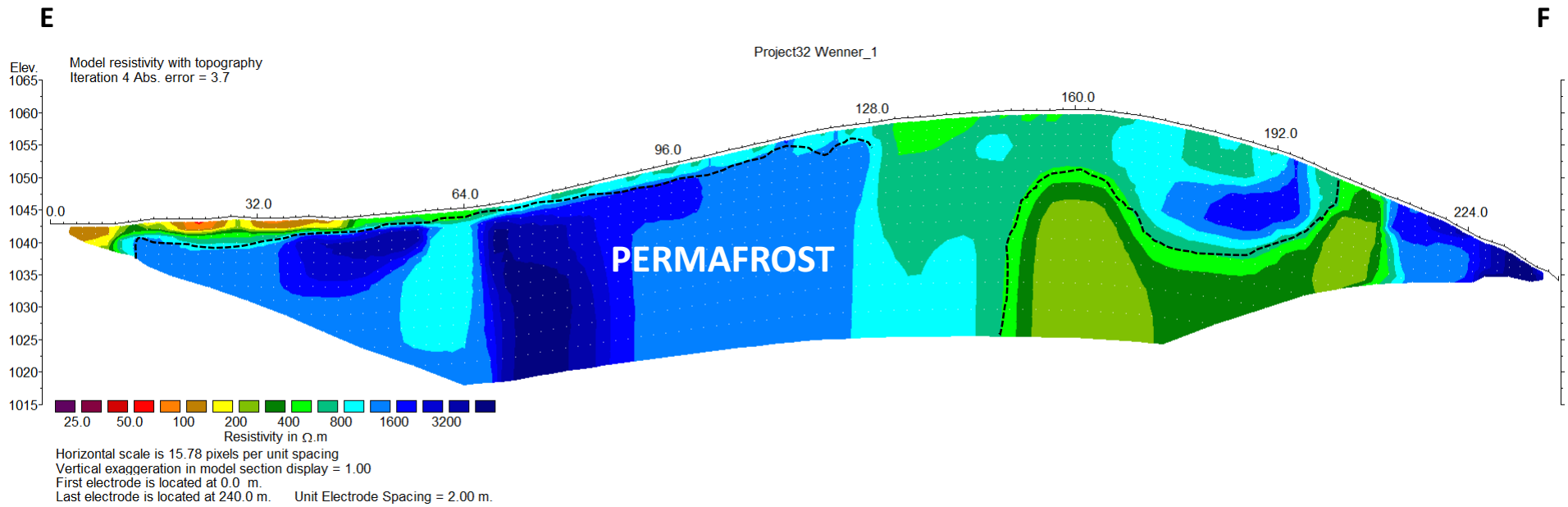


Figure D5: Modelled ERT inversion profile at MP 400 for the ERT 2, with dashed lines representing inferred permafrost. The frozen/unfrozen boundary is taken to be 800 Ω m at this site.

## Appendix E: MP 579

Table E1: Coordinates of the ERT lines at MP 579.

| | Transect starts | | Transect ends | |
|---|---|---|---|---|
| | Latitude | Longitude | Latitude | Longitude |
| Permanent array (A-B) | 59.96471 | -127.53196 | 59.96402 | -127.53170 |
| ERT 1 (C-D) | 59.96434 | -127.53260 | 59.96456 | -127.52980 |
| ERT 2 (E-F) | 59.96468 | -127.53043 | 59.96372 | -127.53157 |

Table E2: Annual Snow Depth Days values (SDD) (cm d) calculated for each station at MP 579.

| Years | Main (SDD) | Sub 1 (SDD) | Sub 2 (SDD) | Average |
|---|---|---|---|---|
| 2010-2011 | 7850 | 8240 | 8590 | 8230 |
| 2011-2012 | 7490 | 6870 | 7750 | 7370 |
| 2012-2013 | 9370 | 11570 | 11630 | 10850 |
| 2013-2014 | 11280 | 10190 | 12160 | 11210 |
| Average | 9000 | 9220 | 10030 | 9410 |

Table E3: Air and ground temperatures (°C) at MP 579. Missing data are represented as blank cells

| | | Main | | | | Sub 1 | | | | Sub 2 | | | |
|---|---|---|---|---|---|---|---|---|---|---|---|---|---|
| Years | MAAT | MAGST 1 | MAGST 2 | MAGT 50 cm | MAGT 100 cm | MAGST 1 | MAGST 2 | MAGT 50 cm | MAGT 100 cm | MAGST 1 | MAGST 2 | MAGT 50 cm | MAGT 100 cm |
| 2010-2011 | -2.8[A] | 0.1 | | | 0.5 | 0.2 | 1.7 | 0.1 | 0.1 | 1.3 | | | -0.2 |
| 2011-2012 | -1.9[A] | | | | | 2.3 | 3.2 | 0.5 | 0.5 | 2.7 | | | 0.2 |
| 2012-2013 | -2.8[A] | 0.4 | 0.6 | 1.1 | 0.6 | 3.0 | 2.9 | 1.0 | 0.6 | 2.4 | 2.8 | | 0.3 |
| Average | -2.5 | 0.3 | 0.6 | 1.1 | 0.5 | 1.8 | 2.6 | 0.5 | 0.4 | 2.1 | 2.8 | | 0.1 |

[A] MAAT presented are from the neighbouring site MP 597, due to serious repeated logger malfunction

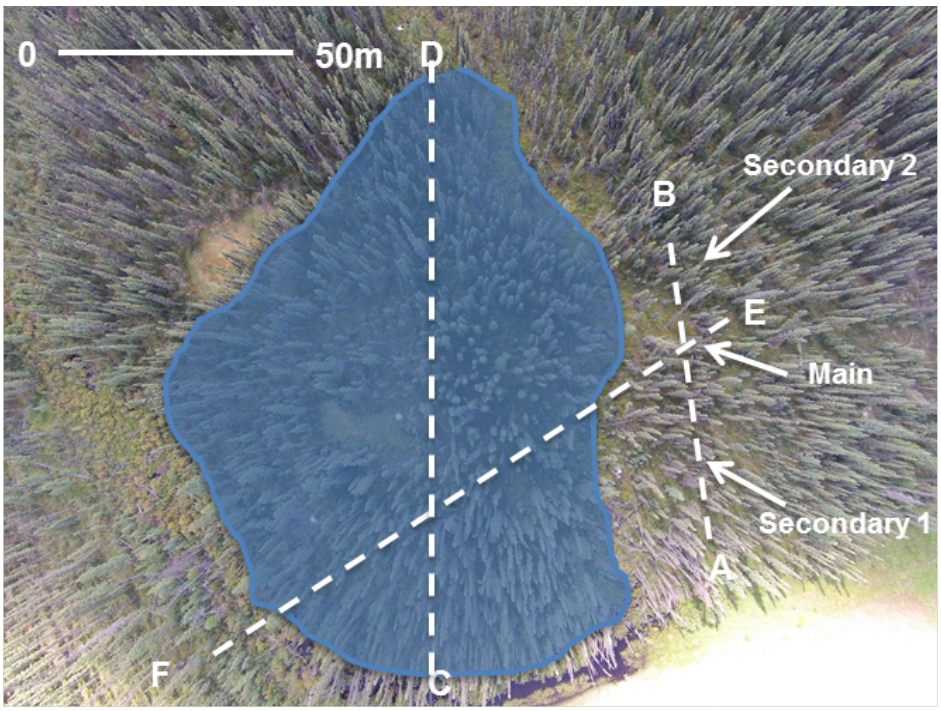


Figure E1: Air photo for MP 579 in 2014. Shaded ellipses represent permafrost patches; dashed lines represent ERT transects and climate monitoring instruments locations are marked. The scale is approximate.

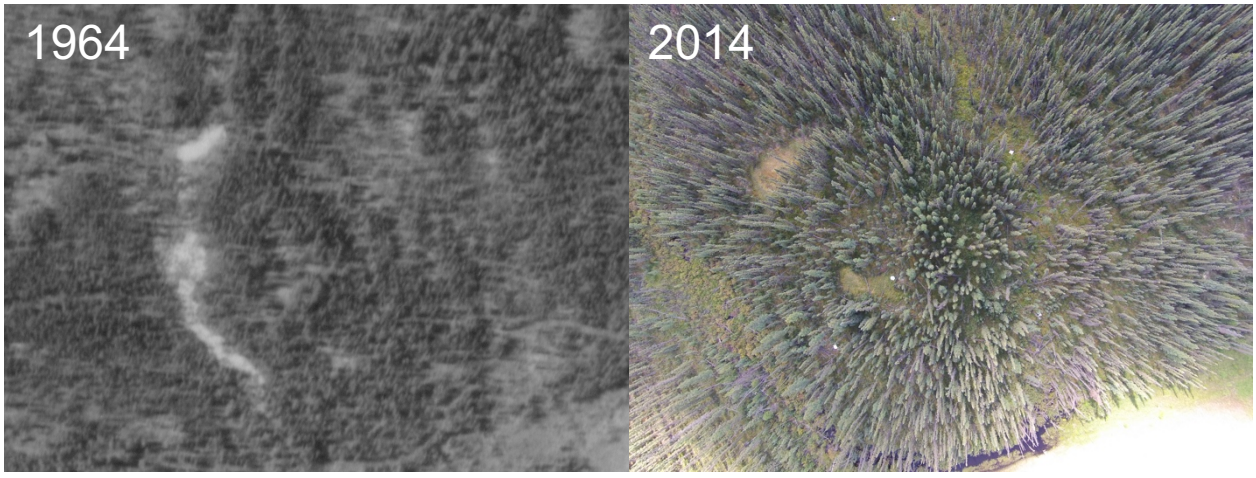


Figure E2: MP 579 Historic air photo analysis from field site in 1964-2014.

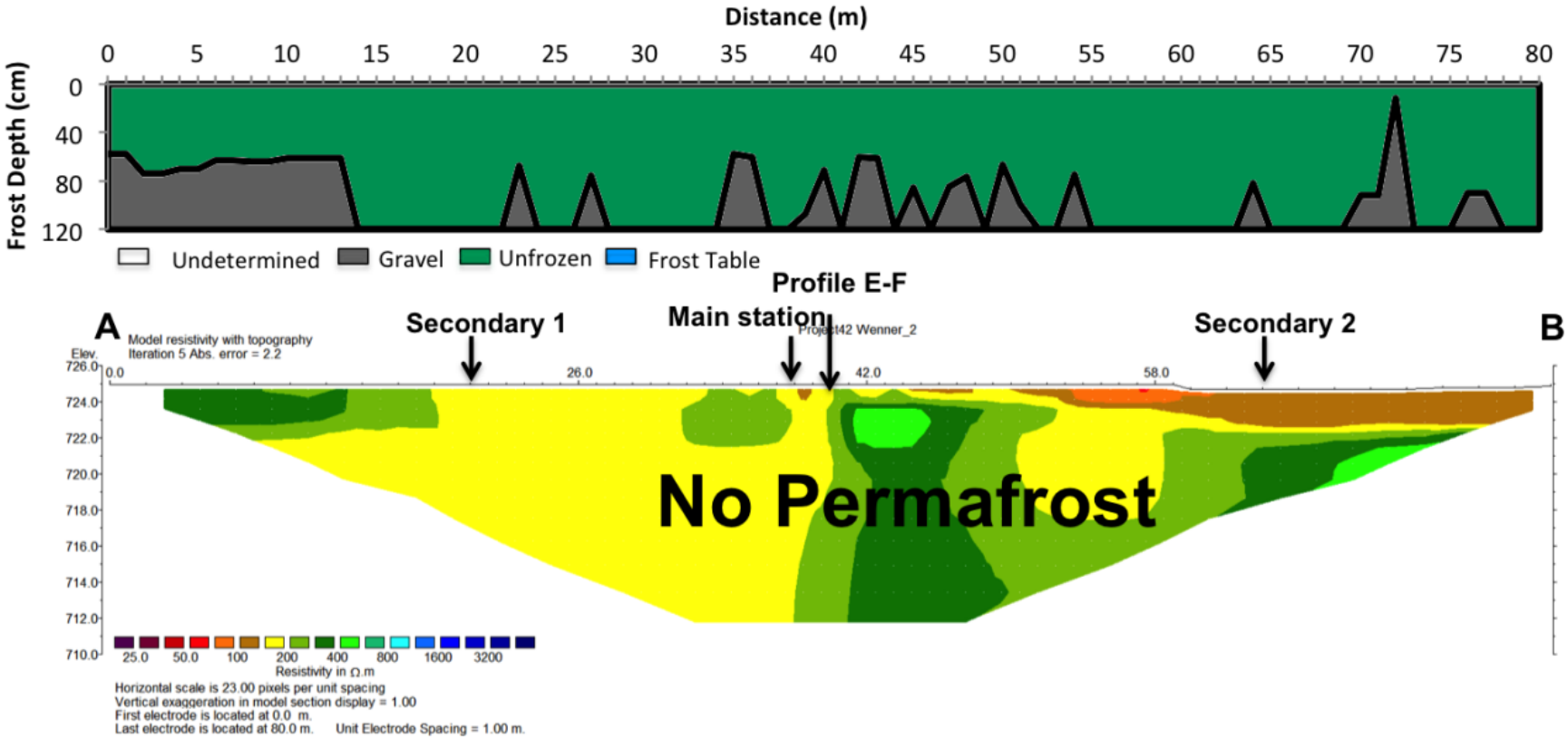


Figure E3: Modelled ERT inversion profile at MP 579 for the permanent array, with dashed lines representing inferred permafrost. The frozen/unfrozen boundary is taken to be 800 Ω m at this site.

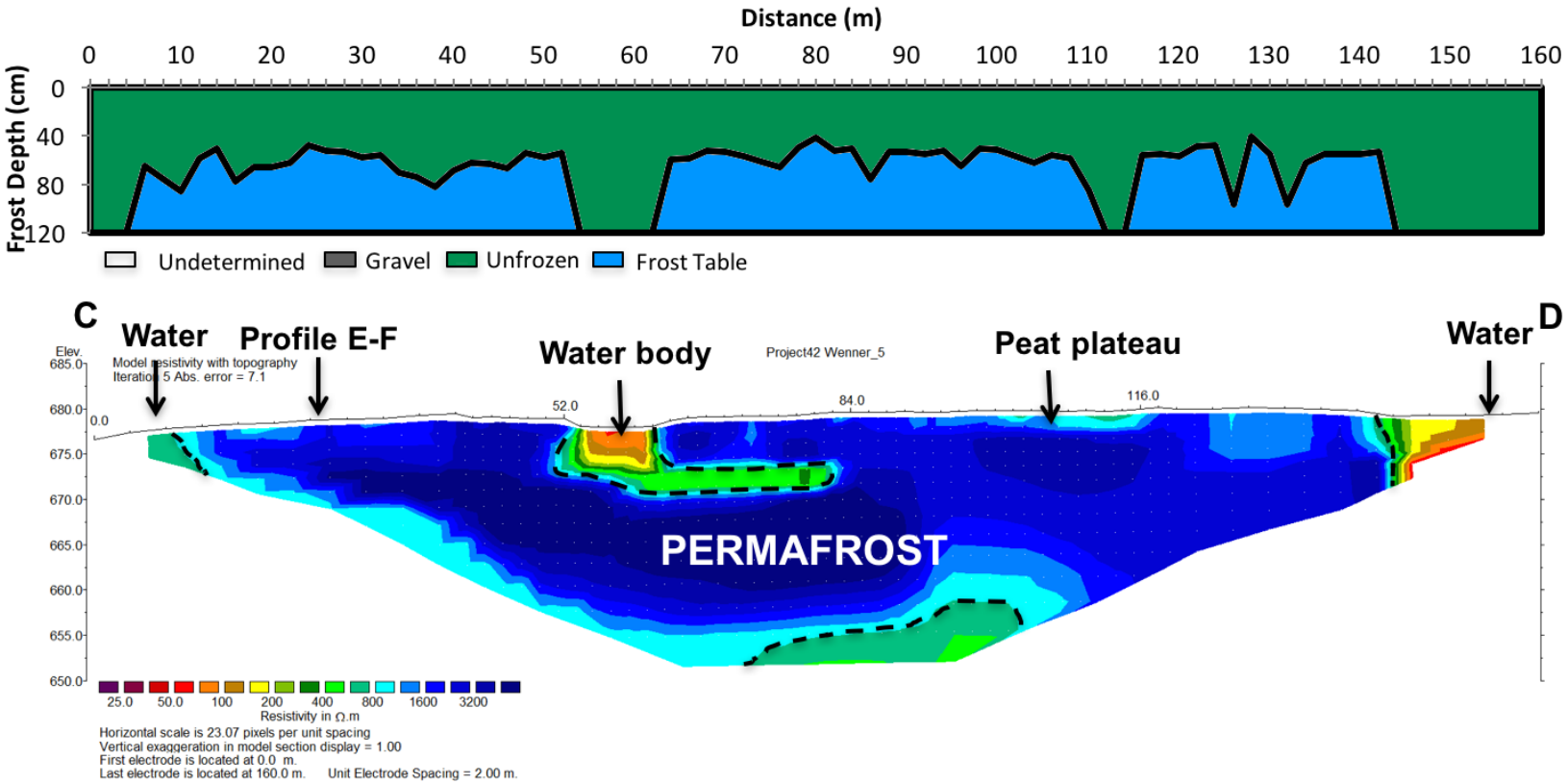


Figure E4: Modelled ERT inversion profile at MP 579 for the ERT 1, with dashed lines representing inferred permafrost. The frozen/unfrozen boundary is taken to be 800 Ω m at this site.

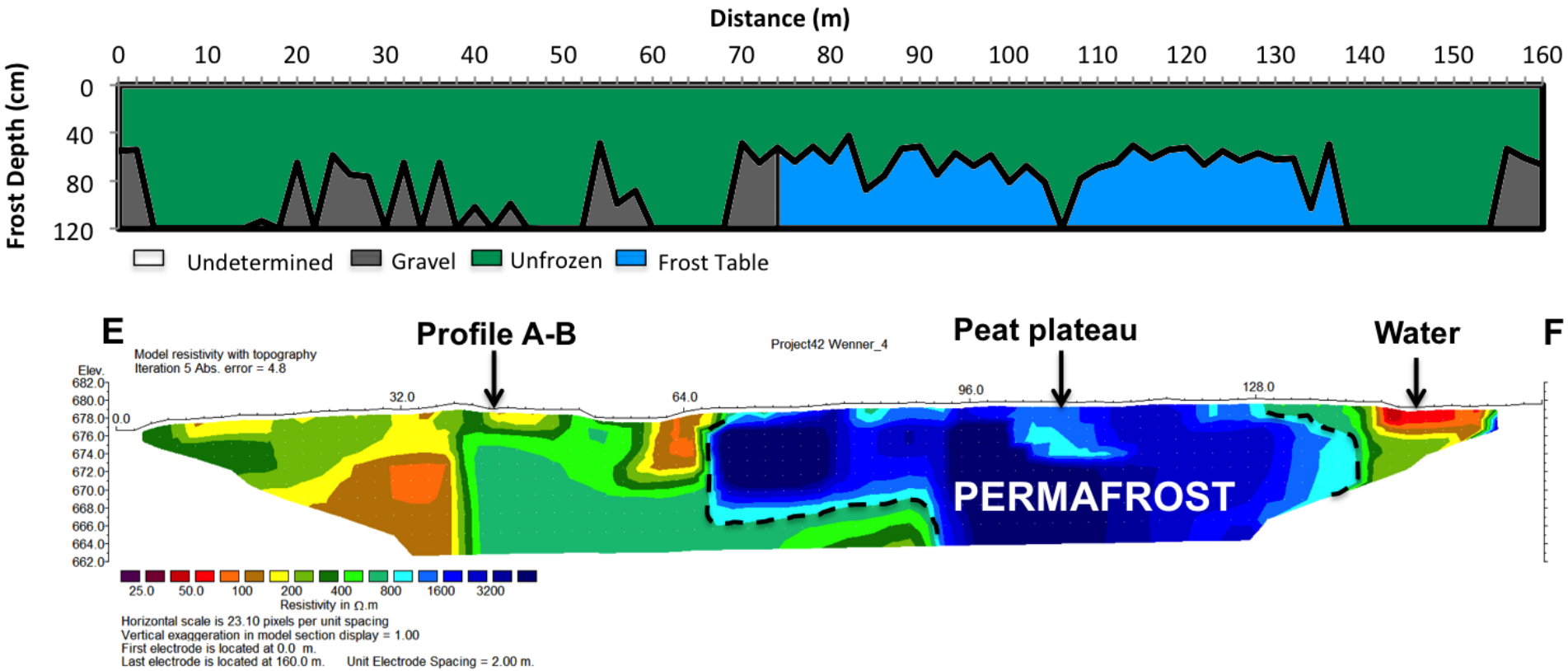


Figure E5: Modelled ERT inversion profile at MP 579 for the ERT 2, with dashed lines representing inferred permafrost. The frozen/unfrozen boundary is taken to be 800 Ω m at this site.

## Appendix F: MP 597

Table F1: Coordinates of the ERT lines at MP 597.

| | Transect starts | | Transect ends | |
|---|---|---|---|---|
| | Latitude | Longitude | Latitude | Longitude |
| Permanent array with extension (A-B) | 59.9959 | -127.95525 | 59.99533 | -127.95444 |
| ERT 1 (C-D) | 59.99518 | -127.95583 | 59.99604 | -127.95359 |

Table F2: Annual Snow Depth Days values (SDD) (cm d) calculated for each station at MP 597.

| Years | Main (SDD) | Sub 1 (SDD) | Sub 2 (SDD) | Average |
|---|---|---|---|---|
| 2010-2011 | 6740 | 7340 | 6450 | 6850 |
| 2011-2012 | 6980 | 6980 | 7620 | 7190 |
| 2012-2013 | 11120 | 9050 | 10510 | 10230 |
| 2013-2014 | 11490 | 8580 | 9070 | 9720 |
| Average | 9080 | 7990 | 8410 | 8490 |

Table F3: Air and ground temperatures (°C) at MP 597. Missing data are represented as blank cells.

| | | Main | | | Sub 1 | | | | Sub 2 | | | |
|---|---|---|---|---|---|---|---|---|---|---|---|---|
| Years | MAAT | MAGST 1 | MAGST 2 | MAGT 100 cm | MAGST 1 | MAGST 2 | MAGT 40 cm | MAGT 50 cm | MAGST 1 | MAGST 2 | MAGT 50 cm | MAGT 100 cm |
| 2010-2011 | -2.8 | 1.2 | 0.4 | 0.7 | 2.1 | 1.7 | 0.1 | -0.1 | | 1.6 | | -0.3 |
| 2011-2012 | -1.9 | 1.2 | 1.1 | -0.1 | 2.1 | | | -0.1 | 2.0 | 1.9 | -0.1 | -0.2 |
| 2012-2013 | -2.8 | 2.0 | 2.0 | 0.1 | 2.3 | 0.9 | 0.0 | -0.1 | 1.4 | 2.3 | 0.0 | -0.2 |
| Average | -2.5 | 1.5 | 1.2 | 0.2 | 2.1 | 1.3 | 0.1 | -0.1 | 1.7 | 1.9 | -0.1 | -0.2 |

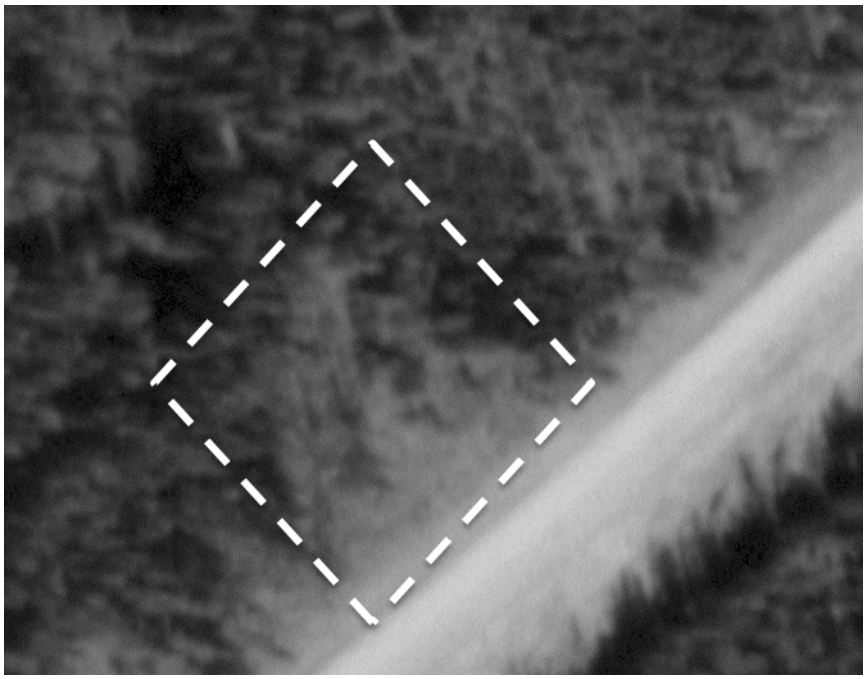

Figure F1: Air photo for MP 597 in 1964. Dashed square represents the study area.

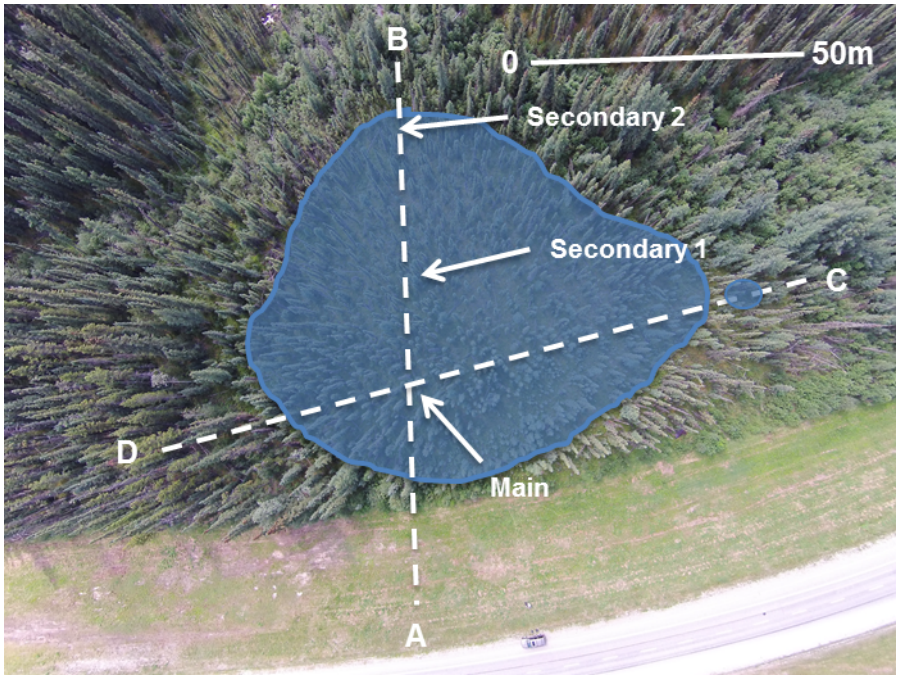


Figure F2: Air photo for MP 597 in 2014. Shaded ellipses represent permafrost patches; dashed lines represent ERT transects and climate monitoring instruments locations are marked. The scale is approximate.

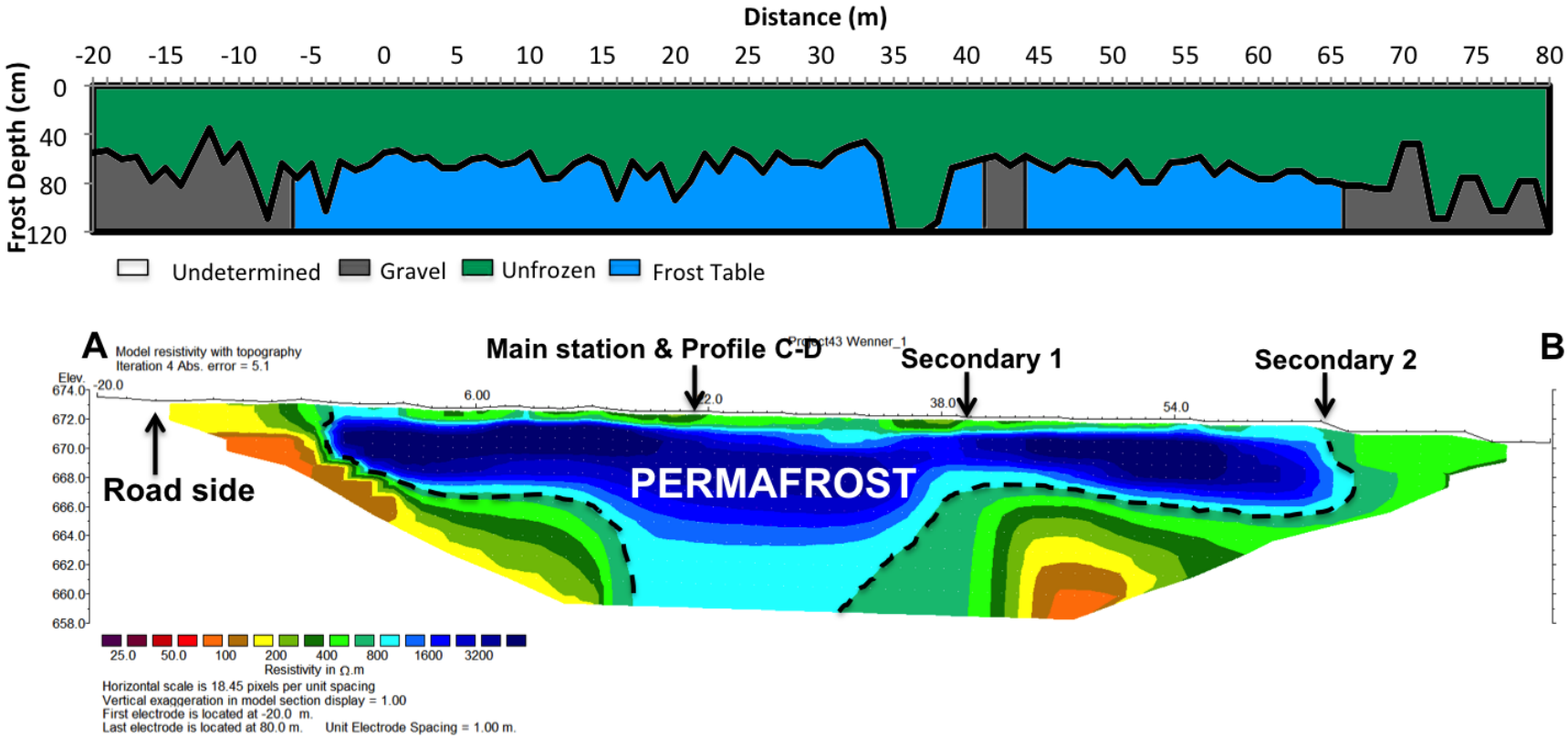


Figure F3: Modelled ERT inversion profile at MP 597 for the permanent array with extension, with dashed lines representing inferred permafrost. The frozen/unfrozen boundary is taken to be 800 Ω m at this site.

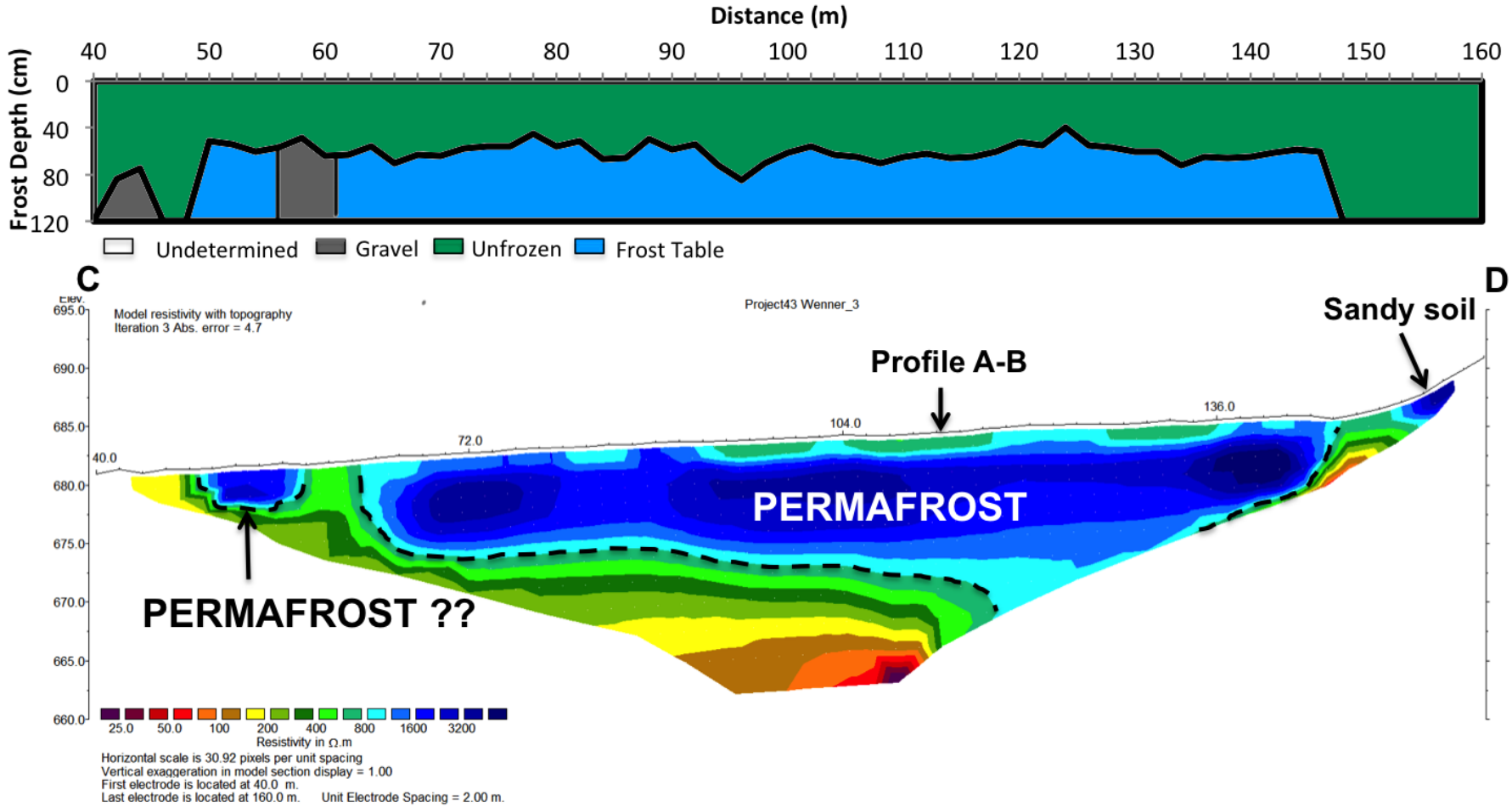


Figure F4: Modelled ERT inversion profile at MP 579 for the ERT 1, with dashed lines representing inferred permafrost. The frozen/unfrozen boundary is taken to be 800 Ω m at this site

## Appendix G: MP 681

Table G1: Coordinates of the ERT lines at MP 681.

| | Transect starts | | Transect ends | |
|---|---|---|---|---|
| | Latitude | Longitude | Latitude | Longitude |
| Permanent array with extension (A-B) | 60.18810 | -129.89973 | 60.18849 | -129.89905 |
| ERT 1 (C-D) | 60.18865 | -129.90004 | 60.18827 | -129.89757 |

Table G2: Annual Snow Depth Days values (SDD) (cm d) calculated for each station at MP 681.

| Years | Main (SDD) | Sub 1 (SDD) | Sub 2 (SDD) | Average |
|---|---|---|---|---|
| 2010-2011 | 8890 | 8160 | 8480 | 8510 |
| 2011-2012 | 9690 | 7740 | 7720 | 8380 |
| 2012-2013 | 10450 | 11200 | 9570 | 10400 |
| 2013-2014 | 9880 | 11670 | 7600 | 9720 |
| Average | 9730 | 9690 | 8340 | 9250 |

Table G3: Air and ground temperatures (°C) at MP 681. Missing data are represented as blank cells.

| | | Main | | Sub 1 | | | Sub 2 | | |
|---|---|---|---|---|---|---|---|---|---|
| Years | MAAT | MAGST | MAGT 50 cm | MAGST | MAGT 65 cm | MAGST 1 | MAGST 2 | MAGT 25 cm | MAGT 65 cm |
| 2010-2011 | -3.3[A] | 0.5 | -0.5 | 1.0 | -0.3 | 1.4 | | 0.9 | |
| 2011-2012 | -3.0[B] | 0.4 | -0.3 | 1.2 | 0.4 | 1.4 | 1.6 | 0.4 | 0.5 |
| 2012-2013 | -3.7[B] | | 0.0 | 2.6 | | 2.3 | 2.6 | 1.1 | 0.8 |
| Average | -3.3 | 0.5 | -0.3 | 1.6 | 0.0 | 1.7 | 2.1 | 0.8 | 0.6 |

[A] Missing data in 2010-2011 estimated through correlation with Watson Lake Environment Canada station and blended with reliable data from MP 681.

[B] Missing data in 2011-2012 and 2012-2013 estimated through correlation with MP 597 station (neighbouring site) and blended with reliable data from MP 681

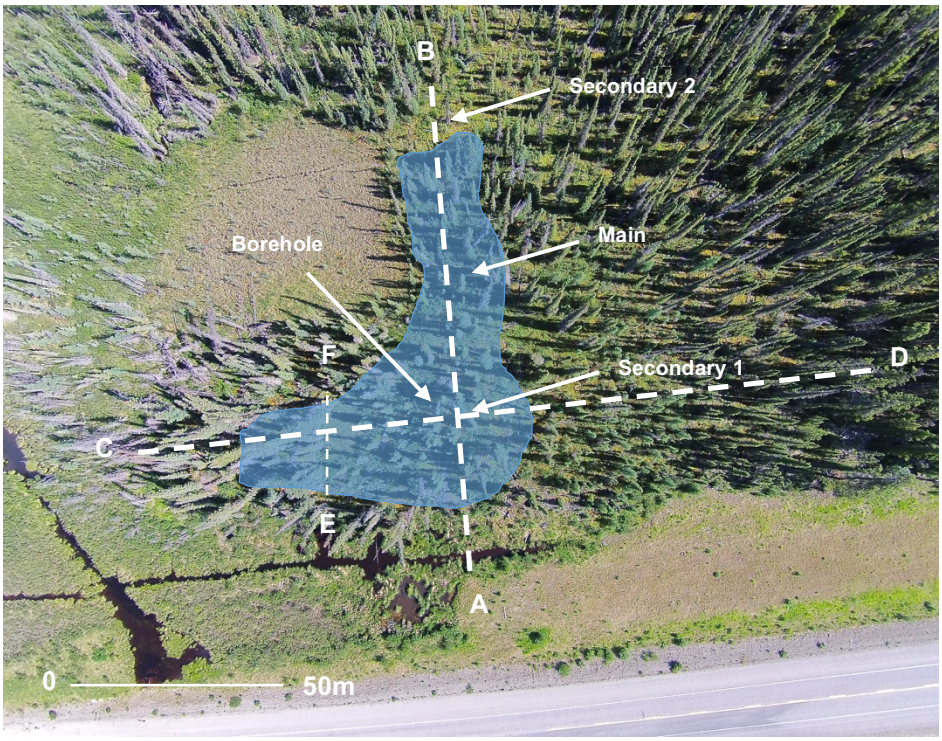


Figure G1: Air photo for MP 681 in 2014. Shaded ellipses represent permafrost patches; dashed lines represent ERT or frost probing transects and climate monitoring instruments locations are marked. The scale is approximate.

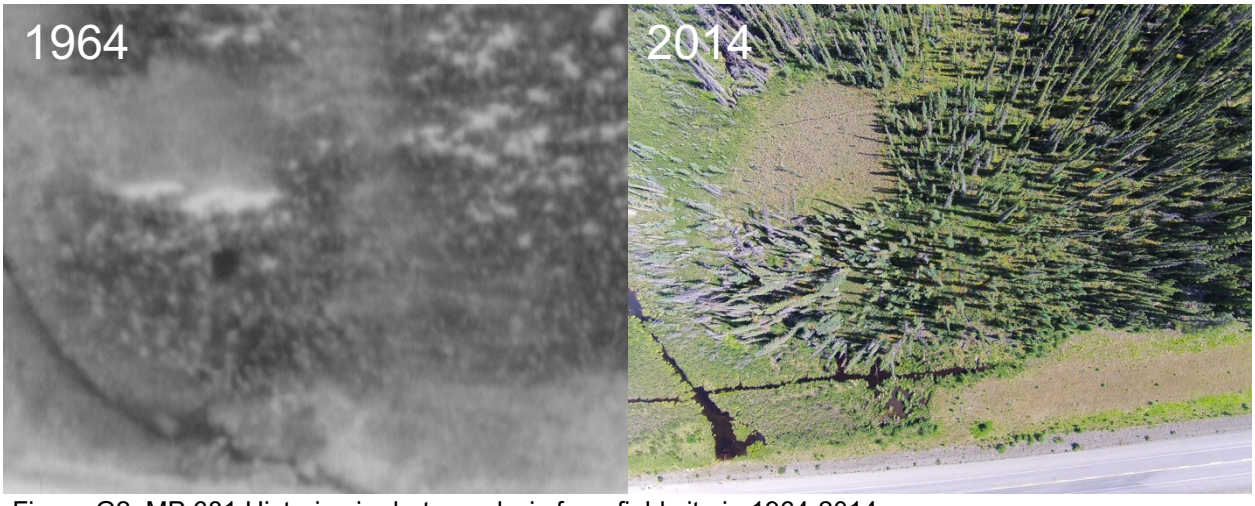


Figure G2: MP 681 Historic air photo analysis from field site in 1964-2014.

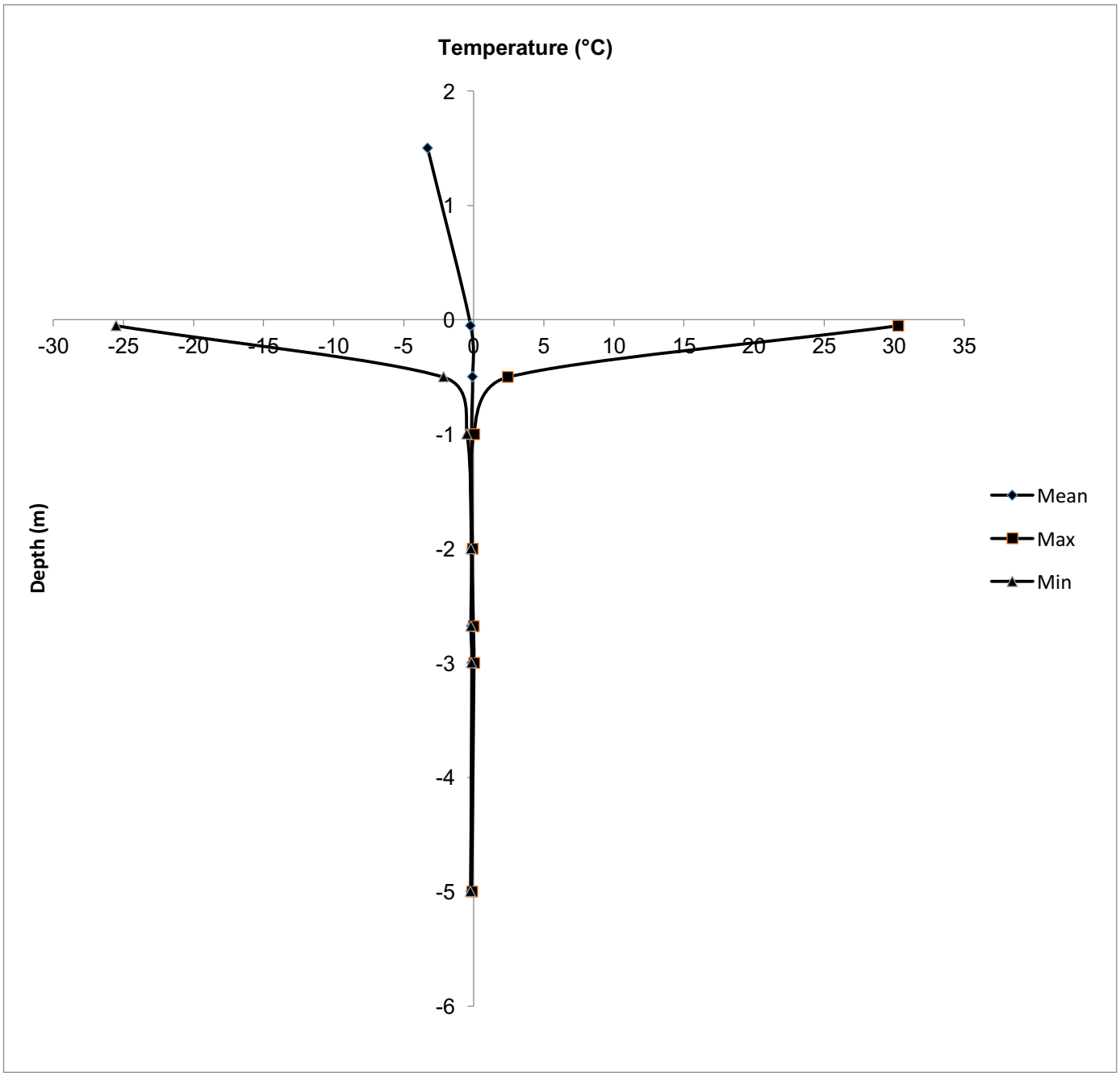


Figure G3: Temperature envelope for the borehole at MP 681 (2013-2014). The temperature at the base of the borehole at 5 m is -0.2°C.

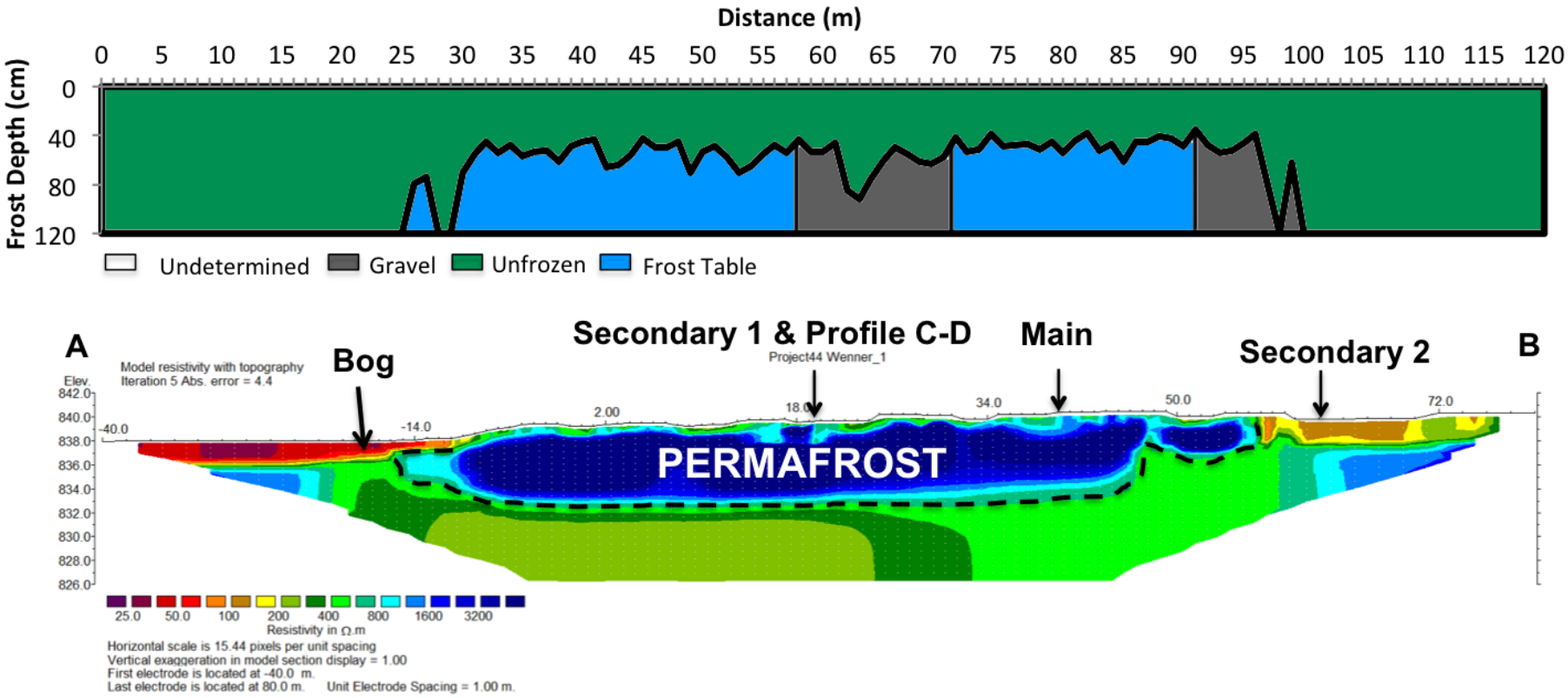


Figure G4: Modelled ERT inversion profile at MP 681 for the permanent array with extension, dashed lines representing inferred permafrost. The frozen/unfrozen boundary is taken to be 800 Ω m at this site.

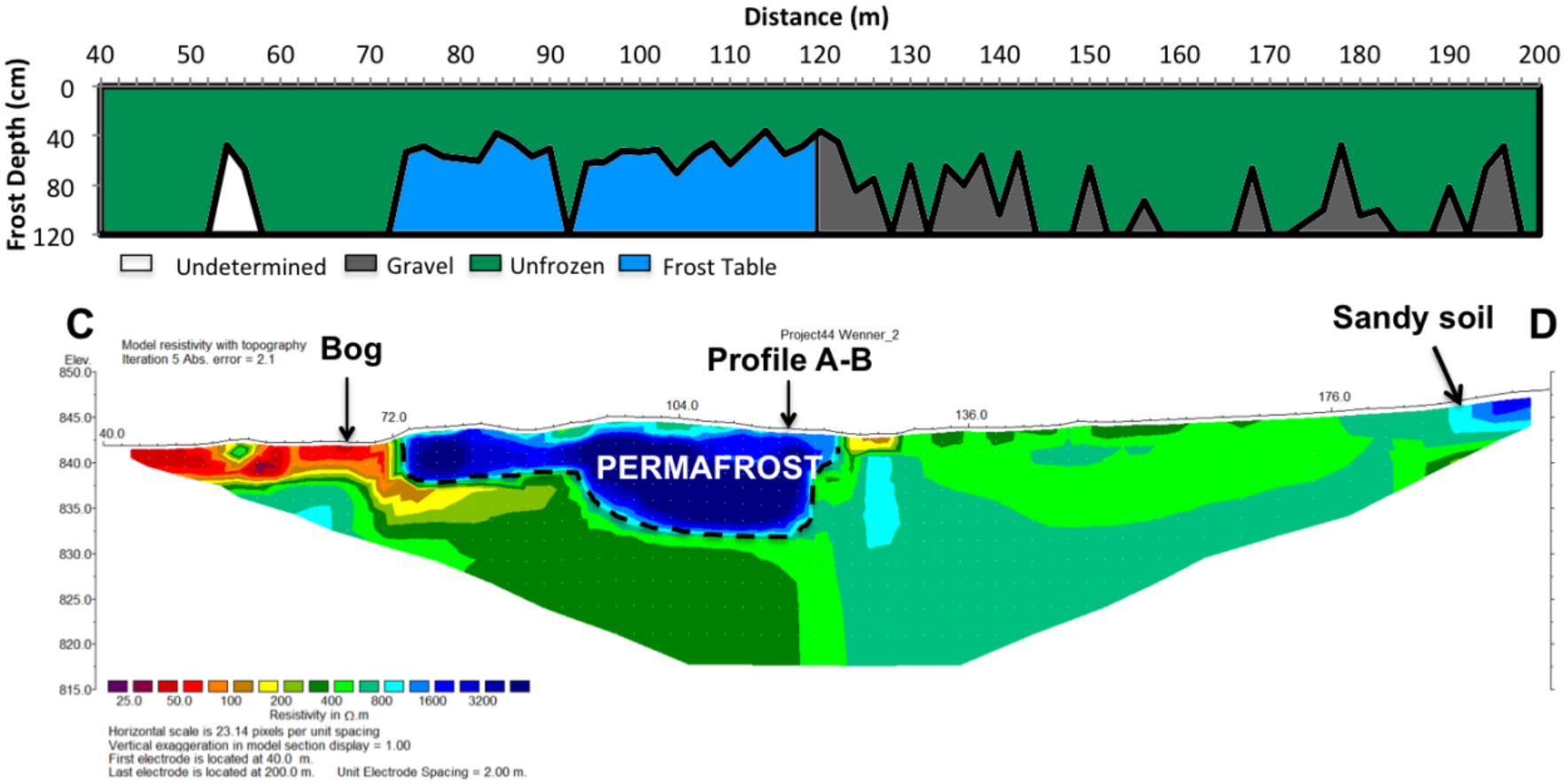


Figure G5: Modelled ERT inversion profile at MP 681 for the ERT 1, with dashed lines representing inferred permafrost. The frozen/unfrozen boundary is taken to be 800 Ω m at this site.

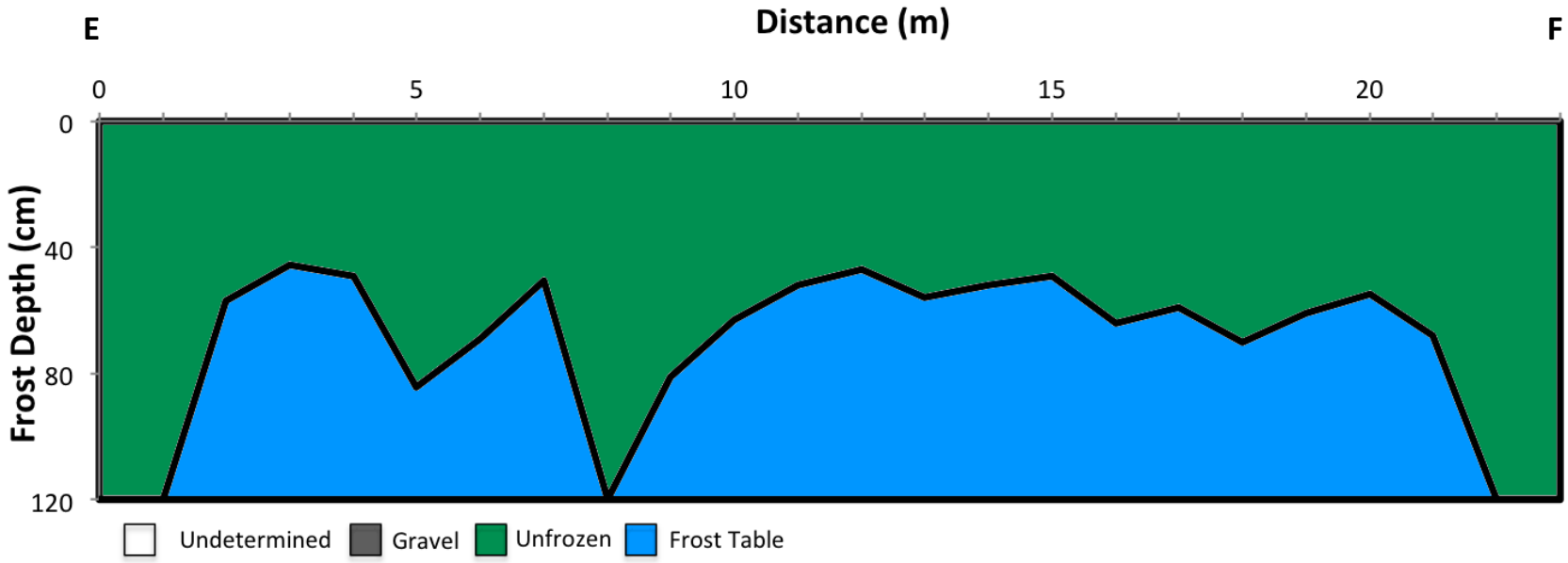


Figure G6: Frost probing survey at MP 681 next to secondary station 1.

## Appendix H: MP 788

Table H1: Coordinates of the ERT lines at MP 788.

| | Transect starts | | Transect ends | |
|---|---|---|---|---|
| | Latitude | Longitude | Latitude | Longitude |
| Permanent array (A-B) | 60.09064 | -132.36815 | 60.09131 | -132.36867 |
| ERT 1 (C-D) | 60.09108 | -132.36826 | 60.09069 | -132.36920 |
| ERT 2 (E-F) | 60.09114 | -132.36838 | 60.09126 | -132.37053 |

Table H2: Annual Snow Depth Days values (SDD) (cm d) calculated for each station at MP 788.

| Years | Main (SDD) | Sub 1 (SDD) | Sub 2 (SDD) | Average |
|---|---|---|---|---|
| 2010-2011 | 4390 | 5090 | 8350 | 5950 |
| 2011-2012 | 4050 | 6030 | 8390 | 6150 |
| 2012-2013 | 3590 | 5480 | 7320 | 5460 |
| 2013-2014 | 7270 | 6150 | 6850 | 6760 |
| Average | 4820 | 5690 | 7730 | 6080 |

Table H3: Air and ground temperatures (°C) at MP 788. Missing data are represented as blank cells.

| | | Main | | | | | Sub 1 | | | Sub 2 | | |
|---|---|---|---|---|---|---|---|---|---|---|---|---|
| Years | MAAT | MAGST | MAGT 50 cm | MAGT 100 cm | MAGST 1 | MAGST 2 | MAGT 50 cm | MAGT 100 cm | MAGST 1 | MAGST 2 | MAGT 50 cm | MAGT 100 cm |
| 2010-2011 | -2.1 | 1.9 | -0.2 | -0.1 | | | 3.3 | | 2.0 | 2.0 | 0.0 | -0.1 |
| 2011-2012 | -0.3 | 2.5 | 0.0 | | | | | | | | | |
| 2012-2013 | -1.1 | 2.7 | -0.1 | -0.1 | 3.5 | | | 1.3 | 2.7 | | | -0.1 |
| Average | -1.1 | 2.4 | -0.1 | -0.1 | 3.5 | | 3.3 | 1.3 | 2.3 | 2.0 | 0.0 | -0.1 |

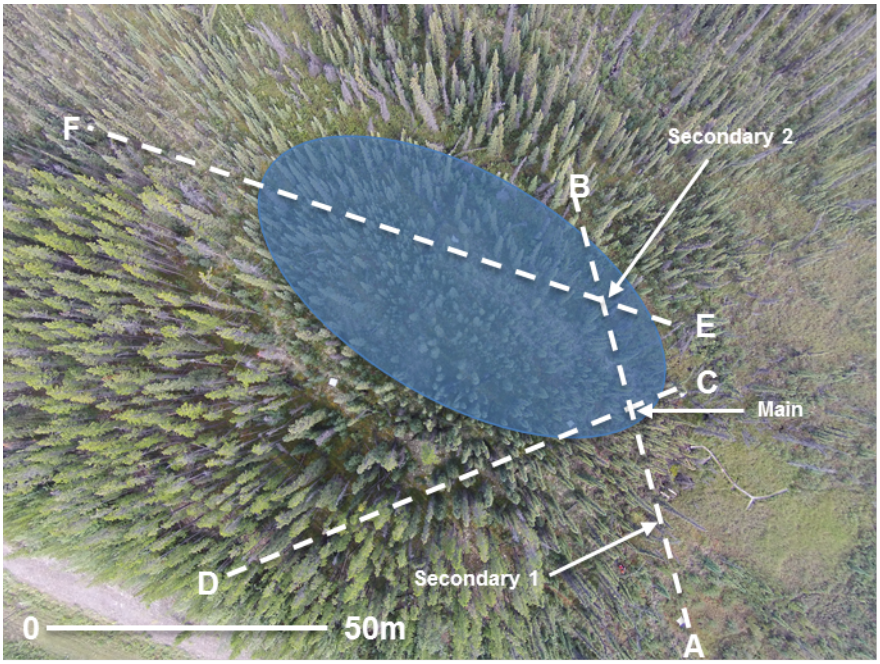


Figure H1: Air photo for MP 788 in 2014. Shaded ellipses represent permafrost patches; dashed lines represent ERT transects and climate monitoring instruments locations are marked. The scale is approximate.

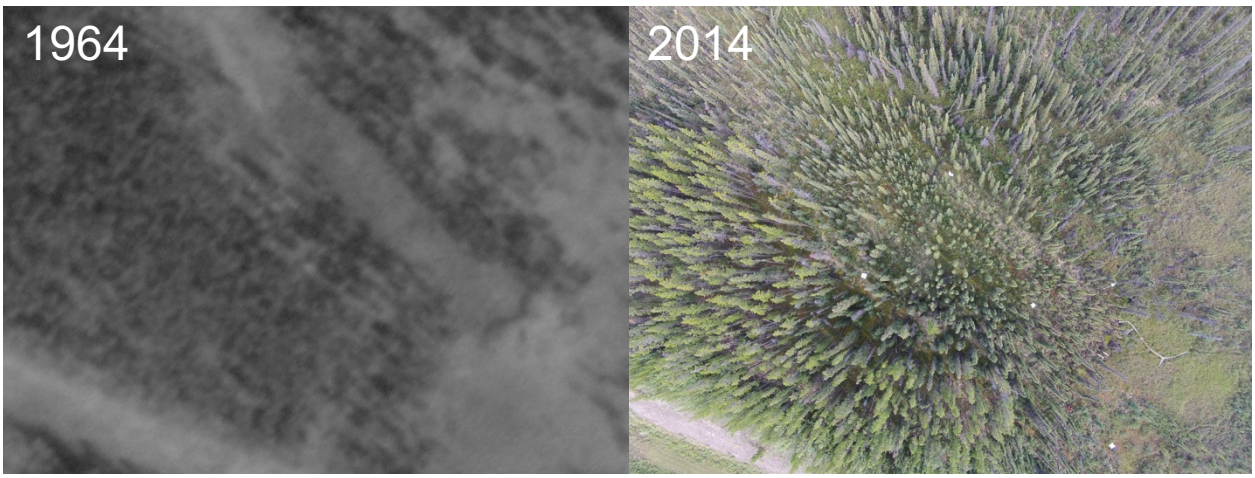


Figure H2: MP 788 Historic air photo analysis from field site in 1964-2014.

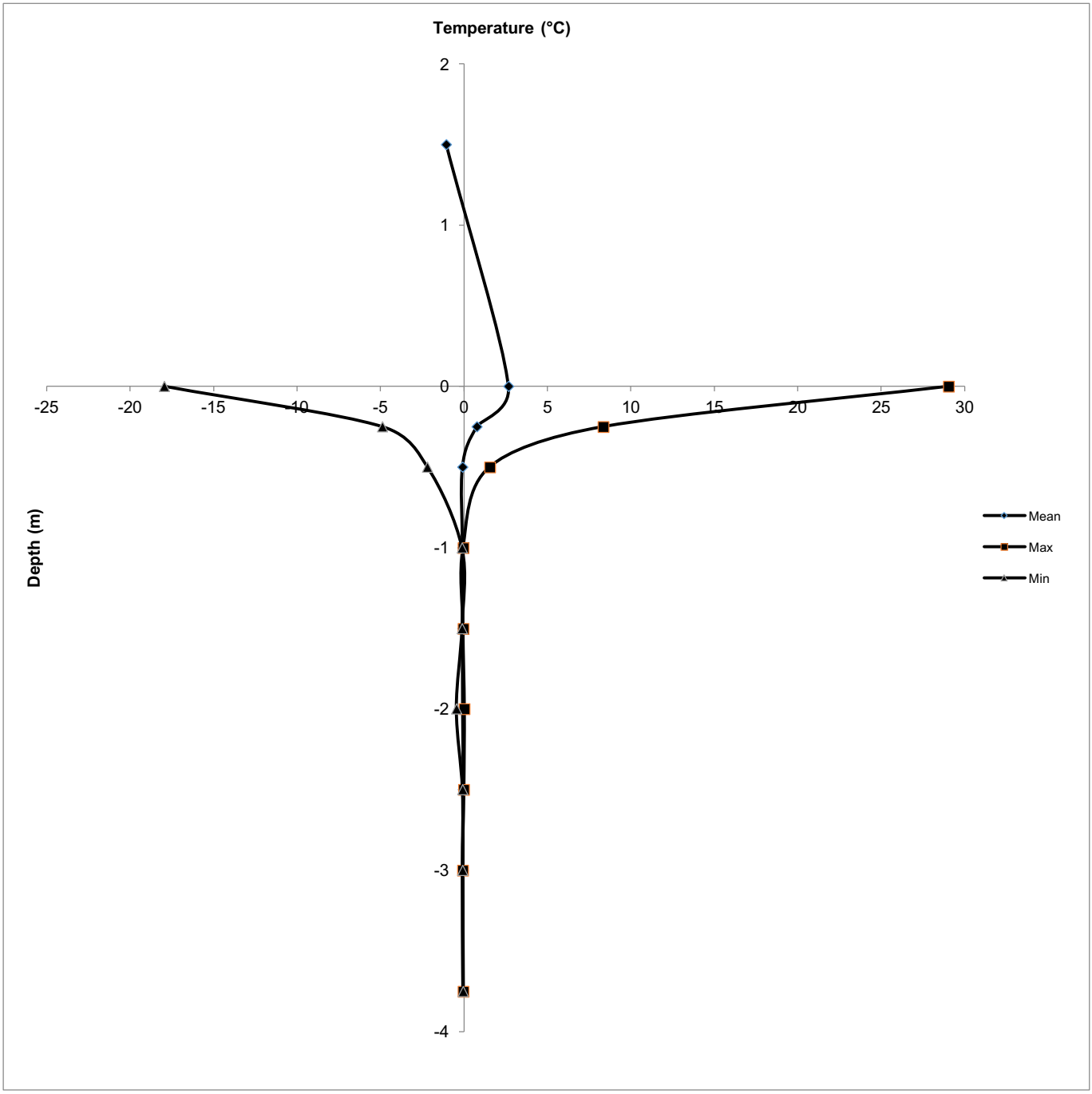


Figure H3: Temperature envelope for borehole at MP 788 (2013-2014). The temperature at the base of the borehole at 3.75 m is -0.1°C

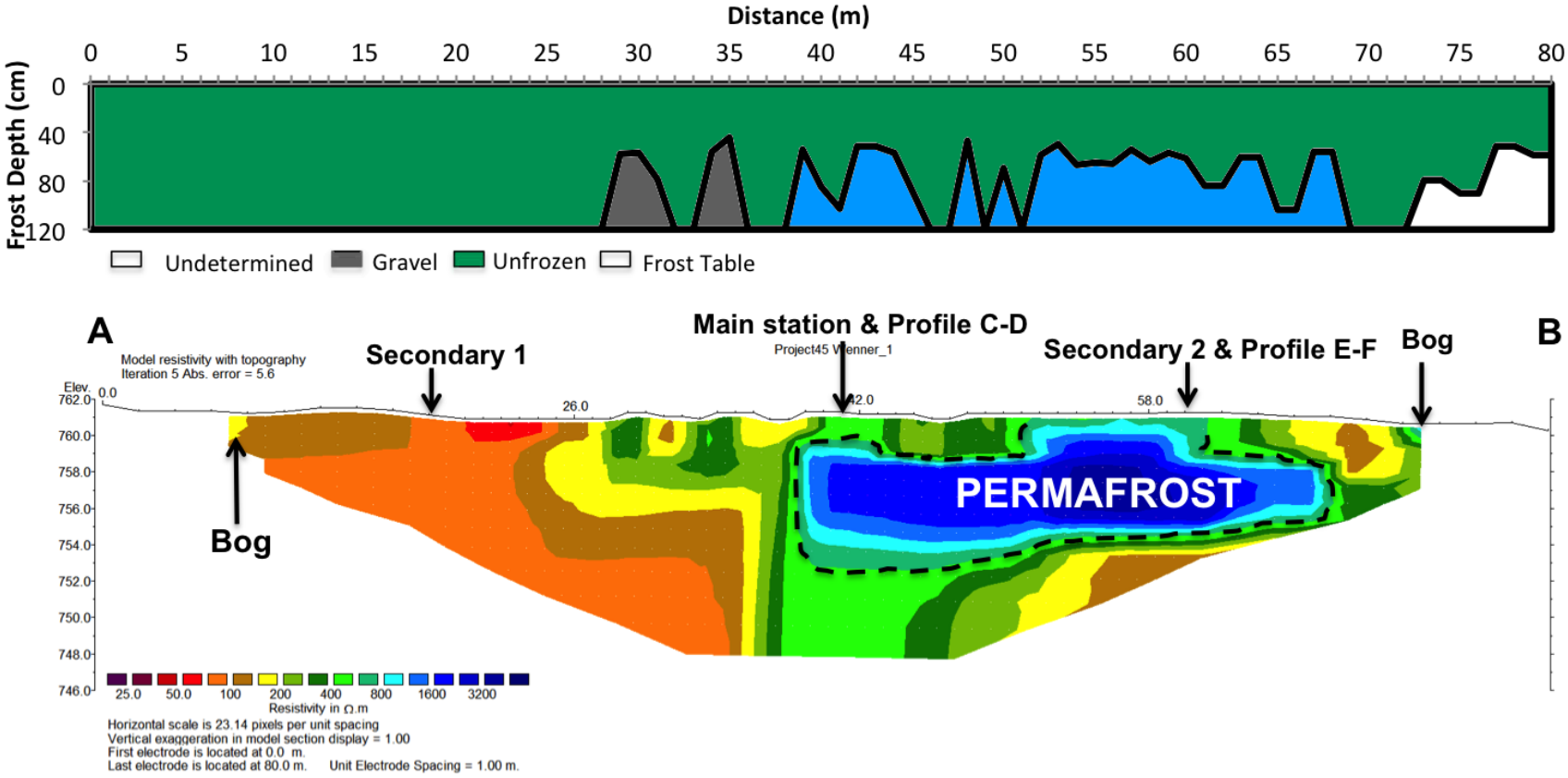


Figure H4: Modelled ERT inversion profile at MP 788 for the permanent array, with dashed lines representing inferred permafrost. The frozen/unfrozen boundary is taken to be 800 Ω m at this site.

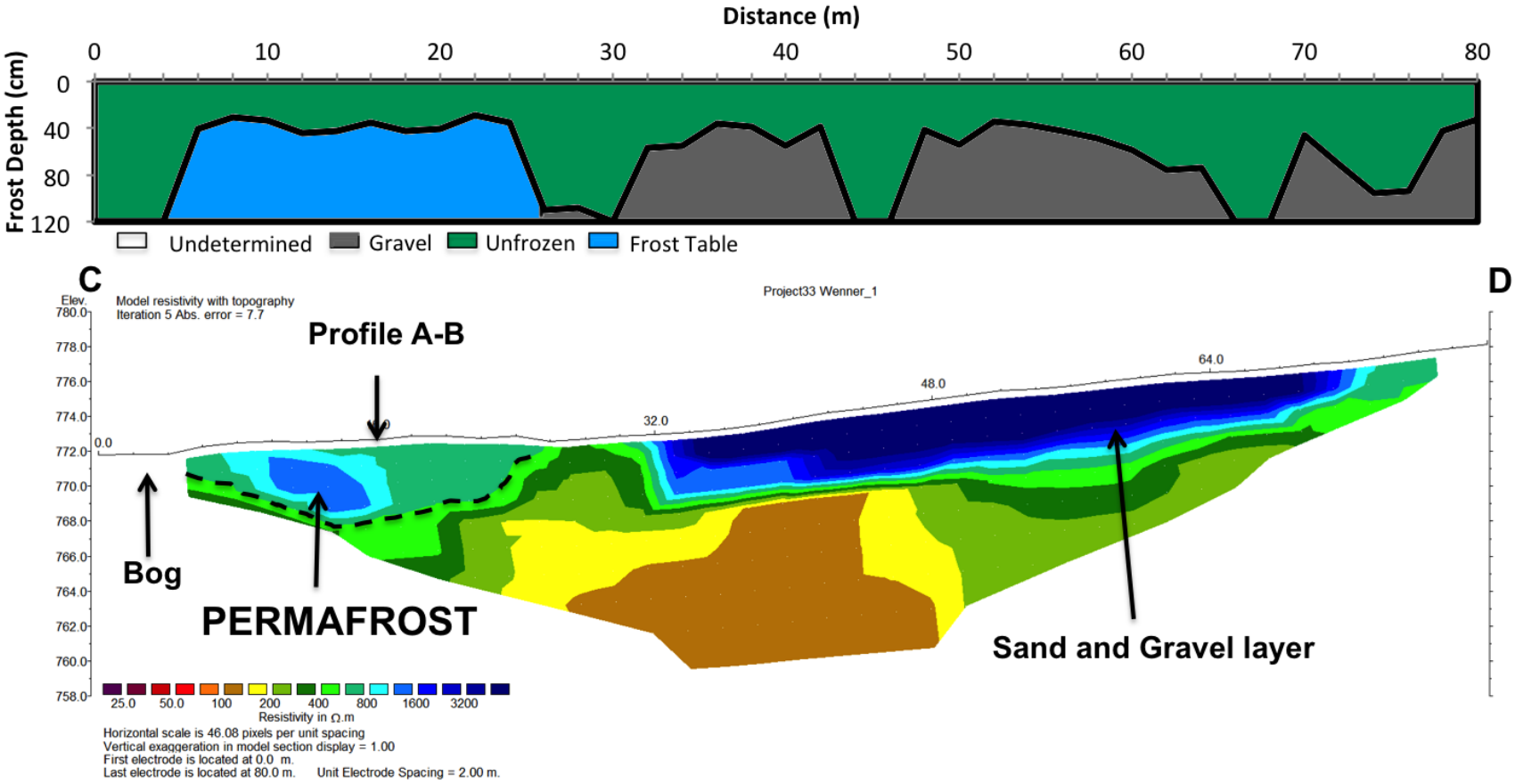


Figure H5: Modelled ERT inversion profile at MP 788 for the ERT 1, with dashed lines representing inferred permafrost. The frozen/unfrozen boundary is taken to be 800 Ω m at this site.

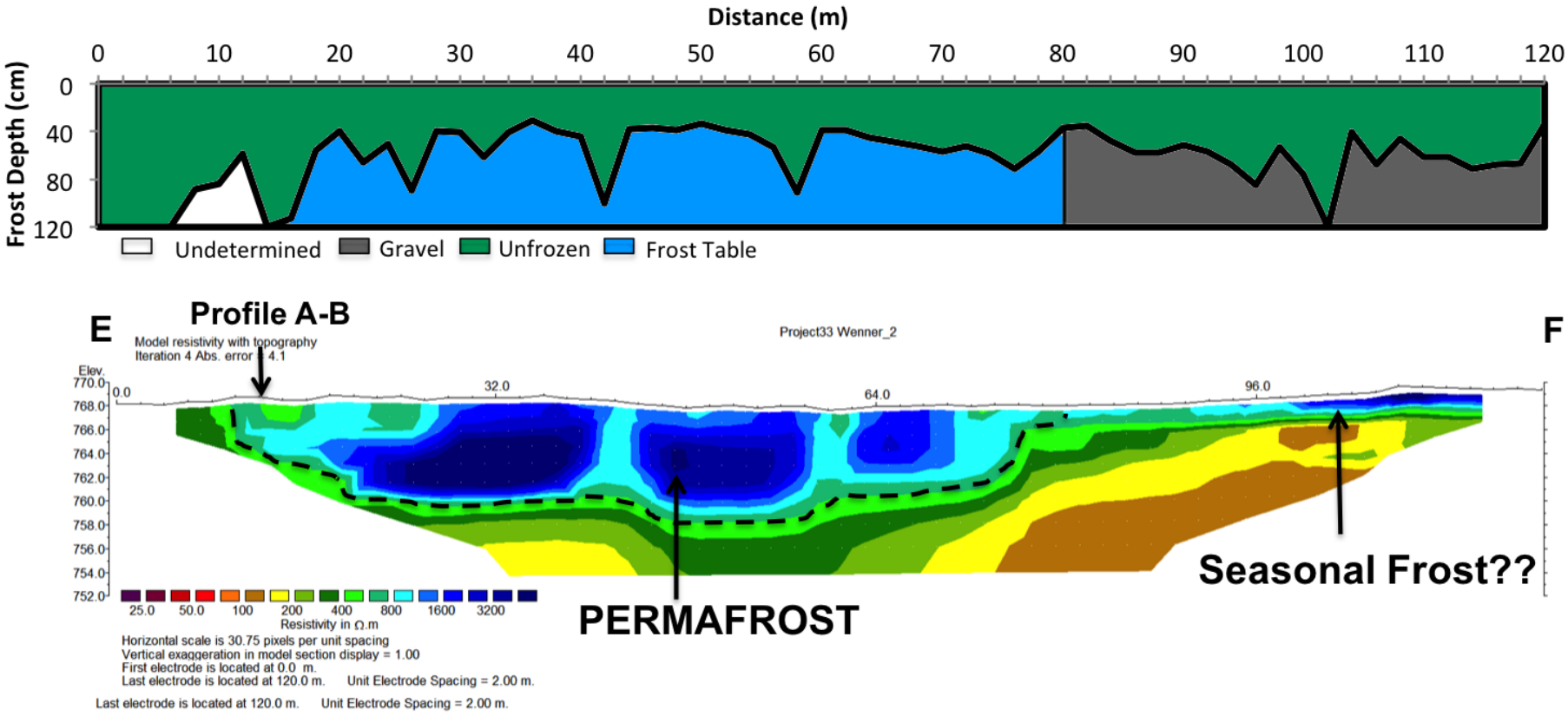


Figure H6: Modelled ERT inversion profile at MP 788 for the ERT 2, with dashed lines representing inferred permafrost. The frozen/unfrozen boundary is taken to be 800 Ω m at this site.

## Appendix I: MP 825

Table I1: Coordinates of the ERT lines at MP 825.

| | Transect starts | | Transect ends | |
|---|---|---|---|---|
| | Latitude | Longitude | Latitude | Longitude |
| Permanent array (A-B) | 60.37161 | -133.11101 | 60.37196 | -133.10980 |
| ERT 1 (C-D) | 60.37151 | -133.11026 | 60.37202 | -133.11086 |
| ERT 2 (E-F) | 60.37157 | -133.11000 | 60.37256 | 133.11043 |

Table I2: Annual Snow Depth Days values (SDD) (cm d) calculated for each station at MP 825.

| Years | Main (SDD) | Sub 1 (SDD) | Sub 2 (SDD) | Average |
|---|---|---|---|---|
| 2013-2014 | 5930 | 5500 | 5790 | 5740 |
| 2012-2013 | 4970 | 5080 | 4650 | 4900 |
| 2011-2012 | 3560 | 5320 | 4740 | 4540 |
| 2010-2011 | 5660 | 7550 | 4970 | 6060 |
| Average | 5030 | 5860 | 5030 | 5310 |

Table I3: Air and ground temperatures (°C) at MP 825. Missing data are represented as blank cells.

| | Main | | Sub 1 | | Sub 2 | | | |
|---|---|---|---|---|---|---|---|---|
| Years | MAAT | MAGST | MAGST | MAGT 100cm | MAGST 1 | MAGST 2 | MAGT 50 cm | MAGT 100 cm |
| 2010-2011 | -1.6[A] | 1.4 | | | 1.0 | 1.0 | 0.2 | 0.0 |
| 2011-2012 | -0.2 | 1.9 | 2.9 | 1.8 | | | | |
| 2012-2013 | -1.3 | 1.3 | 2.9 | 1.4 | 1.6 | 1.5 | 0.3 | 0.1 |
| Average | -1.0 | 1.5 | 2.9 | 1.6 | 1.3 | 1.3 | 0.3 | 0.1 |

[A] Missing data from August 1 to August 18, 2011 estimated by correlation with Whitehorse Environment Canada station.

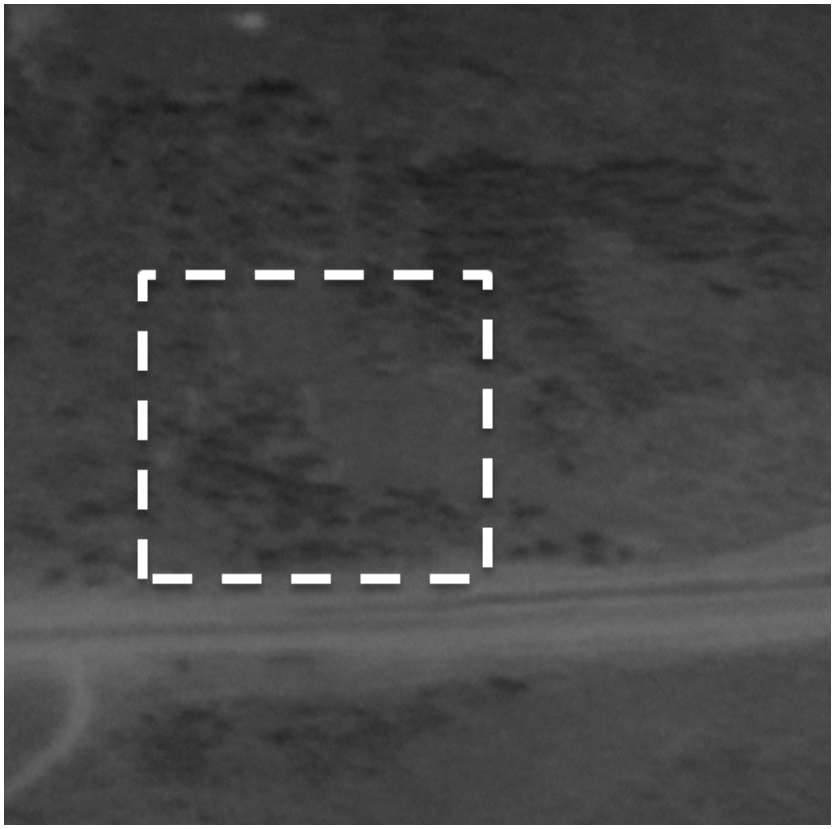

Figure I1: Air photo for MP 825 in 1964. Dashed square represents the study area.

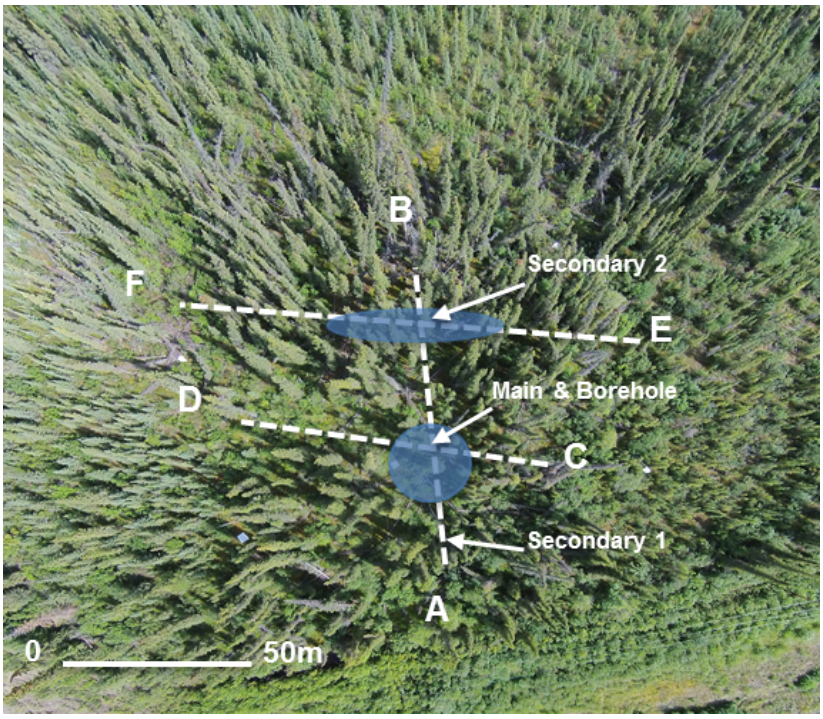


Figure I2: Air photo for MP 825 in 2014. Shaded ellipses represent permafrost patches; dashed lines represent ERT transects and climate monitoring instruments locations are marked. The scale is approximate.

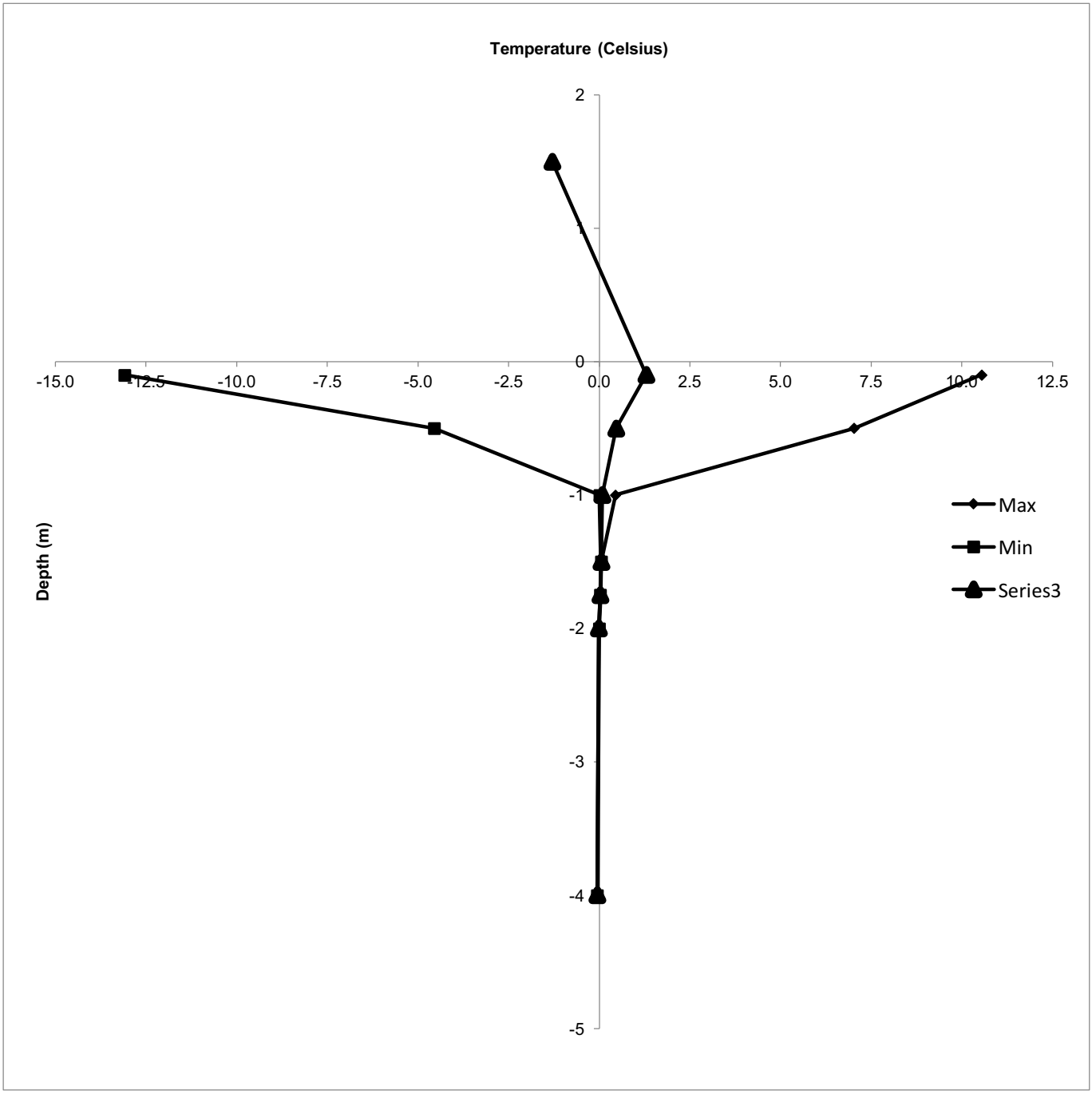


Figure I3: Temperature envelope for borehole at MP 825 (2010-2014). A supra-permafrost talik is present between 1 m and 1.75 m where the ground is perennially thawed. The temperature at the base of the borehole at 4 m is -0.05°C.

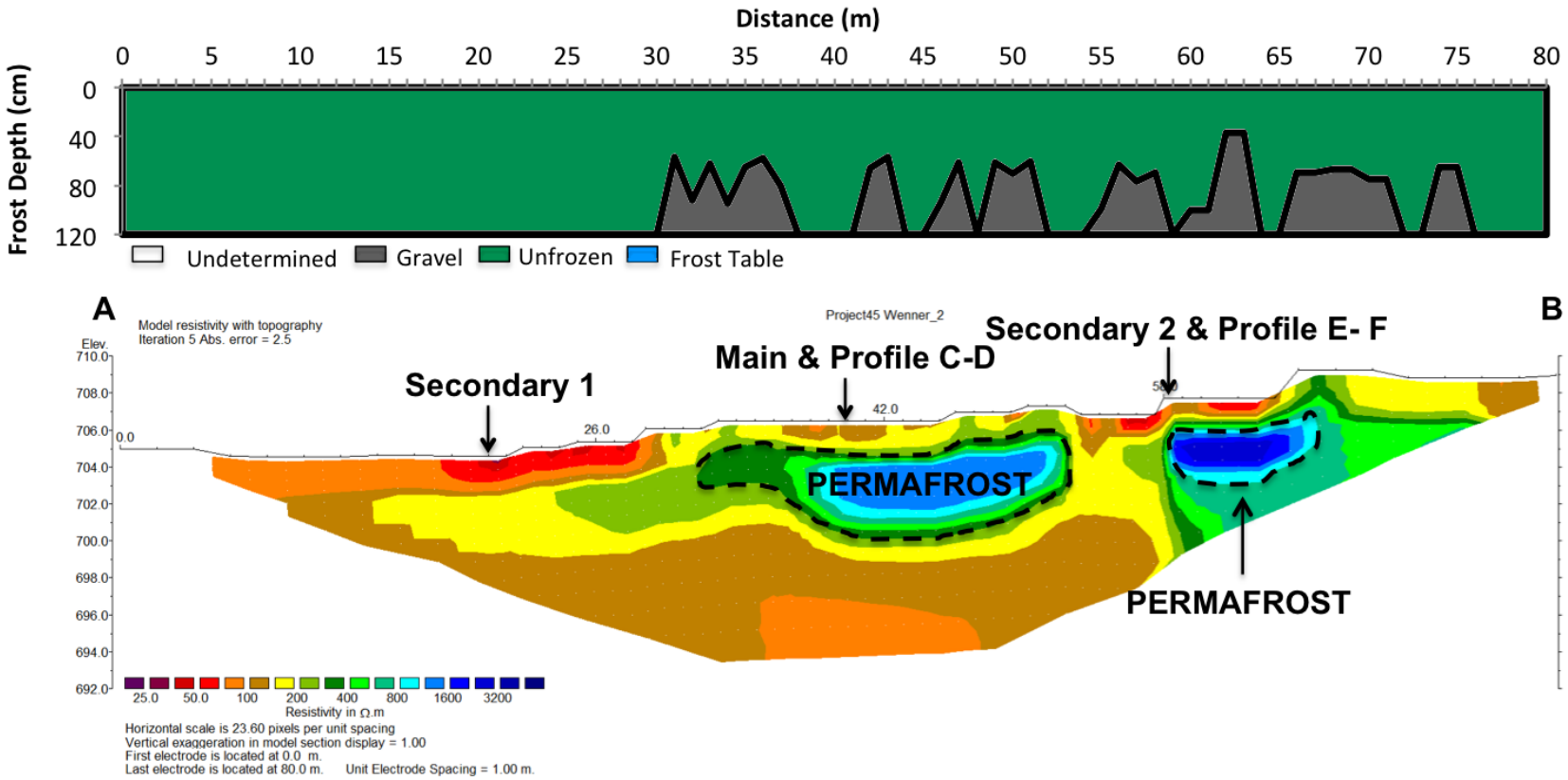


Figure I4: Modelled ERT inversion profile at MP 825 for the permanent array, with dashed lines representing inferred permafrost. The frozen/unfrozen boundary is taken to be 400 Ω m at this site.

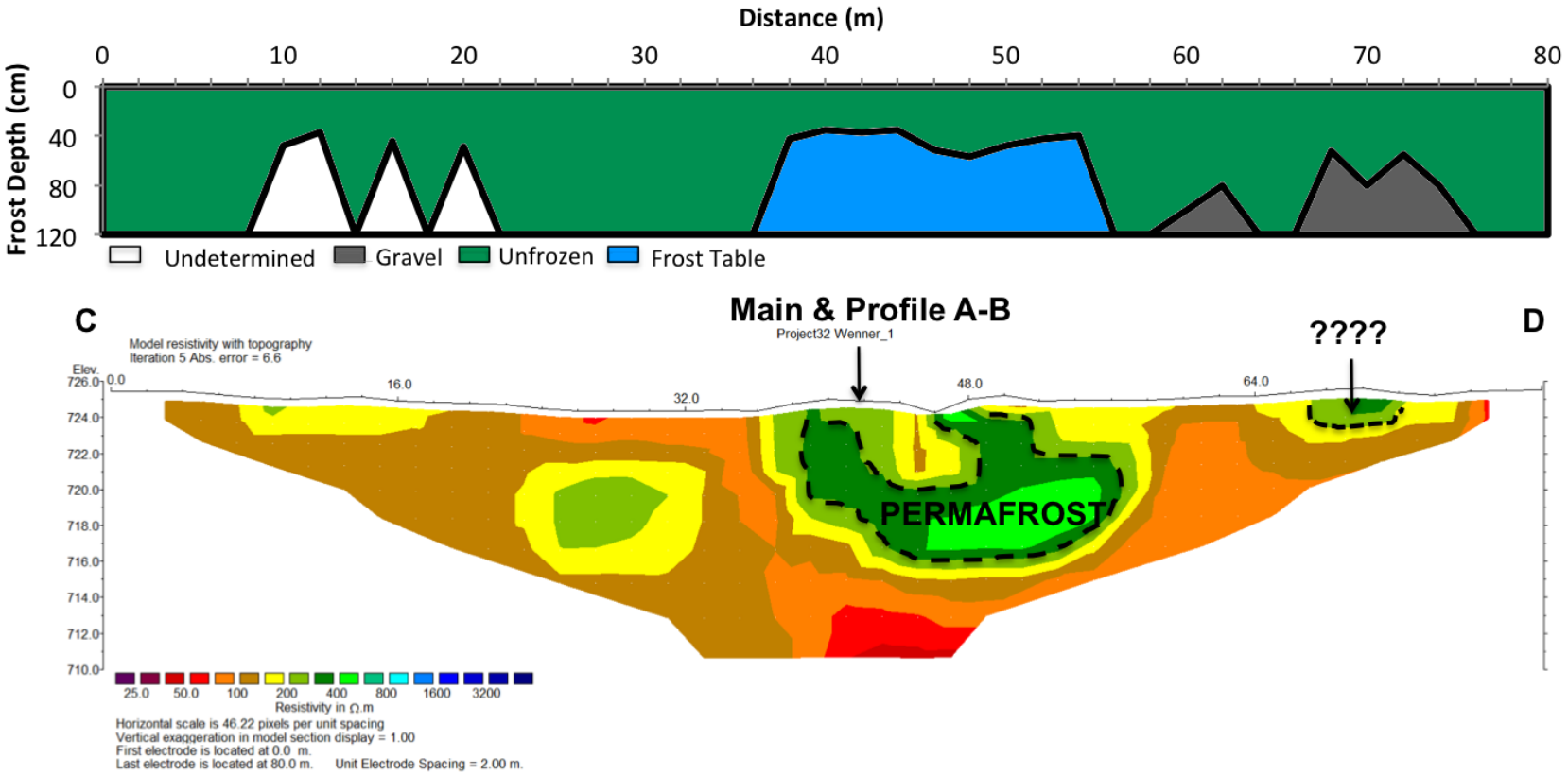


Figure I5: Modelled ERT inversion profile at MP825 for the ERT 1, with dashed lines representing inferred permafrost. The frozen/unfrozen boundary is taken to be 400 Ω m at this site.

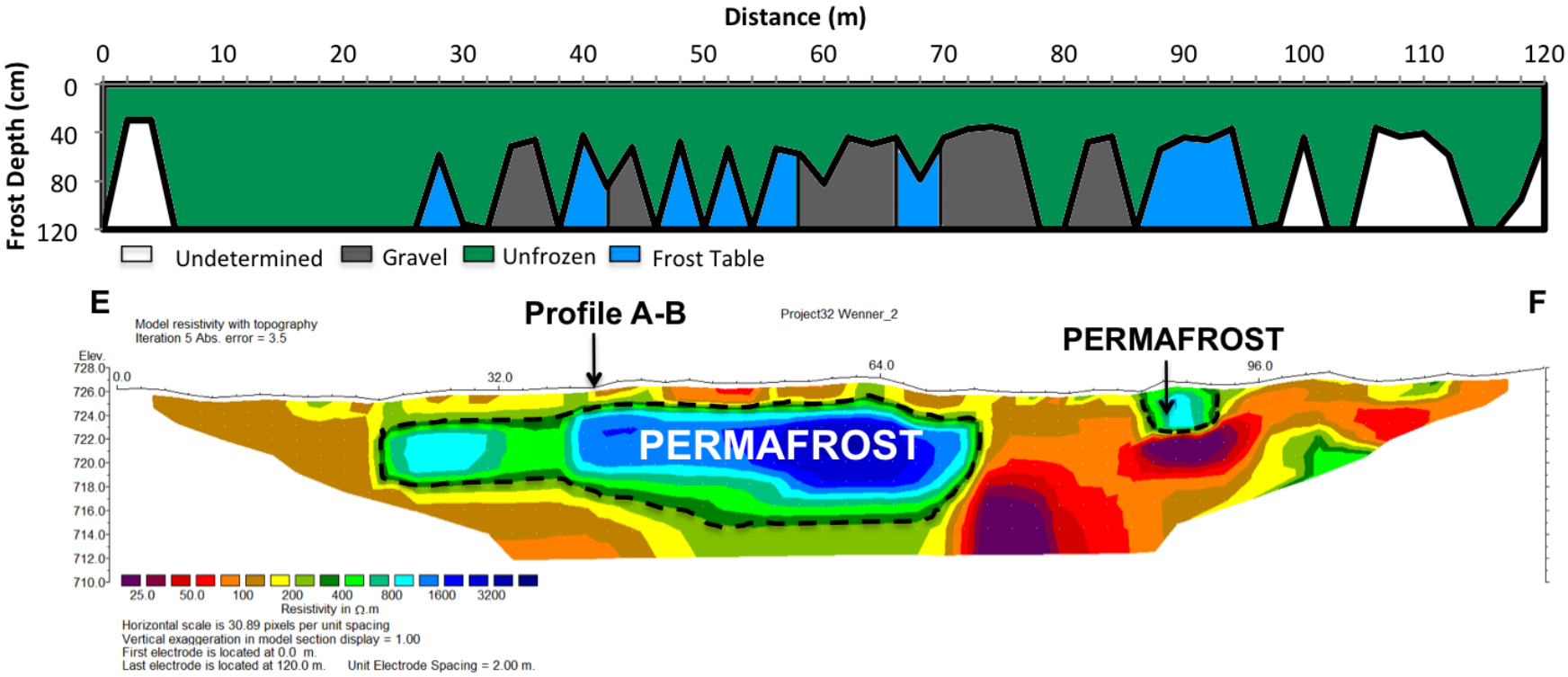


Figure I6: Modelled ERT inversion profile at MP 825 for the ERT 2, with dashed lines representing inferred permafrost. The frozen/unfrozen boundary is taken to be 400 Ω m at this site.

## Appendix J: MP 844

Table J1: Coordinates of the ERT lines at MP 844.

| | Transect starts | | Transect ends | |
|---|---|---|---|---|
| | Latitude | Longitude | Latitude | Longitude |
| Permanent array (A-B) | 60.47620 | -133.48392 | 60.47689 | -133.48459 |
| ERT 1 (C-D) | 60.47691 | -133.48450 | 60.47605 | -133.48380 |
| ERT 2 (E-F) | 60.47613 | -133.48627 | 60.47652 | -133.48427 |

Table J2: Annual Snow Depth Days values (SDD) (cm d) calculated for each station at MP 844.

| Years | Main (SDD) | Sub 1 (SDD) | Sub 2 (SDD) | Average |
|---|---|---|---|---|
| 2010-2011 | 8450 | 10060 | 7820 | 8780 |
| 2011-2012 | 5810 | 5780 | 5470 | 5680 |
| 2012-2013 | 9470 | 8460 | 7560 | 8490 |
| 2013-2014 | 8940 | 9090 | 7760 | 8600 |
| Average | 8170 | 8350 | 7150 | 7890 |

Table J3: Air and ground temperatures (°C) at MP 844. Missing data are represented as blank cells.

| | | Main | | | | | | | | | Sub 1 | | | | Sub 2 | | | |
|---|---|---|---|---|---|---|---|---|---|---|---|---|---|---|---|---|---|---|
| Years | MAAT | MAGST 1 | MAGST 2 | MAGST 3 | MAGT 0 cm | MAGT 10 cm | MAGT 25 cm | MAGT 50 cm | MAGT 75 cm | MAGT 100 cm | MAGST 1 | MAGST 2 | MAGT 50 cm | MAGT 75 cm | MAGST 1 | MAGST 2 | MAGT 25 cm | MAGT 50 cm |
| 2010-2011 | -2.4[A] | | | | | 1.5 | 0.8 | | | | 1.6 | 1.2 | 0.0 | 0.1 | 1.0 | 1.0 | 0.6 | 0.4 |
| 2011-2012 | -1.2[B] | | 1.6 | 0.1 | 1.8 | 1.8 | 1.3 | 1.1 | 0.4 | 0.2 | 1.5 | 1.6 | 0.2 | 0.2 | 1.4 | | | 0.9 |
| 2012-2013 | -2.5 | 1.7 | 1.8 | 1.3 | 1.7 | 1.9 | 1.6 | 0.1 | 0.5 | 0.2 | 1.0 | 1.8 | 0.4 | 0.3 | 1.7 | 1.6 | 1.0 | 0.6 |
| Average | -2.0 | 1.7 | 1.7 | 0.7 | 1.8 | 1.7 | 1.2 | 0.6 | 0.4 | 0.2 | 1.4 | 1.6 | 0.2 | 0.2 | 1.3 | 1.3 | 0.8 | 0.6 |

[A] Missing MAAT in 2010-2011 estimated through correlation with Whitehorse Environment Canada station and blended with reliable data from MP 844.

[B] Missing MAAT in 2011-2012 estimated through correlation with Whitehorse Environment Canada station and blended with reliable data from MP 844.

Figure J1: Air photo for MP 844 in 1964. Dashed square represents the study area.

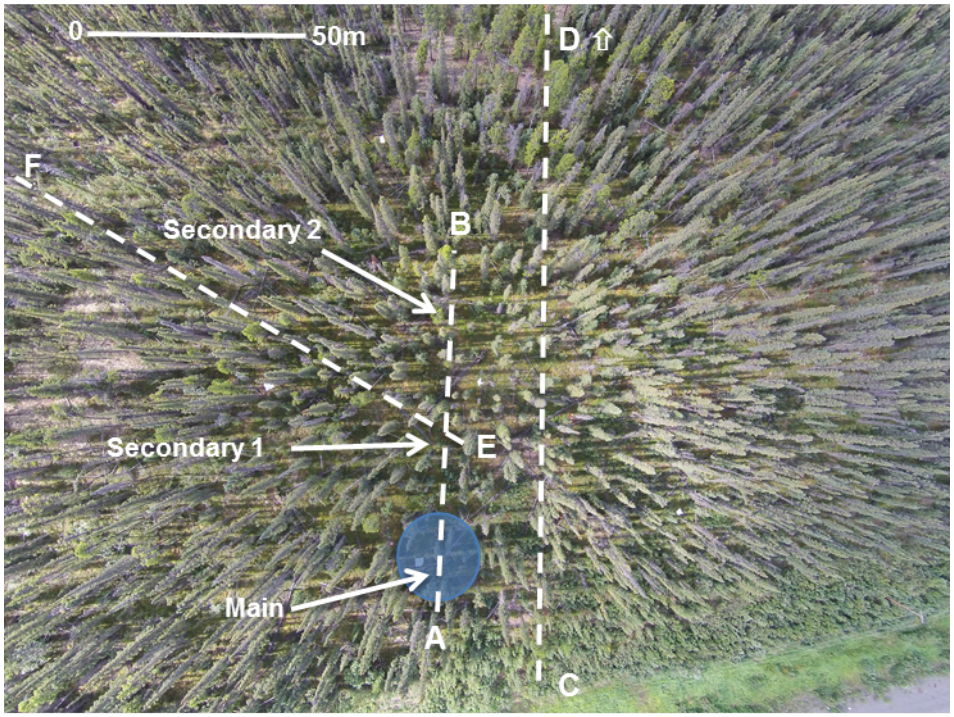


Figure J2: Air photo for MP 844 in 2014. Shaded ellipses represent permafrost patches; dashed lines represent ERT transects and climate monitoring instruments locations are marked. The scale is approximate.

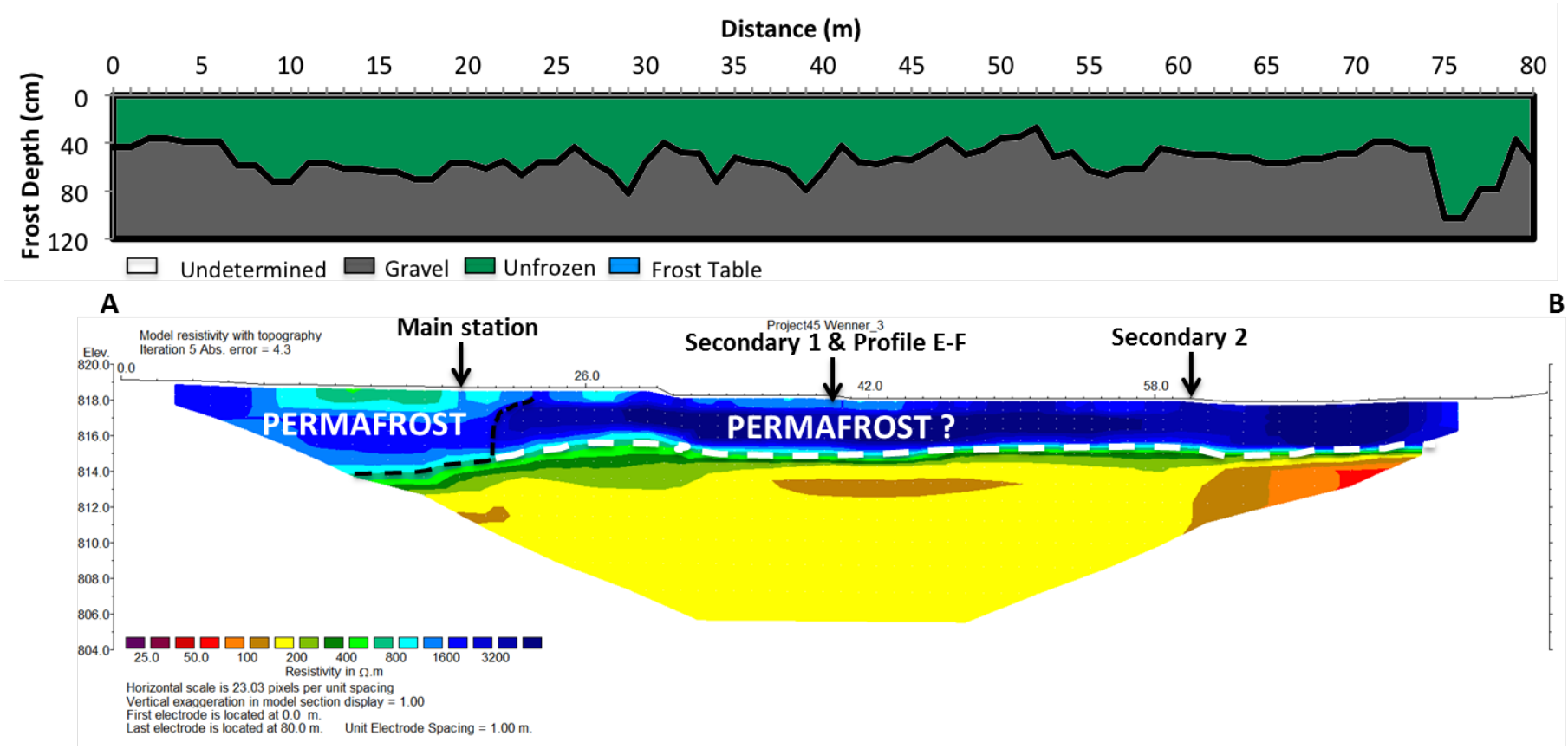


Figure J3: Modelled ERT inversion profile at MP 844 for the permanent array, with black dashed lines representing inferred permafrost and the white dashed lines the areas of uncertainties. The frozen/unfrozen boundary is taken to be 1200 Ω m at this site.

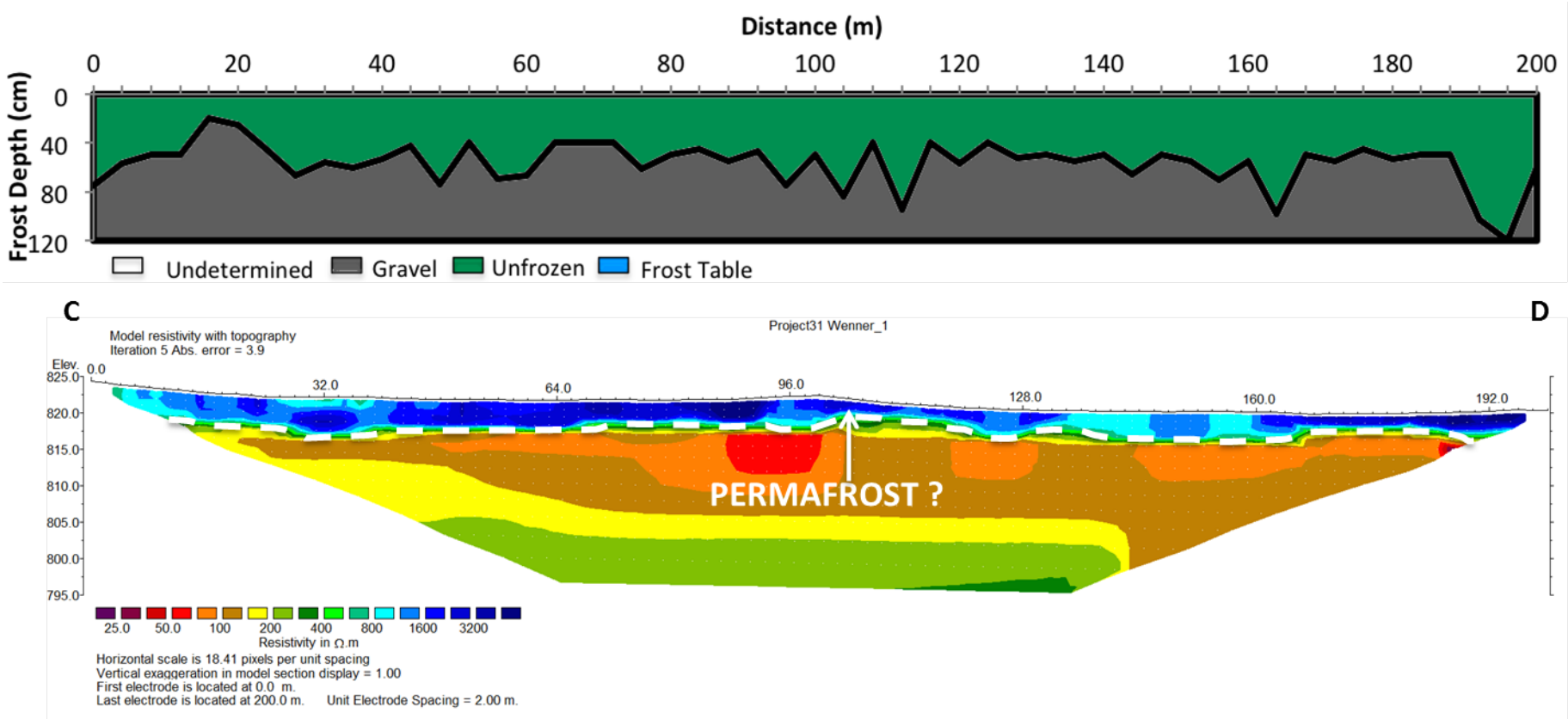


Figure J4: Modelled ERT inversion profile at MP 844 for the ERT 1, with black dashed lines representing inferred permafrost and the white dashed lines the areas of uncertainties. The frozen/unfrozen boundary is taken to be 1200 Ω m at this site.

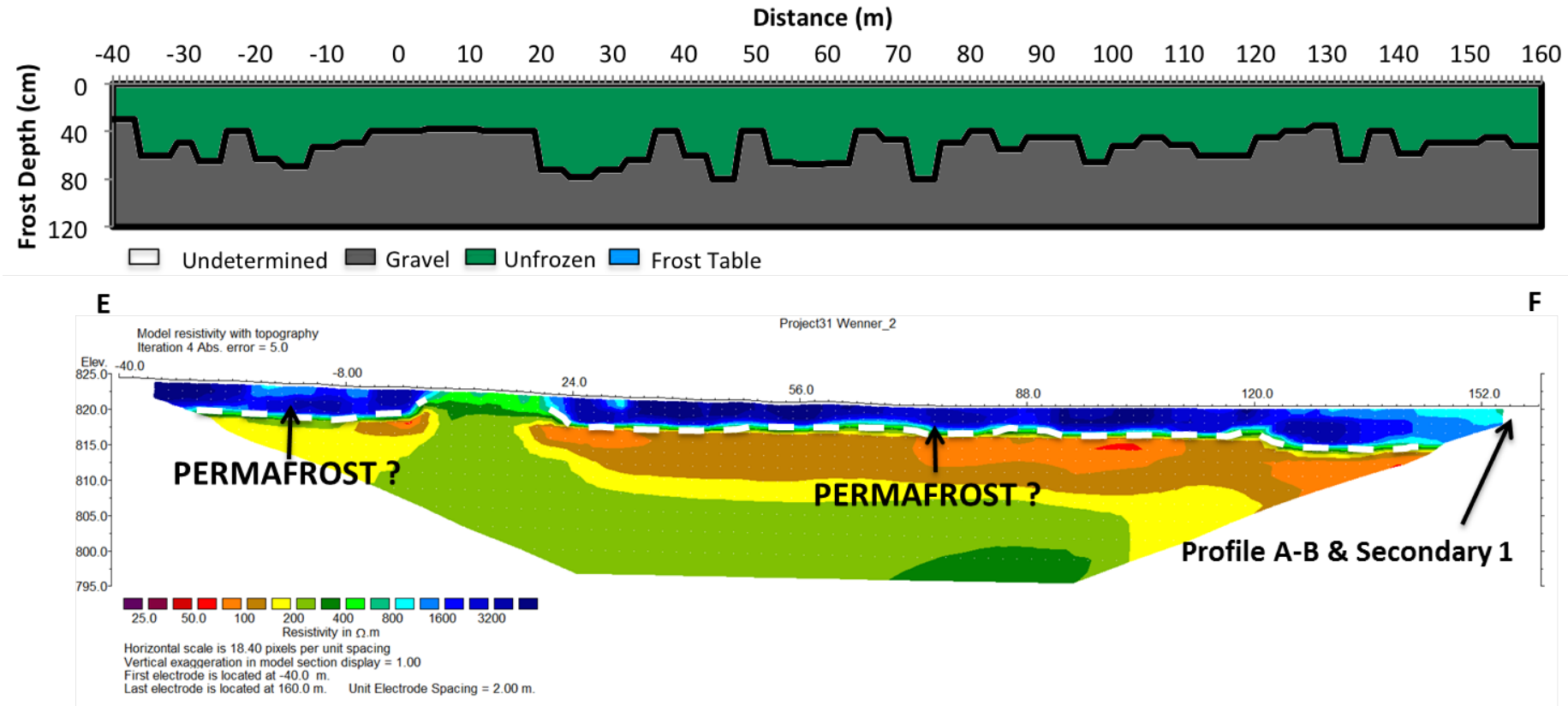


Figure J5: Modelled ERT inversion profile at MP 844 for the ERT 2, with black dashed lines representing inferred permafrost and the white dashed lines the areas of uncertainties. The frozen/unfrozen boundary is taken to be 1200 Ω m at this site.

## Appendix K: Pearson test results

Table K1: Pearson significance test for averages values from 2010-2014. Bold cells are significant at the p = 0.05 level or better.

| | Log 10 Surface Area | Log 10 Max Thickness | Latitude | Longitude | MAAT | MAGST | MAGT | Average SDD | Average Surface Offset | Average Thermal Offset | Average Total Offset |
|---|---|---|---|---|---|---|---|---|---|---|---|
| Log 10 Surface Area | | **0.000** | 0.811 | 0.882 | 0.139 | 0.741 | 0.867 | 0.234 | 0.232 | 0.737 | 0.103 |
| Log10 Max Thickness | | | 0.561 | 0.744 | 0.183 | 0.635 | 0.602 | 0.369 | 0.370 | 0.547 | 0.116 |
| Latitude | | | | **0.001** | 0.890 | 0.582 | 0.462 | 0.976 | 0.526 | 0.706 | 0.742 |
| Longitude | | | | | 0.807 | 0.980 | 0.257 | 0.554 | 0.776 | 0.775 | 0.986 |
| MAAT | | | | | | 0.118 | 0.385 | **0.030** | 0.068 | 0.214 | **0.000** |
| MAGST | | | | | | | 0.657 | 0.517 | 0.297 | **0.000** | 0.134 |
| MAGT | | | | | | | | 0.698 | 0.580 | 0.808 | 0.747 |
| Average SDD | | | | | | | | | 0.137 | 0.637 | **0.031** |
| Average Surface Offset | | | | | | | | | | 0.199 | 0.073 |
| Average Thermal Offset | | | | | | | | | | | 0.181 |

Table K2: Pearson significance test all climate stations average values from 2010-2014. Bold cells are significant at the p = 0.05 level or better.

| | Log10 Permafrost Thickness | SDD | MAGST | MAGT | Average Surface Offset | Average Thermal Offset | Average Total Offset |
|---|---|---|---|---|---|---|---|
| Log10 Permafrost Thickness | | 0.897 | 0.963 | **0.020** | 0.377 | 0.105 | 0.553 |
| SDD | | | **0.030** | 0.850 | 0.315 | **0.023** | **0.001** |
| MAGST | | | | 0.066 | **0.002** | **0.000** | 0.586 |
| MAGT | | | | | 0.719 | **0.020** | **0.011** |
| Average Surface Offset | | | | | | **0.009** | **0.001** |
| Average Thermal Offset | | | | | | | **0.013** |
| Average Total Offset | | | | | | | |

## Appendix L: Air photo information

Table L1: Table of air photo information

| MP Site | Roll number | Line number | Photo number | Scale | Altitude (ft) | Acquisition date | Frame start | Frame end |
|---|---|---|---|---|---|---|---|---|
| MP 178 | A18372 | 2N | 86-87 | 20000 | 10150 | 1964-05-12 | 77 | 113 |
| MP 286 | A18375 | 31W | 93-94 | 15000 | 7500 | 1964-05-20 | 83 | 98 |
| MP 341 | A18393 | 70NE | 5-6 | 15000 | 7300 | 1964-05-29 | 1 | 19 |
| MP 400 | A18392 | 82NW | 118-119 | 20000 | 9310 | 1964-05-28 | 106 | 121 |
| MP 579 | A18392 | 118NW | 64-65 | 15000 | 8120 | 1964-05-28 | 63 | 72 |
| MP 597 | A18392 | 121SW | 83-84 | 15000 | 8200 | 1964-05-28 | 80 | 87 |
| MP 681 | A18390 | 136NE | 118-119 | 20000 | 9050 | 1964-05-26 | 106 | 124 |
| MP 788 | A18388 | 147SE | 103-104 | 20000 | 9405 | 1964-05-28 | 83 | 106 |
| MP 825 | A18404 | 151NW | 37-38 | 20000 | 9740 | 1964-05-27 | 12 | 50 |
| MP 844 | A18388 | 154NE | 129-130 | 20000 | 8840 | 1964-05-28 | 127 | 140 |

## Appendix M: Field site descriptions (data from James, 2010)

Table M1: Field site physical environment description

| *Site* | *Relief* | *Site elevation (m asl)* | *Latitude* | *Longitude* | *Range of organic layer thickness[2] (cm)* | *Tree types[3]* | *Maximum tree height[4] (m)* | *Surface terrain features[5]* | *Soil description* |
|---|---|---|---|---|---|---|---|---|---|
| MP 178 | L | 1098 | 57.425 | -122.865 | > 35 to > 135 | S | 9 | H, M, Lt, Ln | n/a |
| MP 286 | L | 420 | 58.663 | -122.693 | > 47 to > 114 | S, T | 7.5 | (p), H, M, Sph, Lt, Ln | n/a |
| MP 341 | L | 150 | 58.788 | -123.573 | > 42 to > 82 | S, T | 4.5 | H, M, Ln, Sph, Lt, B | Organic |
| MP 400 | L | 1042 | 58.693 | -124.858 | 36 to > 109 | S, W | 6 and 0.7 | (p), H, M, G, Ln, Lt, Se, B | Peaty, Highly cohesive clay |
| MP 579 | L | 675 | 59.965 | -127.531 | 30 to 125 | S | 12 | H, M, Lt, Sph, Ln | Peaty, shallow organic mat. Sandy silt, with scattered stones |
| MP 597 | L | 672 | 59.996 | -127.955 | 39 to > 75 | S, T | 13.5 | (p), Ln, Lt, Sph, M | Organic with coarse sand, sand and silt increase with depth. Presence of scattered stones |
| MP 681 | L | 838 | 60.188 | -129.898 | 12 to 31 | S, T, W | 15 | H, M, Sph, Ln, Lt, B | Wet, moderately cohesive, silty, organic-rich |
| MP 788 | L | 762 | 60.091 | -132.368 | 32 to > 132 | S | 12 | (p), H, M, Sph, Ln, Lt | n/a |
| MP 825 | L | 706 | 60.371 | -133.111 | 18 to 56 | S | 15 | H, M, Ln, Lt | Cohesive silt with sand and scattered stones |
| MP 844 | L | 820 | 60.476 | -133.483 | 21 to > 100 | S, W | 9 and 2 | M, Lt | Silty soil with rocks and gravel |

1: Relief. Legend: “L” site was low-lying with no significant slope.
2: Minimum and maximum range of the organic layer thickness measurements
3: Order of appearance represents order of abundance. Legend: “S” spruce, “T” tamarack, “W” willow.
4: Visual assessment of tree height, in order of appearance.
5: Surface features and low vegetation cover. Order of appearance represents order of abundance. Legend: “H” hummocky, “(p)” peat plateau, “M” non-sphagnum mosses, “Sph” sphagnum mosses, “Ln” lichens, “Lt” Labrador tea, “B” ground birch, “G” grasses, “Se” sedges, “Ht” horsetail.

## Appendix N: Snow Depth Days vs Maximum Snow Depth analyses

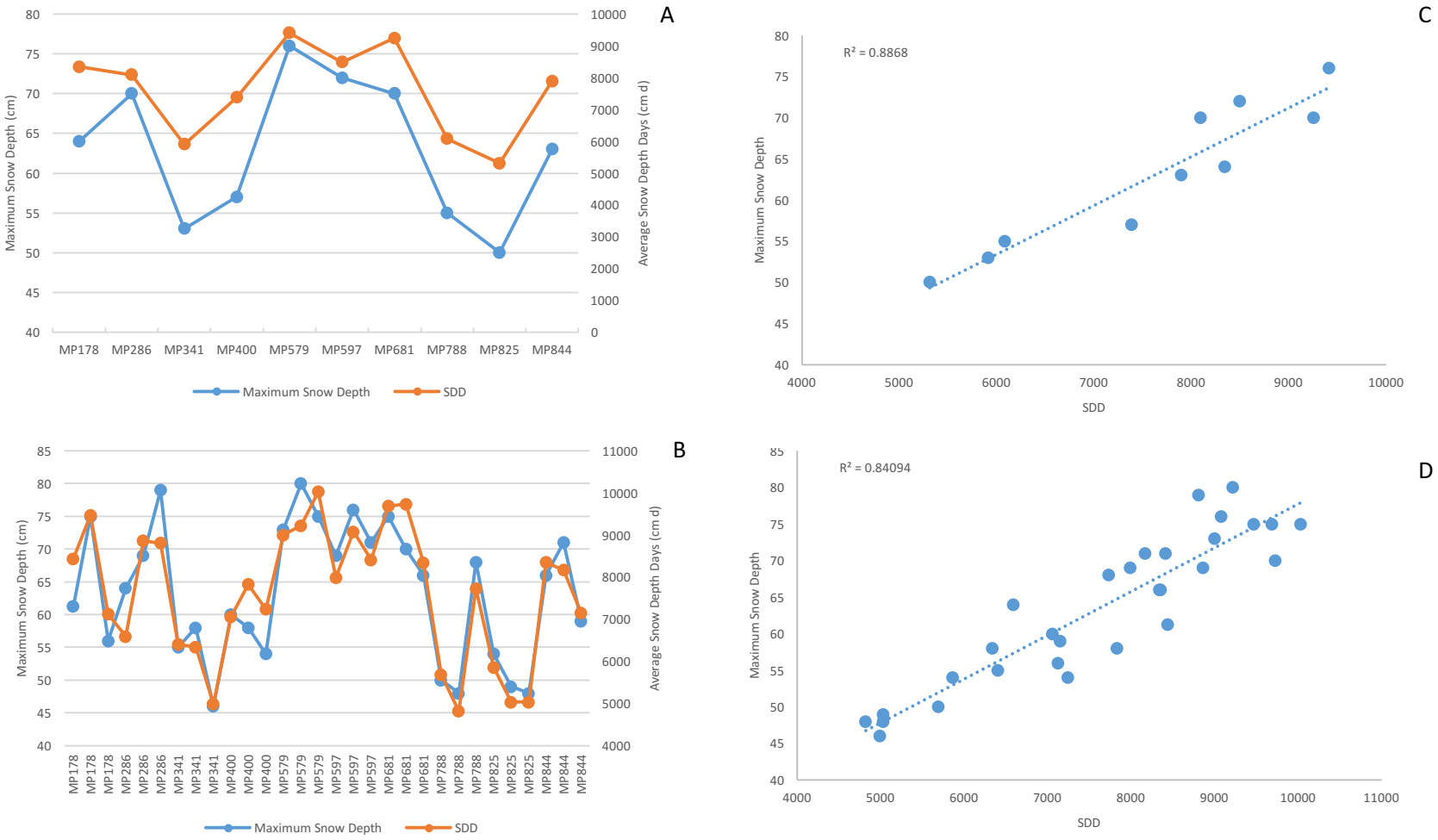


Figure N1: A-B Maximum snow depth and Snow Depth Days at each sites for site average (n=10) and all measurement stations (n=30). C-D scatterplot of Maximum snow depth against SDD.

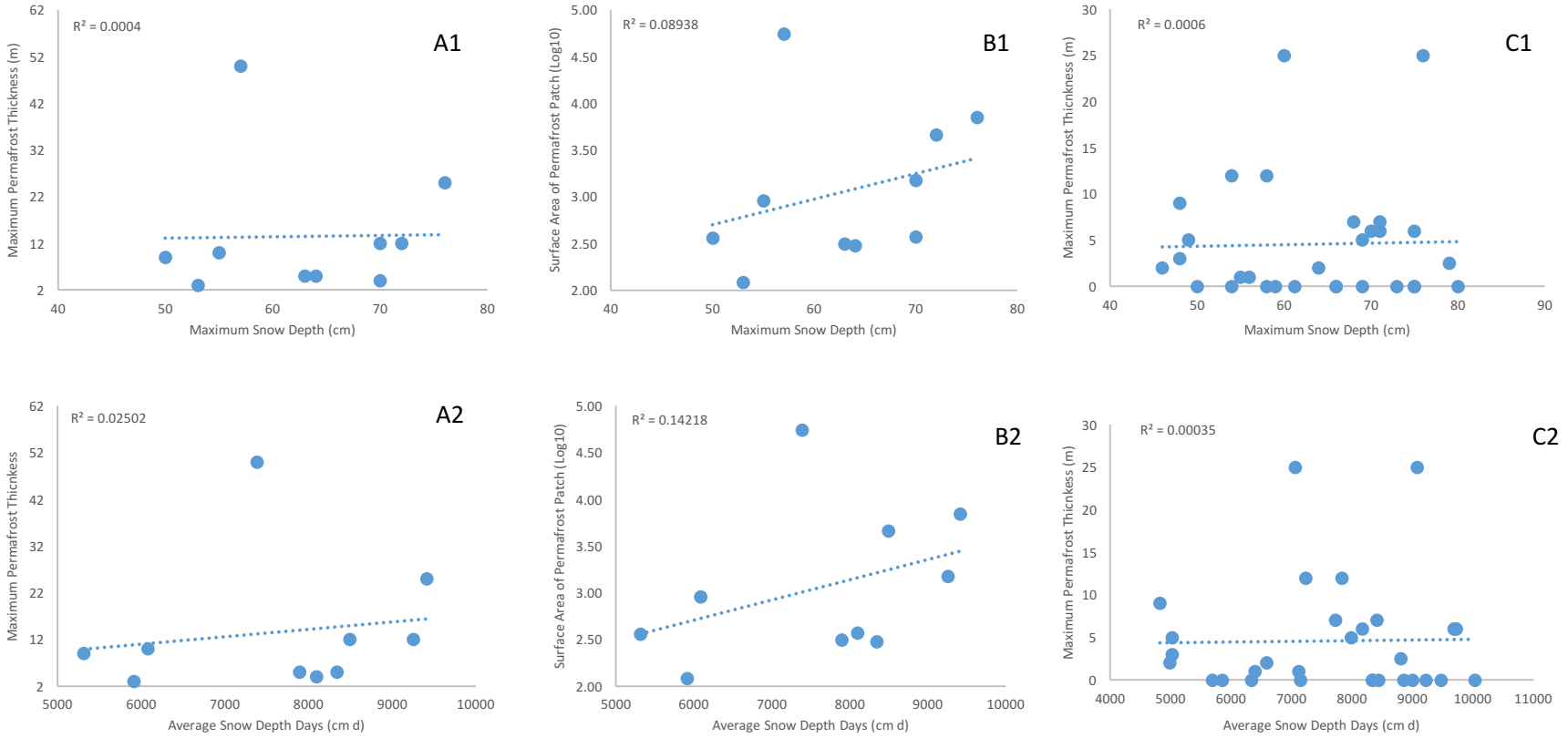


Figure N2: Comparative correlation plots: A1 – MSD (Maximum Snow Depth) vs Maximum permafrost thickness, A2 – SDD (Snow Depth Days) vs Maximum permafrost thickness (site averages (n= 10)); B1 MSD vs Surface Area of permafrost patch, B2 SDD vs Surface area of permafrost patch (site averages (n= 10)); C1 – MSD vs Maximum permafrost thickness, C2 – SDD vs Maximum permafrost thickness (measurement station averages (n= 30)).